University of California
Santa Barbara

Networks of Coupled Oscillators and Social Network Structures of Teams

A dissertation submitted in partial satisfaction
of the requirements for the degree

Doctor of Philosophy
in
Mechanical Engineering

by

Elizabeth Y. Huang

Committee in charge:

Professor Francesco Bullo, Chair
Professor Bassam Bamieh
Professor Jeff Moehlis
Professor Ambuj K. Singh

December 2020

The Dissertation of Elizabeth Y. Huang is approved.

Professor Bassam Bamieh

Professor Jeff Moehlis

Professor Ambuj K. Singh

Professor Francesco Bullo, Committee Chair

December 2020

Networks of Coupled Oscillators

and

Social Network Structures of Teams

Copyright © 2020

by

Elizabeth Y. Huang

To my mom.

Acknowledgements

First and foremost, I would like to thank my advisor, Francesco Bullo, who provided me with guidance and opportunities throughout my graduate studies. He taught me to never compromise on quality, think critically, and strive to go above and beyond. In addition, he taught me to be detail oriented with his unmatched eye for finding typos and highly organized file system. Working under Francesco has allowed me to grow exponetially both personally and professionally, and the lessons he passed on will be invaluable to me in all aspects of the rest of my career.

I am thankful for all of my committee members. Thanks to Bassam Bamieh for teaching my favorite controls course at UCSB, due to his intuitive explanations of linear systems theory. Thanks to Ambuj Singh for organizing the weekly MURI meetings, which cultivated many new collaborations and ideas. And thanks to Jeff Moehlis for his intuitive explanations of dynamical systems theory, ongoing work to improve various aspects of the Mechanical Engineering department, and being a dependable source of support for graduate students in their professional endeavors.

My research was supported by the U.S. Army Research Laboratory and the U.S. Army Research Office under grant number W911NF-15-1-0577 and the U.S. Department of Energy (DOE) Solar Energy Technologies Office under Contract No. DE-EE0000-1583, for which I am very thankful for.

I would like to thank all my collaborators, Omid, Ambuj, Kevin, Saber, Wenjun, and Dario. Without their discerning questions and feedback, I may still be at a dead end in my research. I am grateful for the support and comraderie of my past and present lab mates: Xiaoming, Shadi, Mishel, and Francesco. I am also lucky to have been surrounded by UCSB's fantastic controls and dynamical systems community, with special mention to Pascal, Karthik, Poorva, Emily, Sharad, Raphael, Murat, Henrique, Matina, Shara, and

Danny for their friendship, professional support, and being a soundboard for my scientific ideas. In particular, I'd like to highlight my gratitude to Guosong, for endless discussions regarding research and LaTeX formatting. I always walked away from conversations with him with so much more insight into my own research and his passion for controls was obvious to everyone around him.

I am indebted to Katelynn, Laura, Richard, Josh, and Tim, whose work behind-the-scenes made research possible and helped me navigate academic life. Thanks also to UCSB's CSEP program and everyone involved, for providing me an opportunity to explore teaching and mentoring.

I would like to thank my family and friends from UCSB, UCSD, and beyond. Their company at coffee shops for weekend workdays, companionship in backpacking adventures, food exploration opportunities, professional advice and mentorship, and support through thick and thin have made this achievement possible. And the biggest thank you to my mom, because the opportunity to pursue a Ph.D. would not be possible without her hardwork, support, and reminders to eat healthy.

Curriculum Vitæ

Elizabeth Y. Huang

Education

2020	**Ph.D. in Mechanical Engineering** University of California, Santa Barbara.
2016	**B.S. in Mechanical Engineering** University of California, San Diego.

Professional Experience

2016 – 2020	**Graduate Student Researcher** University of California, Santa Barbara.
Summer 2015/16	**Engineering Intern** Solar Turbines, San Diego, CA

Teaching Experience

Fall 2017/ Summer 2020	**Teaching Assistant** Course: ME 14 *Statics* Mechanical Engineering, University of California, Santa Barbara
Spring 2017/18/20	**Teaching Assistant** Course: ME 155A *Control System Design* Mechanical Engineering, University of California, Santa Barbara
Winter 2019	**Teaching Assistant** Course: ME 179P *Introduction to Robotics: Planning and Kinematics* Mechanical Engineering, University of California, Santa Barbara
Winter 2017	**Teaching Assistant** Course: ME 151B *Thermosciences* Mechanical Engineering, University of California, Santa Barbara
Fall 2016	**Teaching Assistant** Course: ME 104 *Mechatronics* Mechanical Engineering, University of California, Santa Barbara

Mentoring

Summer 2019	Emily Lopez Program: Undergraduate Research through *Early Undergraduate Research and Knowledge Acquisition* University of California, Santa Barbara

Summer 2019	Jess Gomez, Ezequiel Martinez, Lorenzo Sanders Program: Undergraduate Research through *Summer Institute in Mathematics and Science* University of California, Santa Barbara
Summer 2018	Nicholas Garcia, Luis Gonzalez, Amanda Harper Program: Engineering Internship through *Problem-based Initiatives for Powerful Engagement and Learning In Naval Engineering and Science* University of California, Santa Barbara

Professional Service

Reviewer	IEEE Transactions on Automatic Control IEEE Conference on Decision and Control

Publications

1. O. Askarisichani and E. Y. Huang and K. S. Sato and N. E. Friedkin and F. Bullo and A.K. Singh. Expertise and confidence explain how social influence evolves along intellective tasks. *Proceedings of the National Academy of Sciences*. Note: Submitted.
2. E. Y. Huang and D. Paccagnan and W. Mei and F. Bullo. Assign and Appraise: Achieving Optimal Performance in Collaborative Teams. *IEEE Transactions on Automatic Control*. Note: Submitted.
3. S. Jafarpour and E. Y. Huang and K. D. Smith and F. Bullo. Flow and Elastic Networks on the n-Torus: Geometry, Analysis and Computation. *SIAM Review*. Note: Submitted.
4. S. Jafarpour and E. Y. Huang and F. Bullo. Synchronization of Kuramoto oscillators: Inverse Taylor Expansions. *SIAM Journal on Control and Optimization*. 57(5):3388-3412, 2019.
5. E. Y. Huang and S. Jafarpour and F. Bullo. Synchronization of Coupled Oscillators: The Taylor Expansion of the Inverse Kuramoto Map. In IEEE Conf. on Decision and Control, Miami, USA, pages 5340-5345, December 2018.

Abstract

Networks of Coupled Oscillators

and

Social Network Structures of Teams

by

Elizabeth Y. Huang

Networks are ubiquitous in nature and engineering, with applications in areas such as modeling power grids, population dynamics, and social networks. Applying network science to complex dynamical systems provides us with powerful tools to study the interactions between agents. Moreover, these tools can also be used to study the nonlinear dynamics of the network itself and he combination of dynamics *over* networks and dynamics *of* networks paves the way for new models that accurately capture the rich behavior in sociological processes. In this thesis, we first study synchronization in networks of coupled oscillators. Second we model and analyze the dynamics of influence networks of human teams.

Regarding coupled oscillators, we study the frequency synchronization problem for networks of Kuramoto oscillators with arbitrary topology and heterogeneous edge weights. We propose a novel equivalent transcription for the equilibrium synchronization equation. Using this transcription, we develop a power series expansion to compute the synchronized solution of the Kuramoto model as well as a sufficient condition for the strong convergence of this series expansion. Truncating the power series provides (i) an efficient approximation scheme for computing the synchronized solution, and (ii) a simple-to-check, statistically-correct hierarchy of increasingly accurate synchronization tests. This hierarchy of tests provides a theoretical foundation for and generalizes the

best-known approximate synchronization test in the literature.

Regarding the dynamics of social networks of human teams, we focus on modeling and analyzing how performance and expertise impact the level of influence team members have on each other. First, we propose a novel quantitative model describing the decentralized process by which individuals in a team learn who has what abilities, while concurrently assigning tasks to each of the team members. Our theoretical analysis characterizes a team's ability, or inability, to learn each other's skill and thus converge to a work allocation maximizing the team performance. Second, we propose a cognitive dynamical model to describe the process by interpersonal influences are adjusted in small teams over a sequence of intellective tasks with fixed workload. We provide analytical results on the model's asymptotic behavior for the case with identically performing individuals and verify the accuracy of the proposed model on experimental data.

Contents

List of Figures

List of Tables

Chapter 1

Dynamics of Coupled Oscillators Over a Network

This chapter was first published in *SIAM Journal on Control and Optimization* in Volume 57, Issue 5, by the Society for Industrial and Applied Mathematics (SIAM). © 2019, Society for Industrial and Applied Mathematics. See [1].

1.1 Introduction

Collective synchronization is an interesting behaviour which lies at the heart of various natural phenomena. The celebrated Kuramoto model [2] is one of the simplest models for studying synchronization in a network of coupled oscillators. Kuramoto model has been successfully used to model the synchronization behaviour of a wide range of physical, chemical, and biological systems [3]. Examples include the power grids [4, 5], automated vehicle coordination [6, 7], pacemakers in heart [8], clock synchronization [9], and neural networks [10]; see also [11, Chapter 13] for additional examples. One of the most interesting types of synchronization is frequency synchronization, where all oscillators reach

the same rotational frequency with possibly different phases. It is well-known that the Kuramoto model can exhibit a transition from incoherence to frequency synchronization. For many applications, such as frequency regulation in power networks, it is important to have an accurate estimate of this transition to synchronization. Finding sharp conditions to determine when this transition happens continues to be a challenging as well as a critical problem.

Literature Review

The problem of finding conditions for existence of a stable synchronized solution for the Kuramoto model of coupled oscillators has been studied extensively in the literature. For complete graphs with homogeneous weights, the order parameter is used to implicitly determine the exact critical coupling needed for a synchronized solution [12–14]. For acyclic graphs with heterogeneous weights, a necessary and sufficient condition is developed for synchronization of the heterogeneous Kuramoto model [15]. In addition, Lyapunov analysis applied to the complete graph is used in [16] to give a sufficient condition and in [17] to give an explicit necessary and sufficient condition for existence of a synchronized solution. However for general topology graphs, such a complete characterization of frequency synchronization does not exist. For general graphs with heterogeneous weights, several necessary conditions and sufficient conditions for existence of stable synchronized solution have been reported in the literature. [18] requires sufficiently large nodal degrees relative to the natural frequencies, [19] uses the cutset in the graph, and [20] states that the algebraic connectivity must be sufficiently large compared to the difference in natural frequencies of connected oscillators. Recently, a novel cutset projection operator has been introduced to rigorously prove a simple-to-check, sufficient condition for synchronization of Kuramoto model [21]. Using numerous simulations, it is shown

that this new sufficient condition scales better to large networks [21]. In a vast majority of literature on the Kuramoto model, the interactions between oscillators are considered symmetric. However, it is worth mentioning that Kuramoto model with nonsymmetric interactions can exhibit synchronizing behaviors [22] and several conditions for existence and uniqueness of the synchronized solution have been obtained in the literature [23],[24].

Despite these deep results in the literature, the existing synchronization conditions usually provide conservative estimates for the synchronization threshold. In an effort to come closer to finding the exact synchronization threshold, [15] and [25] introduce a statistically accurate approximate test for synchronization that depends on the network parameters and topology derived from the linearized Kuramoto map and the converging power series expansion of the phase angles of the Kuramoto oscillators, respectively.

If existence of a frequency synchronized solution can be guaranteed, then the next step is computing the synchronized solutions. A common method to approximate the solution is to linearize the equations. This will result in studying the equations of the form $\omega = L\theta$, where L is the Laplacian matrix of the network, ω is the vector of natural frequencies, and θ is the vector of angles [26–28]. The angles θ can be approximately solved very efficiently, even for extremely large, sparse graphs [29, Theorem 3.1]. However, when phase differences of the oscillators are large, this linear approximation is not very accurate.

In order to compute the synchronization manifold of the nonlinear Kuramoto equations, one can employ iterative numerical algorithms such as Newton–Raphson or Gauss–Seidel [30–32]. Unfortunately, these algorithms do not guarantee convergence to the synchronized solutions and failure of these algorithms could be due to numerical instability, an initialization issue, or non-existence of the solution. Another approach is to use numerical polynomial homotopy continuation (NPHC). It is guaranteed that NPHC will find all stable and unstable manifolds of the Kuramoto model, but this method is not

computationally tractable for large networks; [33] uses NPHC to study the homogeneous Kuramoto model for particular graph topologies with up to 18 nodes. Finally, [34] gives an approximate analytical solution for stable synchronization manifolds using the order parameter. However, this approximation scheme is only applicable to the Kuramoto model with all-to-all connections and uniform weights.

A wide range of methods for finding synchronized solutions of the Kuramoto model stems from the power network literature, where different techniques are used to find the solutions of the AC power flow equations. Here, we only review two of these approaches. The first approach is called holomorphic embedding load-flow method (HELM) and has been proposed to find all the solutions of power flow equations [35]. While HELM is based on advanced results and concepts from complex analysis, its numerical implementation is recursive and straightforward [35, 36]. However, HELM is reported to be much slower than the Newton–Raphson methods [36]. The second approach is the optimization approach, where an optimal power flow problem (OPF) is used to solve for the AC power flow equations. The OPF problems have been studied extensively in the power network literature, e.g., see [37–39]. Thus, one can use the numerical algorithms for the optimization problem to find the synchronized solution of the Kuramoto model. Unfortunately, due to the non-convex nature of the OPFs, these algorithms usually result in an approximation of the synchronized solution.

Contribution

The contributions of this chapter are both theoretical and computational. From a theoretical viewpoint, as a minor contribution, we first provide a rigorous proof for the following well-known folk theorem: frequency synchronization is equivalent with the existence of a stable synchronization manifold (see [13] and [14] for statement of this result

without proof). Second, by introducing the notions of edge vectors and flow vectors in graphs, we propose four equivalent transcriptions for the synchronization manifold of the Kuramoto model: node, flow, constrained edge, and unconstrained edge balance equations. While the first three formulations have already been studied in the literature (see [15] and [21]), the unconstrained edge balance equations provide a novel important characterization of the synchronization manifold. Our main technical results are (1) a sufficient condition for existence of a unique solution for unconstrained edge balance equations and (2) a recursive expression for each term of the Taylor series expansion for this solution of the unconstrained edge balance equations. Additionally, we prove that, if our simple-to-check sufficient condition is satisfied, then the Taylor series expansion for the solution converges strongly. We also provide an algorithm to symbolically compute all terms of the expansion. Third and final, using the one-to-one correspondence between solutions of the unconstrained edge balance equations and synchronized solutions of the Kuramoto model, we propose a power series expansion for the synchronized solutions of the Kuramoto model and an estimate on the region of convergence of the power series.

From a computational viewpoint, first, we propose a method to approximate the synchronization manifold of the Kuramoto model using the truncated power series. We present several numerical experiments using IEEE test cases and random graphs to illustrate (1) the accuracy of the truncated series and (2) the computational efficiency of the new methods for computing the synchronization manifold. We show that the seventh order approximate method has low absolute error when applied to IEEE test cases with weakly coupled oscillators. The truncated series, up to the seventh order, have comparable computational efficiency to Newton–Raphson when computing the synchronized solutions of the Kuramoto model for multiple natural frequencies over a given static graph. Second, based on our novel power series approach, we propose a hierarchy of approximate tests for synchronization of the Kuramoto model; our approach provides a

theoretical basis for and generalize the state-of-the-art approximate synchronization test in the literature [15]. With numerical analysis, we verify the accuracy of our family of approximate tests for several random graphs and numerous IEEE test cases. In each of these cases, we show that our new approximate tests are a significant improvement compared to the best-known approximate condition given in [15].

Finally, we compare this chapter with our preliminary conference article [25]. In short, this chapter presents a substantially more complete and comprehensive treatment of the power series approach to synchronization of Kuramoto oscillators. Specifically, while [25] presents a power series expansion for nodal phase angles, this chapter develops a novel power series expansion for the flows in the network. Using the Banach Fixed-Point Theorem, we provide an estimate on the domain of convergence of the power series which is substantially larger than the estimates given in [25]. Moreover, our numerical analysis shows that the hierarchy of approximate synchronization tests obtained by truncating this power series is more accurate than the estimate tests proposed in [25].

Chapter organization

In Section 1.2, we give preliminaries and notation used in the chapter. In Section 1.3-1.4 we review the Kuramoto model, frequency synchronization, and give several equivalent formulations of the algebraic Kuramoto equation. Sections 1.5 and 1.6 contain the chapter's main theoretical results and a family of approximate synchronization tests. Finally, Section 1.7 contains numerical experiments analyzing the approximate synchronization tests and efficiency of computation methods for the synchronization manifold.

1.2 Preliminaries and notation

Vectors and functions

Let $\mathbb{Z}_{\geq 0}$, $\mathbb{R}^n$, and $\mathbb{C}^n$ denote the set of non-negative integers, the n-dimensional real Euclidean space, and the n-dimensional complex Euclidean space, respectively. For $n \in \mathbb{Z}_{\geq 0}$, let $n! = \prod_{k=0}^{n}(n-k)$ denote the factorial and $n!! = \prod_{k=0}^{\lceil \frac{n}{2} \rceil - 1}(n-2k)$ denote the double factorial. For $r > 0$ and $\mathbf{x} \in \mathbb{R}^n$, the real polydisk with center $\mathbf{x}$ and radius r is

$$\mathrm{D}_n(\mathbf{x}, r) = \{\mathbf{y} \in \mathbb{R}^n \mid \|\mathbf{x} - \mathbf{y}\|_\infty \leq r\}.$$

Similarly, for $r > 0$ and $\mathbf{z} \in \mathbb{C}^n$, the complex polydisk with center $\mathbf{z}$ and radius r is

$$\mathrm{D}_n^{\mathbb{C}}(\mathbf{z}, r) = \{\mathbf{w} \in \mathbb{C}^n \mid \|\mathbf{z} - \mathbf{w}\|_\infty \leq r\}.$$

Let $\mathbb{1}_n$ and $\mathbb{0}_n$ be n-dimensional column vectors of ones and zeros respectively. The orthogonal complement of $\mathbb{1}_n$ in $\mathbb{R}^n$ is denoted by $\mathbb{1}_n^\perp$. For $\mathbf{x} = (x_1, \ldots, x_n)^\top \in \mathbb{C}^n$, let $\sin(\mathbf{x}) = (\sin(x_1), \ldots, \sin(x_n))^\top$ and $\mathrm{diag}(\mathbf{x})$ be the $n \times n$ diagonal matrix with $(\mathrm{diag}(\mathbf{x}))_{ii} = x_i$, for every $i \in \{1, \ldots, n\}$. For $\mathbf{x} = (x_1, \ldots, x_n)^\top \in \mathbb{C}^n$ with $\|\mathbf{x}\|_\infty \leq 1$, let $\arcsin(\mathbf{x}) = (\arcsin(x_1), \ldots, \arcsin(x_n))^\top$, where

$$\arcsin(r) = \sum_{i=0}^{\infty} \frac{(2i-1)!!}{(2i)!!(2i+1)} r^{2i+1}.$$

Let $\mathbf{x}, \mathbf{y} \in \mathbb{C}^n$ be two vectors and $m \in \mathbb{Z}_{\geq 0}$. Then the Hadamard product $\mathbf{x} \circ \mathbf{y} \in \mathbb{C}^n$ is defined by $(\mathbf{x} \circ \mathbf{y})_i = x_i y_i$, for every $i \in \{1, \ldots, n\}$ and the Hadamard power $\mathbf{x}^{\circ m} \in \mathbb{C}^n$ is defined by $(\mathbf{x}^{\circ m})_i = (x_i)^m$, for every $i \in \{1, \ldots, n\}$. For every matrix $A \in \mathbb{R}^{n \times n}$, kernel and image of A in the real vector space $\mathbb{R}^n$ are denoted by $\mathbb{N}(A)$ and $\mathbb{R}(A)$, respectively and kernel and image of A in the complex vector space $\mathbb{C}^n$ are denoted by $\mathbb{N}_{\mathbb{C}}(A)$ and

$\mathbb{R}_{\mathbb{C}}(A)$, respectively. For every vector $v \in \mathbb{R}^n$, the real vector space spanned by v is denoted by $\mathrm{span}(v)$ and the complex vector space spanned by v is denoted by $\mathrm{span}_{\mathbb{C}}(v)$. For every $n \in \mathbb{N}$, we denote the n-torus by $\mathbb{T}^n$. For every $s \in [0, 2\pi)$, the clockwise rotation of $\theta \in \mathbb{T}^n$ by the angle s is the function $\mathrm{rot}_s : \mathbb{T}^n \to \mathbb{T}^n$ defined by

$$\mathrm{rot}_s(\theta) = (\theta_1 + s, \ldots, \theta_n + s)^\top, \qquad \text{for } \theta \in \mathbb{T}^n.$$

Using the rotation function, one defines an equivalence relation $\sim$ on the n-torus $\mathbb{T}^n$ as follows: For every two points $\theta, \eta \in \mathbb{T}^n$, we say $\theta \sim \eta$ if there exists $s \in [0, 2\pi)$ such that $\theta = \mathrm{rot}_s(\eta)$. For every $\theta \in \mathbb{T}^n$, the equivalence class of θ is denoted by $[\theta] = \{\mathrm{rot}_s(\theta) \mid s \in [0, 2\pi)\}$. The quotient space of $\mathbb{T}^n$ under the equivalence relation $\sim$ is denoted by $[\mathbb{T}^n]$.

Algebraic graph theory

Let G be a weighted undirected connected graph with the node set $\mathcal{N} = \{1, \ldots, n\}$ and the edge set $\mathcal{E} \subseteq \mathcal{N} \times \mathcal{N}$ with m elements. We assume that G has no self-loops and the weights of the edges are described by the nonnegative, symmetric adjacency matrix $A \in \mathbb{R}^{n \times n}$. The Laplacian matrix of the graph G is $L = \mathrm{diag}(A\mathbb{1}_n) - A \in \mathbb{R}^{n \times n}$. For an arbitrary enumeration and orientation of edges of G, the incidence matrix $B \in \mathbb{R}^{m \times n}$ of the graph G is defined by

$$B_{ie} = \begin{cases} +1, & \text{if node } i \text{ is the source of edge } e, \\ -1, & \text{if node } i \text{ is the sink of edge } e, \\ 0, & \text{otherwise.} \end{cases}$$

Define the diagonal edge weight matrix by $\mathcal{A} = \operatorname{diag}(a_{ij})_{(i,j)\in\mathcal{E}} \in \mathbb{R}^{m\times m}$. It is known that the Laplacian is $L = B\mathcal{A}B^\top$. Since L is singular, we use the Moore–Penrose pseudoinverse $L^\dagger$ which has the following properties: $LL^\dagger L = L$, $L^\dagger LL^\dagger = L^\dagger$, $L^\dagger L = (L^\dagger L)^\top$, and $LL^\dagger = (LL^\dagger)^\top$. In addition, for a connected graph $L^\dagger L = LL^\dagger = I_n - \frac{1}{n}\mathbb{1}_n^\top \mathbb{1}_n$. The *weighted cutset projection matrix* $\mathcal{P}_{\text{cut}}$ is the oblique projection onto $\mathbb{R}(B^\top)$ parallel to $\mathbb{N}(B\mathcal{A})$ given by

$$\mathcal{P}_{\text{cut}} = B^\top L^\dagger B\mathcal{A}.$$

The weighted cutset projection matrix $\mathcal{P}_{\text{cut}}$ is idempotent, and 0 and 1 are its eigenvalues with algebraic (and geometric) multiplicity $m-n+1$ and $n-1$, respectively. Additional properties of $\mathcal{P}_{\text{cut}}$ are in [21, Theorem 5]. Similarly, the *weighted cycle projection matrix* $\mathcal{P}_{\text{cyc}}$ is the oblique projection onto $\mathbb{N}(B\mathcal{A})$ parallel to $\mathbb{R}(B^\top)$ given by

$$\mathcal{P}_{\text{cyc}} = I_m - B^\top L^\dagger B\mathcal{A}.$$

Analytic functions and power series

A multi-index ν is a member of $(\mathbb{Z}_{\geq 0})^n$. For every $x \in \mathbb{C}^n$, we define $x^\nu = x_1^{\nu_1} x_2^{\nu_2} \dots x_n^{\nu_n}$. For $x_0 \in \mathbb{C}^n$, the formal expression

$$\sum_{\nu\in\left(\mathbb{Z}_{\geq 0}\right)^n} a_\nu (x - x_0)^\nu, \tag{1.1}$$

where $a_\nu \in \mathbb{C}$, for every $\nu \in (\mathbb{Z}_{\geq 0})^n$ is called a formal power series around point x_0. The power series $\sum_{\nu\in\left(\mathbb{Z}_{\geq 0}\right)^n} a_\nu (x - x_0)^\nu$ *converges strongly* at point x if all rearrangement of the terms of the series $\sum_\nu a_\nu (x - x_0)^\nu$ converges. For every $x_0 \in \mathbb{C}^n$, the *domain of convergence of* (1.1) around x_0 is defined as the set $\mathcal{C}_{x_0}$ of all points $x \in \mathbb{C}^n$ such that

the power series $\sum_\nu a_\nu (x - x_0)^\nu$ converges strongly at point x. While for $n = 1$, one can show that the domain of convergence is an open interval around x_0, for $n > 1$ the domain of convergence of a power series is not necessarily an open poly-disk around x_0. An open set $\Omega \subset \mathbb{C}^n$ is a *Reinhardt domain* if, for every $\begin{pmatrix} z_1, \ldots, z_n \end{pmatrix}^\top \in \Omega$ and every $\begin{pmatrix} \theta_1, \ldots, \theta_n \end{pmatrix}^\top \in \mathbb{T}^n$, we have $\begin{pmatrix} e^{i\theta_1} z_1, \ldots, e^{i\theta_n} z_n \end{pmatrix}^\top \in \Omega$. The Reinhardt domains can be considered as the generalization of the disks on the complex plane to higher dimensions. For every $x \in \mathbb{C}$ satisfying $\|x\| < 1$, we have

$$\frac{1}{(1-x)^n} = \sum_{i=1}^{\infty} \tfrac{(n+i)!}{i!n!} x^i. \tag{1.2}$$

For $N \in \mathbb{Z}_{\geq 0}$, the Nth remainder of the power series (1.2) is the function $\mathrm{Rem}_N^n : [0, 1) \to \mathbb{R}$ given by

$$\mathrm{Rem}_N^n(x) = \sum_{i=N+1}^{\infty} \frac{(n+i)!}{i!n!} x^i. \tag{1.3}$$

1.3 The heterogeneous Kuramoto model

The Kuramoto model is a system of n oscillators, where each oscillator has a natural frequency $\omega_i \in \mathbb{R}$ and its state is represented by a phase angle $\theta_i \in \mathbb{S}^1$. The interconnection of these oscillators are described using a weighted undirected connected graph G, with nodes $\mathcal{N} = \{1, \ldots, n\}$, edges $\mathcal{E} \subseteq \mathcal{N} \times \mathcal{N}$, and positive weights $a_{ij} = a_{ji} > 0$. The dynamics for the heterogeneous Kuramoto model is given by:

$$\dot{\theta}_i = \omega_i - \sum_{j=1}^{n} a_{ij} \sin(\theta_i - \theta_j), \qquad \text{for } i \in \{1, \ldots, n\}. \tag{1.4}$$

In matrix language, one can write this differential equations as:

$$\dot{\theta} = \omega - B\mathcal{A}\sin(B^\top\theta), \tag{1.5}$$

where $\theta = (\theta_1, \theta_2, \ldots, \theta_n)^\top \in \mathbb{T}^n$ is the phase vector, $\omega = (\omega_1, \omega_2, \ldots, \omega_n)^\top \in \mathbb{R}^n$ is the natural frequency vector, and B is the incidence matrix for the graph G. One can show that if $\theta : \mathbb{R}_{\geq 0} \to \mathbb{T}^n$ is a solution for the Kuramoto model (1.5) then, for every $s \in [0, 2\pi)$, the curve $\mathrm{rot}_s(\theta) : \mathbb{R}_{\geq 0} \to \mathbb{T}^n$ is also a solution of (1.5). Therefore, for the rest of this chapter, we consider the state space of the Kuramoto model (1.5) to be $[\mathbb{T}^n]$.

Definition 1 (**Frequency synchronization**). *A solution $\theta : \mathbb{R}_{\geq 0} \to [\mathbb{T}^n]$ of the coupled oscillator model* (1.5) *achieves* frequency synchronization *if there exists a frequency $\omega_{\mathrm{syn}} \in \mathbb{R}$ such that*

$$\lim_{t\to\infty} \dot{\theta}(t) = \omega_{\mathrm{syn}}\mathbb{1}_n.$$

By summing all the equations in (1.4), one can show that if a solution of (1.5) achieves frequency synchronization then $\omega_{\mathrm{syn}} = \frac{1}{n}\sum_{i=1}^n \omega_i$. Therefore, without loss of generality, we can assume that for the Kuramoto model (1.5), we have $\omega \in \mathbb{1}_n^\perp$ and $\omega_{\mathrm{syn}} = 0$.

Definition 2 (**Synchronization manifold**). *Let θ^* be a solution of the algebraic equation*

$$\omega = B\mathcal{A}\sin(B^\top\theta^*). \tag{1.6}$$

Then $[\theta^*]$ is called a synchronization manifold *for the Kuramoto model* (1.5).

The following theorem reduces the problem of local frequency synchronization in the Kuramoto model (1.5) to the existence of a solution for the algebraic equations (1.6).

Theorem 3 (**Characterization of frequency synchronization**). *For the heterogeneous Kuramoto model* (1.5) *on graph G, the following statements are equivalent:*

1. *there exists an open set* $U \in [\mathbb{T}^n]$ *such that every solution of the Kuramoto model* (1.5) *starting in set* U *achieves frequency synchronization;*

2. *there exists a locally asymptotically stable synchronization manifold* $[\theta^*]$ *for* (1.5).

Additionally, if any of equivalent conditions 1 or 2 holds, then, for every $\theta(0) \in U$*, we have* $\lim_{t\to\infty}[\theta(t)] = [\theta^*]$.

Proof. Regarding 1 $\implies$ 2, if the solution achieves frequency synchronization, then $\lim_{t\to\infty} \dot{\theta}_i(t) = 0 = \lim_{t\to\infty} \left(\omega_i - \sum_{j=1}^n a_{ij} \sin(\theta_i(t) - \theta_j(t))\right)$ for all $i = \{1, ..., n\}$. Consider a sequence of natural numbers $k \in \mathbb{N}$ and the corresponding sequence $\theta(k)$ in $\mathbb{T}^n$. Since $\mathbb{T}^n$ is a compact metric space, it is sequentially compact [40, Theorem 28.2]. This means that there is a subsequence $\hat{k}$ such that $\theta(\hat{k})$ is convergent. Then $\lim_{\hat{k}\to\infty} \theta(\hat{k})$ exists and $\mathbb{0}_n = \omega - B\mathcal{A}\sin(B^\top \lim_{\hat{k}\to\infty} \theta(\hat{k}))$. Therefore $\lim_{\hat{k}\to\infty} \theta(\hat{k})$ is a synchronization manifold because it is a solution for equation (1.6) and is locally asymptotically stable since all solutions starting in U reach $\lim_{\hat{k}\to\infty} \theta(\hat{k})$.

Regarding 2 $\implies$ 1, by the definition of local asymptotic stability, there exists some $\delta > 0$ such that the open set U is defined to be $U = \{\theta(0) \in [\mathbb{T}^n] \mid \|\theta(0) - \theta^*\| \leq \delta\}$ where $[\theta^*]$ is the synchronization manifold. Then for solutions starting in U, $\lim_{t\to\infty} \dot{\theta}(t) = \omega - B\mathcal{A}\sin(B^\top\theta^*) = 0$ so $[\theta^*]$ is also a frequency synchronized solution for (1.5).

The last statement follows from the proofs of 1 $\implies$ 2 and 2 $\implies$ 1. □

In many application, such as power networks, not only it is important to study the frequency synchronization of the Kuramoto oscillators but also it is essential to bound the position of the synchronization manifold $[\theta^*]$ due to some security constraints for the grid. An important class of security constraints is thermal constraint which is usually expressed as bounds on the geodesic distances $|\theta_i^* - \theta_j^*|$, for $i, j \in \{1, \ldots, n\}$. The geodesic distance $|\theta_i^* - \theta_j^*|$ is defined as the minimum of the clockwise and counterclockwise arc

lengths between the phase angles $\theta_i^*, \theta_j^* \in \mathbb{S}^1$. Let G be an undirected weighted connected graph with edge set $\mathcal{E}$ and let $\gamma \in [0, \pi)$. We define the cohesive subset $\Delta^G(\gamma) \subseteq [\mathbb{T}^n]$ by

$$\Delta^G(\gamma) = \{[\theta] \in [\mathbb{T}^n] \mid |\theta_i - \theta_j| \leq \gamma, \text{for all } (i,j) \in \mathcal{E}\}.$$

For every $\gamma \in [0, \pi)$, we define the *embedded cohesive subset* $S^G(\gamma) \subseteq [\mathbb{T}^n]$ by

$$S^G(\gamma) = \{[\exp(\mathrm{i}\mathbf{x})] \mid \mathbf{x} \in B^G(\gamma), s \in [0, 2\pi)\},$$

where $B^G(\gamma) = \{\mathbf{x} \in \mathbb{1}_n^\perp \mid \left\|B^\top \mathbf{x}\right\|_\infty \leq \gamma\}$. Note that, in general, we have $S^G(\gamma) \subseteq \Delta^G(\gamma)$. We refer to [21] for additional properties of embedded cohesive subset. In particular, it is shown that $S^G(\gamma)$ is diffeomorphic with $B^G(\gamma)$, for every $\gamma \in [0, \frac{\pi}{2})$ [21, Theorem 8]. Using this result, in the rest of this chapter we identify the set $S^G(\gamma)$ with $B^G(\gamma)$.

1.4 Equivalent transcriptions of the equilibrium manifold

Consider an undirected graph G with vertex set $\mathcal{N} = \{1, \ldots, n\}$ and edge set $\mathcal{E} \subseteq \mathcal{N} \times \mathcal{N}$ with $|\mathcal{E}| = m$. We start by introducing three vector spaces defined by G:

1. the *node space* is $\mathbb{R}^n$; elements of this space are called *node vectors*;
2. the *edge space* is $\mathbb{R}^m$; elements of this space are called *edge vectors*; and
3. the *flow vector space* is $\mathbb{R}(B^\top)$; elements of $\mathbb{R}^m$ belonging to this space are called by *flow vectors*.

It is easy to see that an edge vector $\mathbf{z} \in \mathbb{R}^m$ is a flow vector if and only if there exists a node vector $\mathbf{x} \in \mathbb{R}^n$ such that $\mathbf{z} = B^\top \mathbf{x}$.

Next, we introduce four different balance equations on an undirected graph G with incidence matrix B, weight matrix $\mathcal{A}$, cutset projection $\mathcal{P}_{\text{cut}}$, and cycle projection $\mathcal{P}_{\text{cyc}}$. Given a node vector $\omega \in \mathbb{1}_n^\perp$, define the shorthand flow vector $\eta = B^\top L^\dagger \omega \in \mathbb{R}(B^\top)$. The *node balance equation* in the unknown node vector $\mathbf{x} \in \mathbb{1}_n^\perp$ is

$$\omega = B\mathcal{A}\sin(B^\top \mathbf{x}). \tag{1.7}$$

The *flow balance equation* in the unknown flow vector $\mathbf{z} \in \mathbb{R}(B^\top)$ is

$$\eta = \mathcal{P}_{\text{cut}} \sin(\mathbf{z}). \tag{1.8}$$

The *constrained edge balance equation* in the unknown edge vector $\psi \in \mathbb{R}^m$ is

$$\begin{cases} \eta = \mathcal{P}_{\text{cut}} \psi, \\ \arcsin(\psi) \in \mathbb{R}(B^\top), \quad \|\psi\|_\infty \leq 1. \end{cases} \tag{1.9}$$

The *unconstrained edge balance equation* in the unknown edge vector $\phi \in \mathbb{R}^m$ is

$$\eta = \mathcal{P}_{\text{cut}} \phi + \mathcal{P}_{\text{cyc}} \arcsin(\phi), \quad \|\phi\|_\infty \leq 1. \tag{1.10}$$

We now present equivalent characterizations for synchronization manifold of the Kuramoto model (1.5).

Theorem 4 (**Characterization of synchronization manifold**). *Consider an undirected connected graph G with incidence matrix B, weight matrix $\mathcal{A}$, cutset projection $\mathcal{P}_{\text{cut}}$, and cycle projection $\mathcal{P}_{\text{cyc}}$. Given a node vector $\omega \in \mathbb{1}_n^\perp$, define the shorthand*

$\eta = B^\top L^\dagger \omega \in \mathbb{R}(B^\top)$. *Pick an angle* $\gamma \in [0, \frac{\pi}{2})$. *Then the following statements are equivalent:*

1. *there exists a unique locally exponentially stable synchronization manifold* $\mathbf{x}^*$ *for the Kuramoto model* (1.5) *in* $S^G(\gamma)$*;*
2. *the node balance equation* (1.7) *has a unique solution* $\mathbf{x}^*$ *in* $S^G(\gamma)$*;*
3. *the flow balance equation* (1.8) *has a unique solution* $\mathbf{z}^* \in \mathbb{R}(B^\top)$ *with* $\|\mathbf{z}^*\|_\infty \leq \gamma$*;*
4. *the constrained edge balance equation* (1.9) *has a unique solution* $\psi^* \in \mathbb{R}^m$ *with* $\|\psi^*\|_\infty \leq \sin(\gamma)$*;*
5. *the unconstrained edge balance equation* (1.10) *has a unique solution* $\phi^* \in \mathbb{R}^m$ *with* $\|\phi^*\|_\infty \leq \sin(\gamma)$.

Moreover, if one of the above equivalent conditions hold, then

$$\mathbf{z}^* = B^\top \mathbf{x}^*, \quad \textit{and} \quad \psi^* = \phi^* = \sin(B^\top \mathbf{x}^*).$$

Proof. The implications 1 $\implies$ 2 and 2 $\implies$ 3 are easy to show.

Regarding 3 $\implies$ 4, if $\mathbf{z}^* \in \mathbb{R}(B^\top)$ is the unique solution to the flow balance equation (1.8), then $\phi^* = \sin(\mathbf{z}^*) \in \mathbb{R}^m$ satisfies $\|\phi^*\|_\infty \leq \sin(\gamma)$ and is a solution for the edge balance equation (1.9). Now, we show that ϕ^* is the unique solution for the constrained edge balance equation (1.9) such that $\|\phi^*\|_\infty \leq \sin(\gamma)$. Suppose that $\eta^* \neq \phi^*$ is another solution of the constrained edge balance equation (1.9) satisfying $\|\eta^*\|_\infty \leq \sin(\gamma)$. Then, by the constrained edge balance equation (1.9), there exists $\mathbf{y}^* \in \mathbb{R}(B^\top)$ such that $\mathbf{y}^* \neq \mathbf{z}^*$ and $\arcsin(\eta^*) = \mathbf{z}^*$. This implies that $\|\mathbf{y}^*\| \leq \gamma$ and $\mathcal{P}_{\text{cut}} \sin(\mathbf{y}^*) = B^\top L^\dagger \omega$. Therefore, $\mathbf{y}^* \in S^G(\gamma)$ and satisfies the flow balance equation (1.8). However,

this is in contradiction with the facts that $\mathbf{y}^* \neq \mathbf{z}^*$ and that $\mathbf{z}^* \in \mathbb{R}(B^\top)$ is the unique solution of the flow balance equation (1.8).

Regarding 4 $\implies$ 5, if $\psi^* \in \mathbb{R}^m$ is a solution of constrained edge balance equation (1.9) satisfying $\|\psi^*\|_\infty \leq \sin(\gamma)$, then

$$B^\top L^\dagger \omega = \mathcal{P}_{\text{cut}} \psi^*, \tag{1.11}$$

$$\arcsin(\psi^*) \in \mathbb{R}(B^\top). \tag{1.12}$$

Because $\mathbb{N}(\mathcal{P}_{\text{cyc}}) = \mathbb{R}(B^\top)$, the inclusion (1.12) implies that

$$\mathcal{P}_{\text{cyc}} \arcsin(\psi^*) = 0. \tag{1.13}$$

By adding equations (1.11) and (1.13), we obtain $B^\top L^\dagger \omega = \mathcal{P}_{\text{cut}} \psi^* + \mathcal{P}_{\text{cyc}} \arcsin(\psi^*)$. This means that ψ^* satisfies unconstrained edge balance equation (1.10).

Regarding 5 $\implies$ 1, if $\phi^* \in \mathbb{R}^m$ solves the unconstrained edge balance equation (1.10), then

$$B^\top L^\dagger \omega = \mathcal{P}_{\text{cut}} \phi^* + \mathcal{P}_{\text{cyc}} \arcsin(\phi^*). \tag{1.14}$$

Left-multiplying both sides of equation (1.14) by $\mathcal{P}_{\text{cut}}$ and using the facts that $\mathcal{P}_{\text{cut}} B^\top = B^\top$, $\mathcal{P}_{\text{cut}} \mathcal{P}_{\text{cut}} = \mathcal{P}_{\text{cut}}$ and $\mathcal{P}_{\text{cut}} \mathcal{P}_{\text{cyc}} = \mathbb{0}_{m \times m}$, we obtain

$$B^\top L^\dagger \omega = \mathcal{P}_{\text{cut}} \phi^*.$$

Left-multiplying both side of the equation (1.14) by $\mathcal{P}_{\text{cyc}}$ we obtain

$$\mathcal{P}_{\text{cyc}} \arcsin(\phi^*) = \mathbb{0}_m.$$

This last equality implies that $\arcsin(\phi^*) \in \mathbb{N}(\mathcal{P}_{\text{cyc}}) = \mathbb{R}(B^\top)$. Thus, there exists a vector $\mathbf{x}^* \in \mathbb{1}_n^\perp$ such that $\arcsin(\phi^*) = B^\top \mathbf{x}^*$. First, note that $\mathcal{P}_{\text{cut}} \sin(B^\top \mathbf{x}^*) = B^\top L^\dagger \omega$ and, by multiplying both side of this equation by $B\mathcal{A}$, we obtain

$$\omega = B\mathcal{A} \sin(B^\top \mathbf{x}^*).$$

Moreover, $\|\phi^*\|_\infty \leq \gamma$. Thus, we have $\|\arcsin(\phi^*)\|_\infty \leq \gamma$ and $\|B^\top \mathbf{x}^*\|_\infty \leq \gamma$. This implies that $\mathbf{x}^* \in \mathbb{1}_n^\perp$ is a synchronization manifold for the Kuramoto model (1.5) in $S^G(\gamma)$. The uniqueness follows from [21, Theorem 10, statement (ii)]. □

1.5 Solvability of the unconstrained edge balance equations

The unconstrained edge balance equation (1.10) allows us to focus on a single analytic map whose inverse can be used in computing the synchronization solutions of Kuramoto model. In this section, we study the solvability of these equations and find their inverse on a suitable domain. We start with relaxing the condition $\eta \in \mathbb{R}(B^\top)$ and complexifing the equation (1.10). This extension will allow us to use the theory of several complex variables to find the Taylor series expansion for the inversion of the complexified equation and prove the strong convergence of the Taylor series. We then restrict back to real domain and use the constraint $\eta \in \mathbb{R}(B^\top)$ to find the solutions of the unconstrained edge balance equations (1.10). We start with some useful definitions. Given an undirected graph G with cutset projection $\mathcal{P}_{\text{cut}}$ and cycle projection $\mathcal{P}_{\text{cyc}}$, and a phase angle $\gamma \in [0, \pi/2]$, define the *complex edge balance map* $\mathcal{F}_{\mathbb{C}} : \mathrm{D}^{\mathbb{C}}(\mathbb{0}_m, \sin(\gamma)) \to \mathbb{C}^m$ by

$$\mathcal{F}_{\mathbb{C}}(\phi) = \mathcal{P}_{\text{cut}}\phi + \mathcal{P}_{\text{cyc}} \arcsin(\phi)$$

and the *real edge balance map* $\mathcal{F} : \mathrm{D}(\mathbb{0}_m, \sin(\gamma)) \to \mathbb{R}^m$ by

$$\mathcal{F}(\phi) = \mathcal{P}_{\mathrm{cut}}\phi + \mathcal{P}_{\mathrm{cyc}} \arcsin(\phi).$$

With this notation, the unconstrained edge balance equation (1.10) reads $\eta = \mathcal{F}(\phi)$, together with the constraint $\|\phi\|_\infty \leq 1$. Next, we define the scalar function $h : \mathbb{R}_{\geq 0} \to \mathbb{R}$ by:

$$h(x) = (x+1)\sqrt{1 - \left(\frac{x}{x+1}\right)^2} - x \arccos\left(\frac{x}{x+1}\right).$$

The graph of function h on the interval $[0, 30]$ is shown in Figure (1.1). Since h is

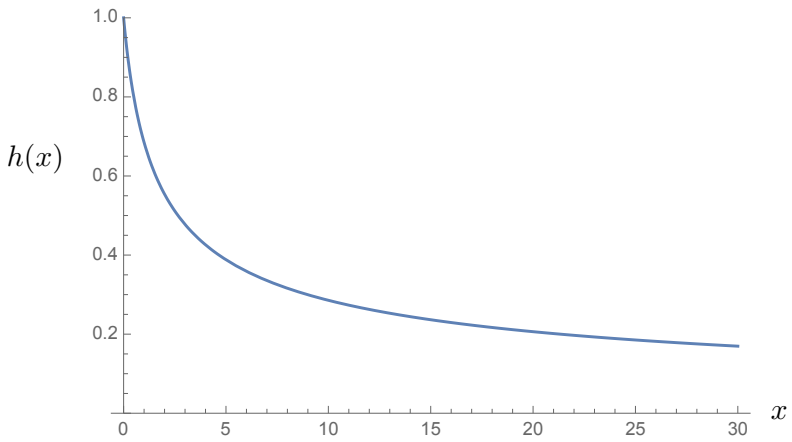

Figure 1.1: The graph of the monotonically-decreasing function h

continuous and strictly monotonically-decreasing, its inverse exists and is denoted by $h^{-1} : \mathbb{R} \to \mathbb{R}_{\geq 0}$. Although we do not have an analytical form for $h^{-1}(y)$, it is simple to compute it numerically.

We are now ready to provide estimates on the image of the maps $\mathcal{F}_{\mathbb{C}}$ and $\mathcal{F}$ and to present power series expansions for the inverse maps $\mathcal{F}_{\mathbb{C}}^{-1}$ and $\mathcal{F}^{-1}$ on suitable domains.

Theorem 5 (Properties of the complex edge balance map). *Consider an undi-*

rected connected graph G with cutset projection $\mathcal{P}_{\mathrm{cut}}$ and cycle projection $\mathcal{P}_{\mathrm{cyc}}$. Select $\eta \in \mathbb{R}^m$ such that $\|\eta\|_\infty < h(\|\mathcal{P}_{\mathrm{cyc}}\|_\infty)$ and define $\gamma^* \in [0, \frac{\pi}{2})$ by

$$\gamma^* = \arccos\left(\frac{h^{-1}(\|\eta\|_\infty)}{h^{-1}(\|\eta\|_\infty)+1}\right).$$

Then the following statements holds:

1. *there exists a unique $\phi^* \in \mathrm{D}^{\mathbb{C}}(\mathbb{0}_m, \sin(\gamma^*))$ such that $\mathcal{F}_{\mathbb{C}}(\phi^*) = \eta$; that is unconstrained edge balance equation has a unique solution;*

2. *there exists a holomorphic map $\mathcal{F}_{\mathbb{C}}^{-1} : \mathrm{D}^{\mathbb{C}}(\mathbb{0}_m, \|\eta\|_\infty) \to \mathcal{F}_{\mathbb{C}}^{-1}(\mathrm{D}^{\mathbb{C}}(\mathbb{0}_m, \|\eta\|_\infty))$ such that*

$$\begin{aligned} &\mathcal{F}_{\mathbb{C}}^{-1} \circ \mathcal{F}_{\mathbb{C}}(\phi) = \phi, && \text{for all } \phi \in \mathcal{F}_{\mathbb{C}}^{-1}(\mathrm{D}^{\mathbb{C}}(\mathbb{0}_m, \|\eta\|_\infty)), \\ &\mathcal{F}_{\mathbb{C}} \circ \mathcal{F}_{\mathbb{C}}^{-1}(\xi) = \xi, && \text{for all } \xi \in \mathrm{D}^{\mathbb{C}}(\mathbb{0}_m, \|\eta\|_\infty); \end{aligned}$$

   that is the edge balance map is invertible on $\mathrm{D}^{\mathbb{C}}(\mathbb{0}_m, \|\eta\|_\infty)$;

3. *the power series*

$$\sum_{i=0}^{\infty} A_{2i+1}(\eta) = A_1(\eta) + A_3(\eta) + A_5(\eta) + \dots,$$

   converges strongly to $\mathcal{F}_{\mathbb{C}}^{-1}(\eta)$, where, for every $i \in \mathbb{Z}_{\geq 0}$, the term $A_i(\eta)$ is a homogeneous polynomial of order i in η defined iteratively by:

$$\begin{aligned} &A_1(\eta) = \eta, \\ &A_{2i+1}(\eta) = -\mathcal{P}_{\mathrm{cyc}}\left(\sum_{k=1}^{i} \frac{(2k-1)!!}{(2k)!!(2k+1)} \sum_{\substack{odd\ \alpha_1,\dots,\alpha_{2k+1}\ s.t. \\ \alpha_1+\dots+\alpha_{2k+1}=2i+1}} A_{\alpha_1}(\eta) \odot \dots \odot A_{\alpha_{2k+1}}(\eta)\right). \end{aligned}$$

4. for every $m \geq 1$,

$$\left\| \mathcal{F}_{\mathbb{C}}^{-1}(\eta) - \sum_{i=1}^{m} A_{2i+1}(\eta) \right\|_{\infty} \leq \sin(\gamma^*) \mathrm{Rem}_{2m+1}^{n} \left(\tfrac{\|\eta\|_{\infty}}{h(\|\mathcal{P}_{\mathrm{cyc}}\|_{\infty})} \right),$$

where Rem_{2m+1}^{n} *is the* $(2m+1)$*th remainder function given by* (1.3).

Proof. Regarding statement 1, define the map $H_\eta : \mathrm{D}^{\mathbb{C}}(\mathbb{0}_m, \sin(\gamma^*)) \to \mathbb{R}^m$ by

$$H_\eta(\phi) = \eta - \mathcal{P}_{\mathrm{cyc}}(\arcsin(\phi) - \phi).$$

Considering equation (1.10), it is clear that the fixed points of the map H_η are the solutions of the unconstrained edge equation (1.10). Therefore, to prove 1, it suffices to show that the map H_η has a fixed point $\phi^* \in \mathrm{D}^{\mathbb{C}}(\mathbb{0}_m, \sin(\gamma^*))$. First, we show that $H_\eta(\mathrm{D}^{\mathbb{C}}(\mathbb{0}_m, \sin(\gamma^*))) \subseteq \mathrm{D}^{\mathbb{C}}(\mathbb{0}_m, \sin(\gamma^*))$. For $\phi \in \mathrm{D}^{\mathbb{C}}(\mathbb{0}_m, \sin(\gamma^*))$, we compute

$$\|H_\eta(\phi)\|_\infty = \|\eta - \mathcal{P}_{\mathrm{cyc}}(\arcsin(\phi) - \phi)\|_\infty \leq \|\eta\|_\infty + \|\mathcal{P}_{\mathrm{cyc}}\|_\infty \|\phi - \arcsin(\phi)\|_\infty.$$

Moreover, for $\phi \in \mathrm{D}^{\mathbb{C}}(\mathbb{0}_m, \sin(\gamma^*))$, we have $\|\phi - \arcsin(\phi)\|_\infty \leq \gamma^* - \sin(\gamma^*)$. These equalities imply that

$$\begin{aligned} \|H_\eta(\phi)\|_\infty &\leq \|\eta\|_\infty + \|\mathcal{P}_{\mathrm{cyc}}\|_\infty (\gamma^* - \sin(\gamma^*)) \\ &\leq \|\eta\|_\infty + h^{-1}(\|\eta\|_\infty)(\gamma^* - \sin(\gamma^*)), \end{aligned} \tag{1.15}$$

where, for the last inequality, we used the fact that $\|\mathcal{P}_{\mathrm{cyc}}\|_\infty \leq h^{-1}(\|\eta\|_\infty)$. By the

definition of h, we have

$$\|\eta\|_\infty = (h^{-1}(\|\eta\|_\infty)+1)\sqrt{1-\left(\frac{h^{-1}(\|\eta\|_\infty)}{h^{-1}(\|\eta\|_\infty)+1}\right)} - h^{-1}(\|\eta\|_\infty)\arccos\left(\frac{h^{-1}(\|\eta\|_\infty)}{h^{-1}(\|\eta\|_\infty)+1}\right).$$

Noting the fact that $\arccos\left(\frac{h^{-1}(\|\eta\|_\infty)}{h^{-1}(\|\eta\|_\infty)+1}\right) = \gamma^*$, we obtain

$$\|\eta\|_\infty = (h^{-1}(\|\eta\|_\infty)+1)\sin(\gamma^*) - h^{-1}(\|\eta\|_\infty)\gamma^*.$$

Now, by replacing the above equation into inequality (1.15), we have

$$\begin{aligned}\|H_\eta(\phi)\|_\infty &\le \|\eta\|_\infty + h^{-1}(\|\eta\|_\infty)(\gamma^* - \sin(\gamma^*)) \\ &= (h^{-1}(\|\eta\|_\infty)+1)\sin(\gamma^*) - h^{-1}(\|\eta\|_\infty)\gamma^* + h^{-1}(\|\eta\|_\infty)(\gamma^* - \sin(\gamma^*)) \\ &= \sin(\gamma^*).\end{aligned}$$

Thus, by the Banach Fixed-Point Theorem, there exists a unique fixed point $\phi^* \in \mathrm{D}^{\mathbb{C}}(\mathbb{0}_m, \sin(\gamma^*))$ for H_η. By construction, this fixed point $\phi^* \in \mathrm{D}^{\mathbb{C}}(\mathbb{0}_m, \sin(\gamma^*))$ satisfies

$$\eta = \mathcal{P}_{\mathrm{cyc}}\arcsin(\phi^*) + \mathcal{P}_{\mathrm{cut}}\phi^* = \mathcal{F}_{\mathbb{C}}(\phi^*).$$

This completes the proof of statement 1.

Regarding statement 2, by statement 1, for every $\eta \in \mathbb{C}^m$ such that $\|\eta\|_\infty < h(\|\mathcal{P}_{\mathrm{cyc}}\|_\infty)$, there exists a unique $\phi \in \mathbb{R}^m$ such that $\eta = \mathcal{F}_{\mathbb{C}}(\phi)$. This implies that $\mathcal{F}_{\mathbb{C}}$ has a unique inverse $\mathcal{F}_{\mathbb{C}}^{-1} : \mathcal{F}_{\mathbb{C}}(\mathrm{D}^{\mathbb{C}}(\mathbb{0}_m, \|\eta\|_\infty)) \to \mathrm{D}^{\mathbb{C}}(\mathbb{0}_m, \|\eta\|_\infty)$ which satisfies the equalities in statement 2. Now we show that both $\mathcal{F}_{\mathbb{C}}$ and $\mathcal{F}_{\mathbb{C}}^{-1}$ are holomorphic on their domains. Note that, for every $\phi \in \mathrm{D}^{\mathbb{C}}(\mathbb{0}_m, \|\eta\|_\infty)$, the derivative of the map $\mathcal{F}_{\mathbb{C}}$ at point

ϕ is given by:

$$D_\phi \mathcal{F}_{\mathbb{C}} = \mathcal{P}_{\text{cut}} + \mathcal{P}_{\text{cyc}} \operatorname{diag}\Big(\frac{1}{\sqrt{1-\phi_i^2}}\Big).$$

We start by showing that, for every $\phi \in \mathrm{D}^{\mathbb{C}}(\mathbb{0}_m, \|\eta\|_\infty)$, the map $D_\phi \mathcal{F}_{\mathbb{C}}$ is invertible. Let us fix ϕ. In order to show that $D_\phi \mathcal{F}_{\mathbb{C}}$ is invertible, it suffices to show that $\mathbb{N}_{\mathbb{C}}(D_\phi \mathcal{F}_{\mathbb{C}}) = \{\mathbb{0}_n\}$. Suppose that, there exists $\mathbf{x} \in \mathbb{C}^m$ such that $D_\phi \mathcal{F}_{\mathbb{C}}(\mathbf{x}) = \mathbb{0}_n$. This means that $\mathcal{P}_{\text{cut}}\mathbf{x} = \mathbb{0}_m$ and $\mathcal{P}_{\text{cyc}} \operatorname{diag}\Big(\frac{1}{\sqrt{1-\phi_i^2}}\Big)\mathbf{x} = \mathbb{0}_m$. The first equality implies that $\mathbf{x} \in \mathbb{N}_{\mathbb{C}}(B\mathcal{A})$ and the second inequality implies that $\operatorname{diag}\Big(\frac{1}{\sqrt{1-\phi_i^2}}\Big)\mathbf{x} \in \mathbb{R}_{\mathbb{C}}(B^\top)$. Therefore, there exists $\alpha \in \mathbb{C}^n$ such that $\operatorname{diag}\Big(\frac{1}{\sqrt{1-\phi_i^2}}\Big)\mathbf{x} = B^\top \alpha$. Thus, we get

$$B\mathcal{A} \operatorname{diag}(\sqrt{1-\phi_i^2}) B^\top \alpha = B\mathcal{A}\mathbf{x} = \mathbb{0}_n. \tag{1.16}$$

Moreover, $\mathcal{A} \operatorname{diag}(\sqrt{1-\phi_i^2})$ is a positive definite diagonal matrix. Therefore, equation (1.16) implies that $\alpha \in \operatorname{span}_{\mathbb{C}}\{\mathbb{1}_n\}$ and as a result $\mathbf{x} = \operatorname{diag}(\sqrt{1-\phi_i^2}) B^\top \alpha = \mathbb{0}_n$. This implies that $\mathbb{N}_{\mathbb{C}}(D_\phi \mathcal{F}_{\mathbb{C}}) = \{\mathbb{0}_n\}$. As a result, for every $\phi \in \mathrm{D}^{\mathbb{C}}(\mathbb{0}_m, \|\eta\|_\infty)$, the map $D_\phi \mathcal{F}_{\mathbb{C}}$ is invertible. Now, by the Inverse Function Theorem [41, Theorem 2.5.2], the maps $\mathcal{F}_{\mathbb{C}}$ and $\mathcal{F}_{\mathbb{C}}^{-1}$ are locally holomorphic and therefore they are holomorphic on their domains. This completes the proof of statement 2.

Regarding statement 3, we first find the formal power series representation for $\mathcal{F}_{\mathbb{C}}^{-1}$. Suppose that $\sum_{i=1}^{\infty} A_i(\eta)$ is the formal power series for $\mathcal{F}_{\mathbb{C}}^{-1}$. Then we have

$$\mathcal{P}_{\text{cyc}} \arcsin(\mathcal{F}_{\mathbb{C}}^{-1}(\eta)) + \mathcal{P}_{\text{cut}} \mathcal{F}_{\mathbb{C}}^{-1}(\eta) = \eta, \qquad \text{for all } \eta \in \mathbb{R}^m.$$

By replacing the power series $\sum_{i=1}^{\infty} A_i(\eta)$ for $\mathcal{F}_{\mathbb{C}}^{-1}$ and using the power series expansion

of arcsin, we obtain

$$\mathcal{P}_{\text{cyc}}\left(\sum_{k=1}^{\infty}\frac{(2k-1)!!}{(2k)!!(2k+1)}\big(\sum_{i=1}^{\infty}A_i(\eta)\big)^{\odot(2k-1)}\right)+\mathcal{P}_{\text{cut}}\sum_{i=1}^{\infty}A_i(\eta)=\eta. \tag{1.17}$$

By equating the same order terms on the both side of equation (1.17) and using the fact that $\mathcal{P}_{\text{cyc}}+\mathcal{P}_{\text{cut}}=I_m$, we obtain that $A_1(\eta)=\eta$ and $A_{2i}(\eta)=\mathbb{0}_m$, for every $i\in\mathbb{Z}_{\geq 0}$. Simple book-keeping shows that the recursive formula in statement 3 holds for the odd terms in the power series.

Finally, we prove that the formal power series $\sum_{i=1}^{\infty}A_{2i+1}(\eta)$ converges on the domain $\mathrm{D}^{\mathbb{C}}(\mathbb{0}_m,\eta)$. Note that statement 2 implies that the map $\mathcal{F}_{\mathbb{C}}^{-1}:\mathrm{D}^{\mathbb{C}}(\mathbb{0}_m,\eta)\to\mathcal{F}_{\mathbb{C}}^{-1}(\mathrm{D}^{\mathbb{C}}(\mathbb{0}_m,\eta))$ is holomorphic and and that the set $\mathrm{D}^{\mathbb{C}}(\mathbb{0}_m,\eta)$ is a Reinhardt domain. Therefore, [42, Theorem 2.4.5] implies that the power series converges strongly on the domain $\mathrm{D}^{\mathbb{C}}(\mathbb{0}_m,\eta)$.

Regarding statement 4, define the sets

$$\Omega=\{z\in\mathbb{C}^n\mid\|z\|_\infty<h(\|\mathcal{P}_{\text{cyc}}\|_\infty)\},$$
$$T_\delta=\{t\in\mathbb{C}^n\mid\|t_i\|\leq 1+\delta\}.$$

First note that $\|\eta\|_\infty<h(\|\mathcal{P}_{\text{cyc}}\|_\infty)$ and therefore $\eta\in\Omega$. Moreover, for every $0<\epsilon<\frac{h(\|\mathcal{P}_{\text{cyc}}\|_\infty)}{\|\eta\|_\infty}-1$ and every $t\in T_\epsilon$, we have $(t_1\eta_1,\ldots,t_n\eta_n)\in\Omega$. Note that $\sum_{i=1}^{\infty}A_{2i+1}(\eta)$ is the Taylor series expansion of the holomorphic function $\mathcal{F}_{\mathbb{C}}^{-1}(\eta)$. Therefore, $\mathcal{F}_{\mathbb{C}}^{-1}(\eta)-\sum_{i=1}^{m}A_{2i+1}(\eta)$ is a holomorphic function and its Taylor series only contains terms of order

higher than $2m+1$ in η. Using [43, Theorem 2.2.1 and Theorem 2.4.5], we can compute

$$\mathcal{F}_{\mathbb{C}}^{-1}(\eta) - \sum_{i=1}^{m} A_{2i+1}(\eta) = \sum_{\substack{\alpha_1,\dots,\alpha_n \in \mathbb{Z}_{\geq 0} \text{ s.t.} \\ \alpha_1+\dots+\alpha_n \geq 2m+2}} \left(\frac{1}{2\pi \mathrm{i}}\right)^n \int_{\partial T_\epsilon} \mathcal{F}_{\mathbb{C}}^{-1}(t_1\eta_1,\dots,t_n\eta_n) t_1^{-\alpha_1-1}\dots t_n^{-\alpha_n-1} dt_1\dots dt_n. \quad (1.18)$$

For every $t \in \partial T_\epsilon$ and every $i \in \{1,\dots,n\}$, we know that $\|t_i\| \leq 1+\epsilon$ and $\|\mathcal{F}_{\mathbb{C}}^{-1}(t_1\eta_1,\dots,t_n\eta_n)\|_\infty \leq \sup_{\xi\in\Omega} \|\mathcal{F}_{\mathbb{C}}^{-1}(\xi)\|_\infty$. Therefore, by taking the ∞-norm of both side of equation (1.18), we get

$$\left\| \mathcal{F}_{\mathbb{C}}^{-1}(\eta) - \sum_{i=1}^{m} A_{2i+1}(\eta) \right\|_\infty \leq \left(\frac{1}{2\pi}\right)^n \sup_{\xi\in\Omega} \|\mathcal{F}_{\mathbb{C}}^{-1}(\xi)\|_\infty \sum_{\substack{\alpha_1,\dots,\alpha_n \in \mathbb{Z}_{\geq 0} \text{ s.t.} \\ \alpha_1+\dots+\alpha_n \geq 2m+2}} (1+\epsilon)^{-(\alpha_1+\dots+\alpha_n)-n} \int_{\partial T_\epsilon} dt_1\dots dt_n.$$

Note that by statement 1, for every $\xi \in \Omega$, there exists a unique $\phi^* \in \mathrm{D}^{\mathbb{C}}(\mathbb{0}_m, \sin(\gamma^*))$ such that $\mathcal{F}_{\mathbb{C}}(\phi^*) = \xi$. This implies that, for every $\xi \in \Omega$, we have $\mathcal{F}_{\mathbb{C}}^{-1}(\xi) \in \mathrm{D}^{\mathbb{C}}(\mathbb{0}_m, \sin(\gamma^*))$. Therefore,

$$\sup_{\xi\in\Omega} \|\mathcal{F}_{\mathbb{C}}^{-1}(\xi)\|_\infty \leq \sin(\gamma^*).$$

Moreover, a simple book-keeping shows that

$$\sum_{\substack{\alpha_1,\dots,\alpha_n \in \mathbb{Z}_{\geq 0} \text{ s.t.} \\ \alpha_1+\dots+\alpha_n \geq 2m+2}} (1+\epsilon)^{-(\alpha_1+\dots+\alpha_n)-n} = \sum_{j=2m+2}^{\infty} \tfrac{(n+j)!}{n!j!} (1+\epsilon)^{j-n}.$$

Finally, we can compute the integral $\int_{t\in\partial T_\epsilon} dt_1\dots dt_n = (2\pi)^n(1+\epsilon)^n$. Using all the above

observations, we get

$$\left\| \mathcal{F}_{\mathbb{C}}^{-1}(\eta) - \sum_{i=1}^{m} A_{2i+1}(\eta) \right\|_{\infty} \leq \sin(\gamma^*) \sum_{j=2m+2}^{\infty} \tfrac{(n+j)!}{n!j!}(1+\epsilon)^j. \tag{1.19}$$

Since equation (1.19) holds for every $\epsilon < \frac{h(\|\mathcal{P}_{\mathrm{cyc}}\|_\infty)}{\|\eta\|_\infty} - 1$, we conclude that

$$\left\| \mathcal{F}_{\mathbb{C}}^{-1}(\eta) - \sum_{i=1}^{m} A_{2i+1}(\eta) \right\|_{\infty} \leq \sin(\gamma^*) \mathrm{Rem}_{2m+1}^{n} \left(\frac{\|\eta\|_\infty}{h(\|\mathcal{P}_{\mathrm{cyc}}\|_\infty)} \right).$$

This completes the proof of statement 4. □

Remark 6 (**Properties of the real edge balance map**). *A similar result as Theorem 5 holds for the real edge balance map $\mathcal{F}$ by replacing the complex variables by their real counterparts. The proof is straightforward by restricting the results in Theorem 5 to the real Euclidean space.*

1.6 Inverse Taylor expansion for Kuramoto model

In this section we study the synchronization of the Kuramoto model (1.5) by applying the results on the unconstrained edge balance equation (1.10) from Theorem 5 in the previous section.

Theorem 7 (**Inverse Taylor expansion**). *Consider the Kuramoto model* (1.5) *with undirected connected graph G, weighted cutset projection $\mathcal{P}_{\mathrm{cut}}$, and weighted cycle projection $\mathcal{P}_{\mathrm{cyc}}$. Given frequencies $\omega \in \mathbb{1}_n^{\perp}$ satisfying*

$$\|B^\top L^\dagger \omega\|_\infty < h(\|\mathcal{P}_{\mathrm{cyc}}\|_\infty), \tag{T0}$$

define $\gamma^* \in [0, \frac{\pi}{2})$ *by*

$$\gamma^* = \arccos\left(\frac{h^{-1}(\|B^\top L^\dagger \omega\|_\infty)}{h^{-1}(\|B^\top L^\dagger \omega\|_\infty) + 1}\right).$$

Then the following statements hold:

1. *there exists a unique locally stable synchronization manifold* $\mathbf{x}^*$ *in* $S^G(\gamma^*)$*; and*

2. *the power series*

$$\sum_{i=0}^{\infty} A_{2i+1}(B^\top L^\dagger \omega) = A_1(B^\top L^\dagger \omega) + A_3(B^\top L^\dagger \omega) + \dots, \tag{1.20}$$

   converges strongly to $\sin(B^\top \mathbf{x}^*)$ *where, for every* $i \in \mathbb{Z}_{\geq 0}$*, the term* $A_i(\eta)$ *is a homogeneous polynomial of order* i *in* η *defined iteratively as in Theorem 53.*

3. *for every* $m \geq 1$*,*

$$\left\| \sin(B^\top x^*) - \sum_{i=1}^{m} A_{2i+1}(B^\top L^\dagger \omega) \right\|_\infty \leq \sin(\gamma^*) \mathrm{Rem}_{2m+1}^n \left(\frac{\|B^\top L^\dagger \omega\|}{h(\|\mathcal{P}_{\mathrm{cyc}}\|_\infty)}\right),$$

   where Rem_{2m+1}^n *is the* $(2m+1)$*th remainder function given by* (1.3)*.*

This theorem is an immediate application of Theorem 4 on the equivalent transcriptions and of Theorem 5 on the properties of the maps $\mathcal{F}_{\mathbb{C}}$ and $\mathcal{F}$.

Proof of Theorem 7. Regarding statement 1, we use (the real version of) Theorem 51 with $\eta = B^\top L^\dagger \omega$. Since $\|B^\top L^\dagger \omega\|_\infty < h(\|\mathcal{P}_{\mathrm{cyc}}\|_\infty)$, there exists a unique $\phi^* \in \mathrm{D}(\mathbb{0}_m, \sin(\gamma^*))$ such that $\mathcal{F}(\phi) = B^\top L^\dagger \omega$. This means that

$$B^\top L^\dagger \omega = \mathcal{P}_{\mathrm{cyc}} \arcsin(\phi^*) + \mathcal{P}_{\mathrm{cut}} \phi^*.$$

Since $\mathbb{R}(B^\top) = \mathbb{R}(\mathcal{P}_{\text{cut}}) = \mathbb{N}(\mathcal{P}_{\text{cyc}})$, we obtain $\mathcal{P}_{\text{cut}}\phi^* = B^\top L^\dagger \omega$ and $\arcsin(\phi)^* \in \mathbb{R}(B^\top)$. The result follows by the equivalence of parts 1 and 4 in Theorem 4.

Regarding statements 2 and 3, the result follows from (the complex version of) Theorem 53 and 54, respectively. □

Some remarks are in order.

Remark 8 (Power series expansion for $\sin(B^\top \mathbf{x}^*)$). *1. It is instructive to apply the iterative procedure in Theorem 72 to compute the first four odd terms in the power series* (1.20) *where* $\eta = B^\top L^\dagger \omega$*:*

$$
\begin{aligned}
A_1(\eta) &= \eta, \\
A_3(\eta) &= -\mathcal{P}_{\text{cyc}}\left(\frac{1}{6}\eta^{\odot 3}\right), \\
A_5(\eta) &= -\mathcal{P}_{\text{cyc}}\left(\frac{1}{12}A_3(\eta) \odot \eta^{\odot 2} + \frac{3}{40}\eta^{\odot 5}\right), \\
A_7(\eta) &= -\mathcal{P}_{\text{cyc}}\left(\frac{5}{112}\eta^{\odot 7} + \frac{3}{8}A_3(\eta) \odot \eta^{\odot 4} + \frac{1}{2}(A_3(\eta))^{\odot 2} \odot \eta + \frac{1}{2}A_5(\eta) \odot \eta^{\odot 2}\right).
\end{aligned}
$$

The iterative procedure in Theorem 72 is amenable to implementation on a mathematical software manipulation system; we report its implementation in Mathematica code in Algorithm 1 in Appendix 1.8.

2. If $\mathcal{P}_{\text{cyc}}$ *and* $\text{diag}(\eta)$ *commute, then, for every* $i \in \mathbb{Z}_{>0}$*:*

$$
A_{2i+1}(\eta) = -\frac{(2i-1)!!}{(2i)!!(2i+1)}\mathcal{P}_{\text{cyc}}\left(\eta\right)^{\odot(2i+1)}.
$$

For example, if the graph G *is acyclic, then* $\mathcal{P}_{\text{cyc}} = \mathbb{0}_{n\times n}$ *and, therefore,* $\mathcal{P}_{\text{cyc}}$ *and*

$\mathrm{diag}(\eta)$ *commute. Thus, for acyclic graphs, we have*

$$A_1(\eta) = \eta,$$
$$A_{2i+1}(\eta) = 0, \qquad \text{for all } i \in \mathbb{Z}_{\geq 0}$$

so that $\sin(B^\top \mathbf{x}^*) = B^\top L^\dagger \omega$. *Therefore, the Kuramoto model* (1.5) *on an acyclic graph has a unique locally stable synchronization manifold inside* $S^G(\gamma)$ *if and only if* $\|B^\top L^\dagger \omega\|_\infty \leq \sin(\gamma)$. *Moreover, if this condition holds, then the synchronization manifold is given by*

$$\mathbf{x}^* = L^\dagger B \mathcal{A} \arcsin(B^\top L^\dagger \omega).$$

This result is known for example as [15, Theorem 2 (Supporting Information)].

3. *While for acyclic graphs we have* $\mathcal{P}_{\mathrm{cyc}} = \mathbb{0}_{n\times n}$, *the matrix* $\mathcal{P}_{\mathrm{cyc}}$ *is non-zero and idempotent for cyclic graphs and it satisfies* $\|\mathcal{P}_{\mathrm{cyc}}\|_\infty \geq 1$. *The jump from* $\|\mathcal{P}_{\mathrm{cyc}}\|_\infty$ *equals* 0 *to values greater than or equal to* 1 *can be attributed to the discontinuity of the projection matrix* $\mathcal{P}_{\mathrm{cyc}}$ *with respect to edge weights of the graph. The following example shows that the infinity norm of the projection matrix* $\mathcal{P}_{\mathrm{cyc}}$ *is, in general, a discontinuous function of the weights of the graphs. Consider the family of 3-cycle graph* $\{G(\epsilon)\}_{\epsilon\geq 0}$ *with the node set* $V = \{1, 2, 3\}$, *the edge set* $\mathcal{E} = \{(1, 2), (1, 3), (2, 3)\}$, *and the adjacency matrix* $A(\epsilon) \in \mathbb{R}^{3\times 3}$ *given by*

$$A(\epsilon) = \begin{pmatrix} 0 & 1 & 1 \\ 1 & 0 & \epsilon \\ 1 & \epsilon & 0 \end{pmatrix}.$$

Then, for every $\epsilon > 0$, one can show that

$$\mathcal{P}_{\rm cyc}(\epsilon) = I_3 - B^\top L^\dagger B\mathcal{A} = \begin{pmatrix} \epsilon & \epsilon & \epsilon \\ \epsilon & \epsilon & \epsilon \\ 1-2\epsilon & 1-2\epsilon & 1-2\epsilon \end{pmatrix}.$$

This implies that $\lim_{\epsilon\to 0^+} \|\mathcal{P}_{\rm cyc}(\epsilon)\|_\infty = 3$. *However, the graph $G(0)$ is acyclic and therefore we have $\mathcal{P}_{\rm cyc}(0) = \mathbb{0}_{3\times 3}$. Thus, $\lim_{\epsilon\to 0^+} \|\mathcal{P}_{\rm cyc}(\epsilon)\|_\infty \neq \|\mathcal{P}_{\rm cyc}(0)\|_\infty$. This implies that the function $\epsilon \mapsto \|\mathcal{P}_{\rm cyc}(\epsilon)\|_\infty$ is not continuous at $\epsilon = 0$.*

4. *If the condition* (T0) *does not hold, it is still possible that the Kuramoto model* (1.5) *has a unique stable equilibrium manifold inside $S^G(\gamma^*)$ and the power series* (1.20) *converges strongly. We refer to the Numerical Experiments section for several examples on IEEE test cases. However, the upper bound on the error in part 3 is well-defined only when the condition* (T0) *holds. More specifically, if condition* (T0) *does not hold, then the function $x \mapsto \mathrm{Rem}^n_{2m+1}(x)$ diverges for $x = \frac{\|B^\top L^\dagger \omega\|_\infty}{h(\|\mathcal{P}_{\rm cyc}\|_\infty)}$ and for every $m \in \mathbb{Z}_{\geq 0}$.*

In the rest of this section, we use the power series (1.20) to propose a family of statistically-accurate approximate tests that are much less conservative than proven sufficient conditions for existence of a unique synchronization solution inside $S^G(\gamma)$ for $\gamma \in [0, \pi/2)$. Our approximate tests estimate the solution of the unconstrained edge balance equation (1.10) and check that all elements of the estimate are less than or equal to $\sin(\gamma)$. For more insight into these approximate tests, recall from Theorem 72 that ϕ, the solution for unconstrained edge balance equation (1.10) is given by

$$\phi = B^\top L^\dagger \omega + A_3(B^\top L^\dagger \omega) + A_5(B^\top L^\dagger \omega) + \dots.$$

There already exists a first order approximate synchronization test, introduced by reference [15], which truncates the series, given above, after the first order term. By approximating ϕ with $\phi \approx B^\top L^\dagger \omega \in \mathbb{R}(B^\top)$, we write

$$\left\| B^\top L^\dagger \omega \right\|_\infty \leq \sin(\gamma), \tag{AT1}$$

By substituting the third order power series expansion for the edge variable $\phi \in \mathbb{R}^m$ of the Kuramoto model in Theorem 72 into equation (1.9), we can also write the third order approximate synchronization test as

$$\left\| B^\top L^\dagger \omega + \frac{1}{6} \mathcal{P}_{\text{cyc}} (B^\top L^\dagger \omega)^{\odot 3} \right\|_\infty \leq \sin(\gamma).$$

In summary we propose a family of higher order approximate tests as follows.

Definition 9. *For $\gamma \in [0, \pi/2)$ and $k \in 2\mathbb{Z}_{\geq 0} + 1$, the* kth order approximate test *for existence of a unique solution in $S^G(\gamma)$ is defined by*

$$\left\| \sum_{i=0}^{(k-1)/2} A_{2i+1} (B^\top L^\dagger \omega) \right\|_\infty \leq \sin(\gamma). \tag{ATk}$$

Finally, it is valuable to compare our approach with the existing methods in the literature for existence of synchronization manifolds in the Kuramoto model. One of the conventional and well-studied approaches for synchronization is the Lyapunov direct method. In literature, several necessary and sufficient conditions for synchronization of the Kuramoto model are reported based on different Lyapunov functions [5, 16, 20]. Comparing to our power series approach, Lyapunov direct method provides rigorous sufficient conditions with guaranteed region of attraction for synchronization. However, as is shown in the next section, these Lyapunov-based conditions are usually conservative

and do not provide intuition about the role of network parameters in synchronization. On the other hand, our power series approach, proposes a family of approximate but increasingly accurate synchronization tests, identifies the correct functional form of the trade-off between coupling strength and oscillator heterogeneity, and provides good estimates for the synchronization manifolds.

1.7 Numerical Experiments

In this section we illustrate the usefulness of the Taylor series expansion given by Theorem 7. First, for large IEEE test cases, we illustrate the accuracy of the truncated series for approximating synchronized solutions of (1.5). In addition, we present results showing the sharpness of the approximate tests (ATk) for existence of a synchronization manifold (9) on several IEEE test cases and random networks.

1.7.1 Accuracy of the Taylor series: approximating the synchronization manifold

Here we evaluate the accuracy of the truncated power series in Theorem 72 for approximating the synchronization manifold. We consider both IEEE test cases and random networks to evaluate these measures of accuracy.

The general numerical setting for the IEEE test cases is as follows. Each IEEE test case can be described by a connected undirected graph G with the nodal admittance matrix $Y \in \mathbb{C}^{n\times n}$. The set of nodes in G are partitioned into load buses $\mathcal{N}_1$ and generator buses $\mathcal{N}_2$. The power demand (resp. power injection) at node $i \in \mathcal{N}_1$ (resp. $i \in \mathcal{N}_2$) is denoted by P_i. V_i and θ_i are the voltage magnitude and phase angle at node $i \in \mathcal{N}_1 \cup \mathcal{N}_2$. For every IEEE test case, we study the following Kuramoto synchronization manifold

equation

$$P_i = \sum_{j \in \mathcal{N}_1 \cup \mathcal{N}_2} a_{ij} \sin(\theta_i - \theta_j), \qquad \text{for all } i \in \mathcal{N}_1 \cup \mathcal{N}_2, \tag{1.21}$$

where $a_{ij} = a_{ji} = V_i V_j \Im(Y_{ij}) > 0$, where $\Im(Y_{ij})$ is the imaginary part of $Y_{ij} \in \mathbb{C}$. The equation (1.21) is exactly the lossless active AC power flow equations for the network. Note that in order to study equation (1.21), we need to apply some modifications to the IEEE test cases. First, we assume that the admittance matrix $Y \in j\mathbb{R}^{n \times n}$ is purely inductive with no shunt admittances $Y_{ii} = 0$. If the IEEE test case has branch resistances or shunt admittances, then they are removed. Second, we assume that all the nodes in the IEEE test case are PV nodes; this assumption is reasonable since the active power injection and output voltage of generators are known. For the loads, we use MATPOWER [44] to solve the coupled AC power flow balance to obtain their terminal voltage V_i. Lastly, for every $i \in \{1, \dots, n\}$, we set $P_i = K P_i^{\text{nom}}$ for some $K \in \mathbb{R}_{\geq 0}$ where P_i^{nom} is the nominal injections given by each test case. Starting with $K = 0$, we increase K by 5×10^{-3} at each step. MATLAB's *fsolve* is used to solve equation (1.21) for θ^*_{fsolve} at each K. The scalar K is increased until whichever situation occurs first: $\|B^\top \theta^*_{\text{fsolve}}\|_\infty$ reaches $\pi/2$ or *fsolve* does not converge to a solution.

To evaluate the accuracy of the truncated Taylor series with k terms, we define the absolute error denoted by S_k by

$$S_k = \left\| \sin(B^\top \theta^*_{\text{fsolve}}) - \sum_{i=0}^{k} A_{2i+1} (B^\top L^\dagger p_{\text{sd}}) \right\|_\infty, \tag{1.22}$$

where $p_{\text{sd}} = [P_1, \dots, P_n]^\top$ is the balanced supply/demand vector, $L = B\mathcal{A}B^\top$, and $\mathcal{A}$ is the diagonal weight matrix with diagonal elements $\{a_{ij}\}_{(i,j) \in \mathcal{E}}$. The errors S_k for IEEE 300 and Pegase 1354 are shown in Figure 1.2.

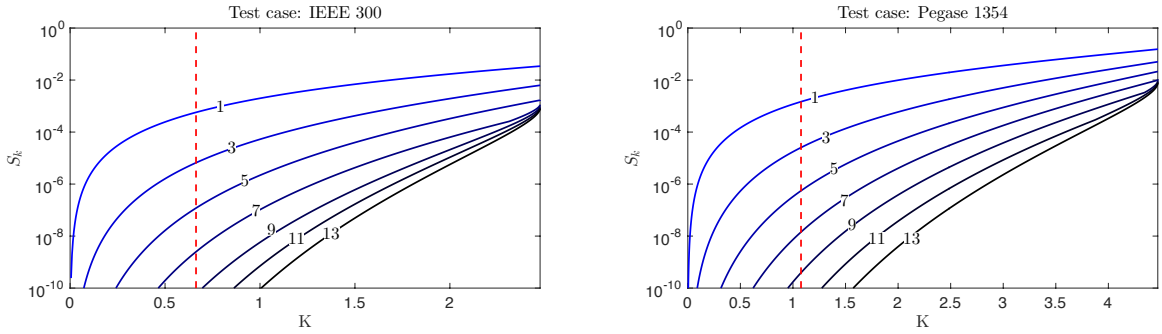

Figure 1.2: Absolute errors of the sine of the phase differences, approximated with the truncated Taylor series in Theorem 72, for different orders and various values of scaling factor K. The number on each line shows the order of truncation. The absolute error is calculated with equation (1.22), using the solution found with *fsolve* as the true value. The errors are decreasing to zero as the scaling factor K decreases to zero. The red dashed line shows the maximum value of the scaling factor K for which test (T0) holds. For the IEEE 300 testcase, the red dashed line is at $K = 0.6631$ and, for Pegase 1354, the red dashed line is at $K = 1.0767$. As can be seen in both figures, the power series (1.20) can converge beyond this threshold.

Summary evaluation Figure 1.2 shows that, for the IEEE test cases, the error of truncated Taylor series for computing the synchronized solutions of the Kuramoto model (1.21) decreases exponentially with the order of the truncations and increases as we approach the threshold of synchronization. For IEEE 300 and Pegase 1354 with the nominal power injections, the error of approximating the synchronized manifold with 5th order or higher truncated series is smaller than 10^{-6}. Finally, Figure 1.2 shows that the power series (1.20) can converge beyond the threshold predicted by the synchronization test (T0).

1.7.2 Accuracy of the Taylor series: approximating the critical coupling

In this section, we compare the approximate synchronization test (ATk) with the existing tests in the literature and evaluate the accuracy of these approximate tests.

We consider both IEEE test cases and random networks to evaluate these measures of accuracy.

For IEEE test cases, we use the same simulation setup given earlier in Section 1.7.1. Denote the critical coupling of equation (1.21) by K_{C}, that is, let K_{C} be the smallest scaling factor such that $\|B^{\top}\theta^{*}_{\mathrm{fsolve}}\|_{\infty}$ reaches $\pi/2$ or *fsolve* does not converge to a solution (whichever occurs first). Let K_{T} denote the smallest scaling factor for which a particular synchronization test fails. Then we denote the critical ratio by $K_{\mathrm{T}}/K_{\mathrm{C}}$; this percentage is a measure of the accuracy of the given test. The conditions are checked on IEEE 118, IEEE 300, and Polish 2383 from [45], and on Pegase test case from [46] with a 10^{-6} tolerance. Table 1.1 compares the accuracy of the approximate test with existing sufficient conditions for synchronization:

The first column contains the critical ratio of the best-known Lyapunov-based synchronization test in the literature (T1) from [47, Theorem 7.2]:

$$\lambda_2(L) > \lambda_{\mathrm{critical}} \triangleq \|B^{\top}p_{\mathrm{sd}}\|_2. \tag{T1}$$

The second column contains the critical ratio of the best-known ∞-norm synchronization test (T2) form [21, Theorem 16]:

$$\|B^{\top}L^{\dagger}p_{\mathrm{sd}}\|_{\infty} \leq g(\|\mathcal{P}_{\mathrm{cut}}\|_{\infty}). \tag{T2}$$

Note that test (T2) is a sufficient condition for existence of a synchronization manifold in $S^{G}(\gamma^{*})$ where $\gamma^{*} = \arccos\left(\frac{\|\mathcal{P}_{\mathrm{cut}}\|_{\infty}-1}{\|\mathcal{P}_{\mathrm{cut}}\|_{\infty}+1}\right) \in [0, \pi/2]$ and $g(x) = \frac{y(x)+\sin(y(x))}{2} - x\frac{y(x)-\sin(y(x))}{2}\Big|_{y(x)=\arccos(\frac{x-1}{x+1})}$.

The third column contains the new sufficient test (T0) proposed in this chapter.

The last four columns contains the critical ratio for the family of approximate

tests (ATk) of order 1, 3, 5 and 7.

Test Case	Critical ratio $K_{\mathrm{T}}/K_{\mathrm{C}}$						
	λ_2 test (T1)[47]	∞-norm test (T2)[21]	New test (T0)	Approx test $k=1$ (AT1)[15]	Approx test $k=3$ (ATk)	Approx test $k=5$ (ATk)	Approx test $k=7$ (ATk)
IEEE 118	0.23 %	43.76 %	29.91 %	86.12 %	90.80 %	93.10 %	94.45 %
IEEE 300	0.02 %	40.45 %	27.25 %	99.64 %	99.80 %	99.84 %	99.88 %
Pegase 1354	0.04 %	34.04 %	23.94 %	89.02 %	97.58 %	99.61 %	99.66 %
Polish 2383	0.03 %	29.49 %	20.60 %	84.53 %	90.62 %	92.60 %	93.95 %

Table 1.1: Comparison of the conservativeness of various sufficient conditions with approximate synchronizations tests applied to IEEE test cases in the domain $S^G(\pi/2)$.

Summary evaluation Table 1.1 shows that, for IEEE test cases with scaled nominal power injections, the following statements holds:

1. Comparing to the approximate tests (ATk), the best-known Lyapunov-based synchronization test (T1) provides conservative estimates of the synchronization threshold of the Kuramoto model;

2. the accuracy of the approximate tests (ATk) increases with the order of the tests;

3. for $\gamma = \frac{\pi}{2}$, the fifth and seventh order approximate tests (ATk) improves the accuracy given by the 1st order approximate test $\left\|B^\top L^\dagger \omega\right\|_\infty \leq 1$ [15] by up to 9%;

4. for $\gamma = \frac{\pi}{2}$, the fifth and seventh order approximate tests (ATk) improves the best-known sufficient synchronization test in the literature [21] by up to 50%.

Next, we consider random graph models with randomly generated natural frequencies. We setup the numerical analysis to assess the correctness of the family of approximate tests (ATk) as follows. Consider a nominal unweighted random networks $\{G, \omega\}$, where

G is a connected undirected graph with $n = 80$ nodes chosen from a parametrized family of random graph models RGM and $\omega \in \mathbb{1}_n^\perp$ are natural frequencies chosen randomly form sampling distribution SD. Then we study the synchronization of the Kuramoto model with uniform coupling gain $K \in \mathbb{R}_{>0}$,

$$\dot{\theta} = \omega - KB\sin(B^\top \theta).$$

The random graph models RGM and the sampling distributions SD are given as follows:

1. *Network topology:* For the network topology, we consider three types of random graph models (RGM), parametrized by $n \geq 2$ nodes and coupling parameter $p \in [0, 1]$. Note that depending on the random graph model, the coupling parameter p represents different notions of edge density. The random graph models we consider are (i) Erdős–Rényi random graph with probability p of an edge existing [48], (ii) Random Geometric graph model with sampling region $(0, 1]^2 \subset \mathbb{R}^2$ and connectivity radius p [48], and (iii) Watts–Strogatz small world model network with initial coupling to the 2 nearest neighbors and rewiring probability p [49]. If there exists an edge, then the coupling weight is $a_{ij} = a_{ji} = 1$. If the graph is not connected, then it is thrown out and a new random graph is generated.
2. *Natural frequencies:* We consider two types of sampling distributions SD. For $n = 80$, random numbers are sampled from either a (i) uniform distribution on the interval $(-1, 1)$ or (ii) bipolar distribution $\{-1, +1\}$ to obtain q_i for $i \in \{1, \ldots, n\}$. Then to ensure that t he natural frequencies satisfy $\omega \in \mathbb{1}_n^\perp$, we take $\omega_i = q_i - \sum_{i=1}^n q_i/n$.
3. *Parametric realizations:* We consider combinations of parameters (RGM, p, SD): the three random graph models, 15 edge connectivity parameters on the interval $p \in [0, 1]$, and two sampling distributions.

For each parametric realization in (iii), we generate 100 nominal models of $\{G, \omega \in \mathbb{1}_n^\perp\}$. For each nominal case, we find the critical coupling, denoted by K_{C}, and the smallest coupling where the approximate test fails (9), denoted by K_{T}, for orders $\{1, 3, 5, 7\}$. K_{C} is found iteratively with MATLAB's *fsolve*. The numerically determined values are found with an accuracy of 10^{-3}. Each data point in Figure 1.3 corresponds to the mean of $K_{\mathrm{T}}/K_{\mathrm{C}}$ over 100 nominal cases of the same parametric realization.

Summary evaluation Figure 1.3 illustrates that, for random graph models with random natural frequency for bipolar and uniform distribution and $\gamma = \frac{\pi}{2}$, the accuracy of the approximate test (ATk) consistently improves. In particular, the fifth and seventh order approximate tests (ATk) improves the accuracy of the 1st order approximate test $\left\|B^\top L^\dagger \omega\right\|_\infty \leq 1$ [15] by up to 30%.

1.7.3 Computational cost of approximating the synchronization manifold

Consider a connected graph G with m edges, n nodes, and no self-loops. Table 1.2 shows the order of the number of operations associated with different methods for approximating the synchronization manifold for the sparse and dense graphs.

For random graph models, we compare the computational time of three different methods for approximating the synchronization manifold of the Kuramoto model: (i) the series approximation of the analytical solution from Theorem 72, (ii) Newton–Raphson method, and (iii) MATLAB's *fsolve*.

For the simulation setup, we consider the random network $\{G, \omega\}$ with $n \geq 2$ nodes, $\omega_i \in (-\alpha, \alpha)$ for $i \in \{1, \ldots, n\}$, and number of edges m depending on the coupling parameter $p \in (0, 1)$. The following lists the random graph parameters:

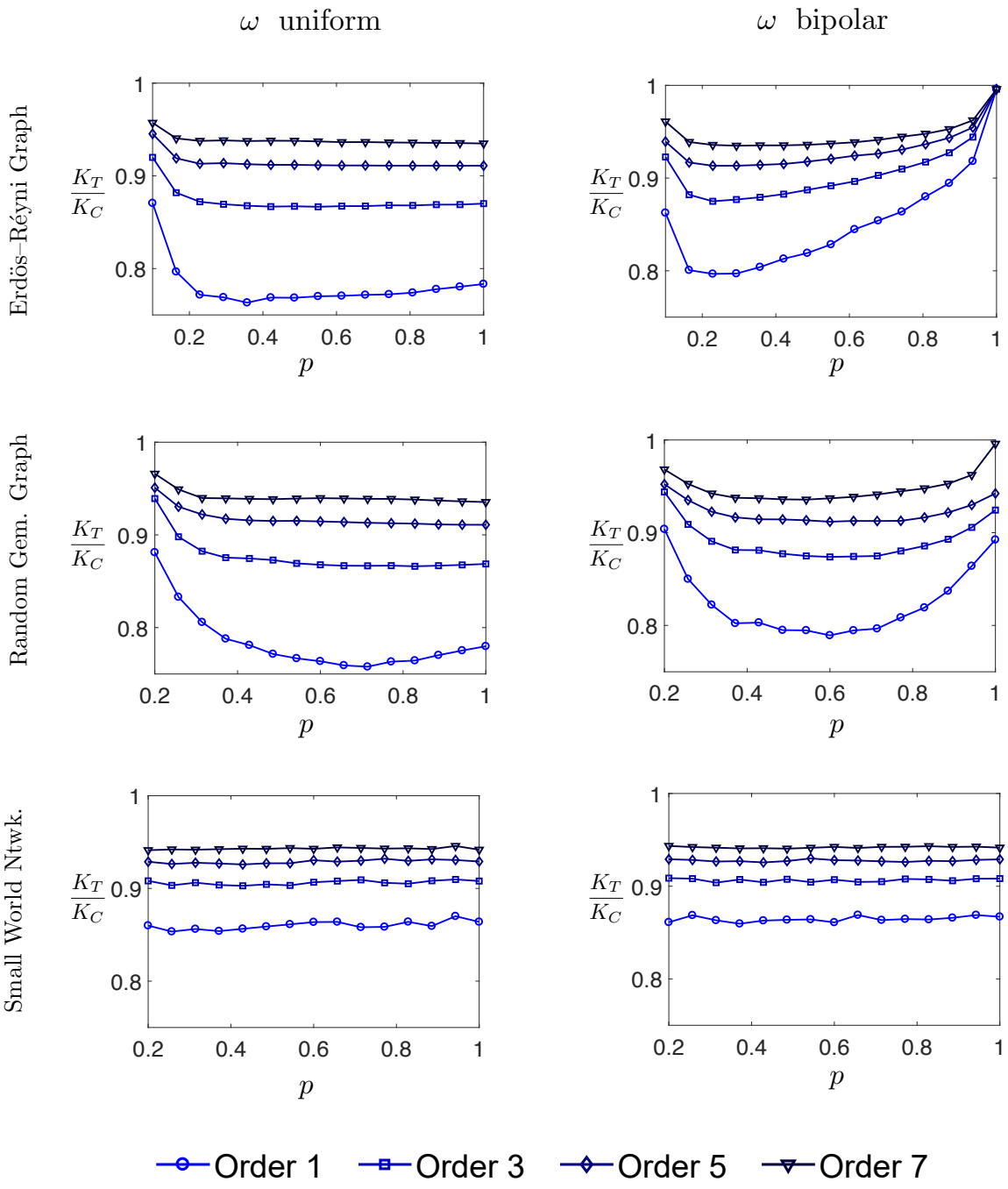

Figure 1.3: Each data point is the critical ratio $K_{\mathrm{T}}/K_{\mathrm{C}}$ averaged over 100 random graphs with $n = 80$ nodes and in the domain $S^G(\pi/2)$. $K_{\mathrm{T}}/K_{\mathrm{C}}$ measures the accuracy of the approximate synchronization tests (ATk). K_{C} is the smallest coupling gain such that there exists a solution to the Kuramoto model. K_{T} is an approximation of K_{C}, estimated using the approximate test (ATk) derived from Theorem 72 for orders $k = 1, 3, 5, 7$.

Method	General	Sparse Graphs $\mathcal{O}(n) = \mathcal{O}(m)$	Dense Graphs $\mathcal{O}(n^2) = \mathcal{O}(m)$
Precomputation	$\mathcal{O}(m^2 n)$	$\mathcal{O}(n^3)$	$\mathcal{O}(n^5)$
Series, 5th order*	$\mathcal{O}(2m^2)$	$\mathcal{O}(2n^2)$	$\mathcal{O}(2n^4)$
Series, 7th order*	$\mathcal{O}(3m^2)$	$\mathcal{O}(3n^2)$	$\mathcal{O}(3n^4)$
Newton–Raphson	$\mathcal{O}(mn^2)$	$\mathcal{O}(n^3)$	$\mathcal{O}(n^4)$

* Denotes that the method precomputes the terms $B^\top L^\dagger$, $L^\dagger B\mathcal{A}$ and $\mathcal{P}_{\text{cyc}}$. The computation complexity of these terms are found in the "Precomputation" row.
The computational complexity of $L^\dagger$ for $L \in \mathbb{R}^{n\times n}$ is $\mathcal{O}(n^3)$.

Table 1.2: Comparison of number of operations required for computing the truncated series and Newton–Raphson.

1. *Network topology:* To construct the random graph, the Erdős–Rényi random graph model was used with probability p of an edge existing. If the graph is not connected, then it is thrown out and a new random graph is generated.
2. *Coupling weights:* Each edge is given a random coupling weight, $a_{ij} = a_{ji} > 0$, sampled on the uniform distribution interval $(0, 10)$.
3. *Natural frequencies:* n random numbers are sampled from a uniform distribution on the interval $(-\alpha, \alpha)$ to obtain q_i for $i \in \{1, \dots, n\}$. Then to ensure that the natural frequencies satisfy $\omega \in \mathbb{1}_n^\perp$, we take $\omega_i = q_i - \sum_{i=1}^n q_i/n$. In our simulations, we choose $\alpha = 0.05$ which is sufficiently small to ensure that the MATLAB's *fsolve* converges to a solution of the Kuramoto model (1.5).
4. *Parametric realizations:* We consider random network parametrization (n, p, α) with combinations of $n = \{10, 20, 30, 60, 120\}$ and $p = \{0.2, 0.4, 0.6, 0.8\}$.

For each parametrization, we generate 3000 nominal graphs and 20 natural frequency vectors for *each* random graph. The results of the execution time for various methods are shown in Figure 1.4 where each point is the computational time for a particular method averaged over 3000 graphs and 20 natural frequency vectors $\omega \in \mathbb{1}_n^\perp$ per graph. The computation time for the series approximation is the total time to complete the

calculations for 1 random nominal graph with 20 different natural frequency vectors. This time *does not* include the computation time for the precomputed terms listed in Table 1.2. The initial guess for Newton–Raphson and *fsolve* is $B^\top L^\dagger \omega$.

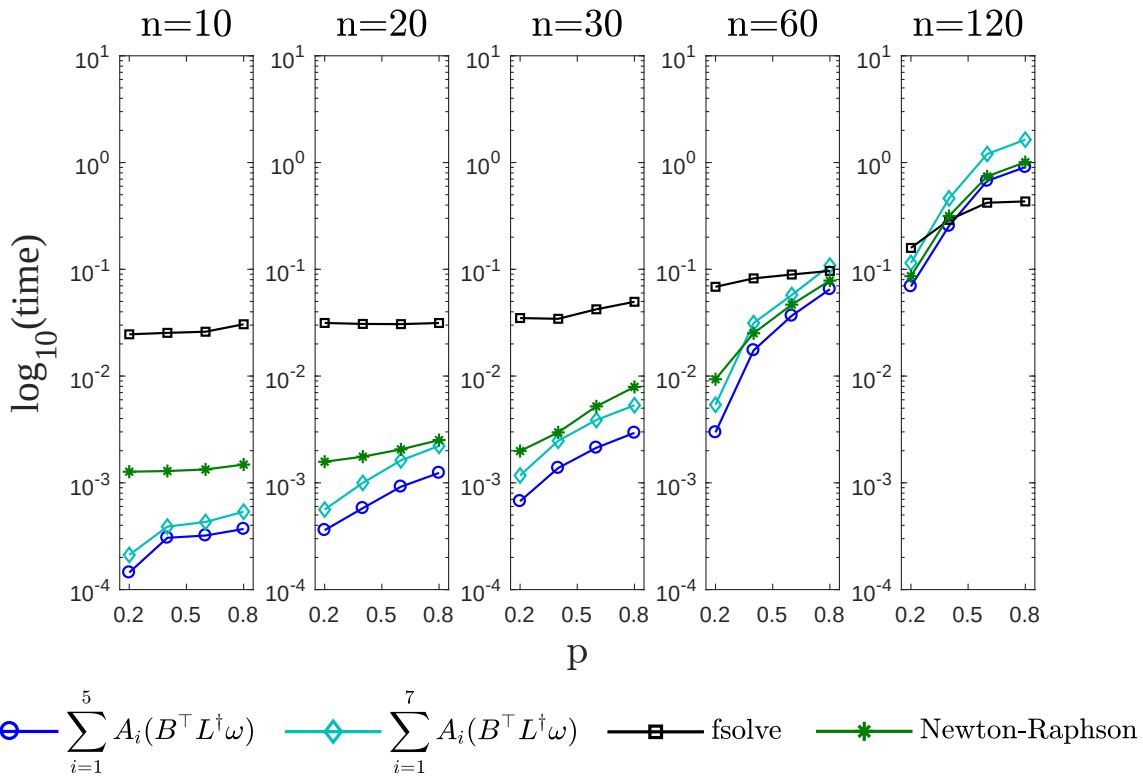

Figure 1.4: Comparison of computation times for 5th order truncated series, the 7th order truncated series, MATLAB's *fsolve*, and Newton–Raphson for random graphs, where p is the probability of an edge existing for Erdős–Rényi graphs. The computation time is how long it takes the various methods to compute the solutions of the unconstrained edge balance equations, for 20 randomly generated natural frequency vector given one randomly generated graph. If a random natural frequency vector does not give a solution, it is thrown out and a new vector is generated. Certain values are precomputed for each graph, but the precomputation time is not included in the graph. Each data point is averaged over 3000 Erdős–Rényi random graphs.

Summary evaluation Figure 1.4 show that the computation time for the truncated power series increases with density of the random graphs. Moreover, the truncated series are more efficient than Newton–Raphson method for small random graphs, while they

are only comparable to Newton–Raphson method for large random graphs.

For IEEE test cases, we compare the computational time of three different methods for calculating the synchronization manifold: (i) the series approximation of the analytical solution from Theorem 72, (ii) Newton–Raphson method, and (iii) MATLAB's *fsolve*. The setting for the IEEE test cases are the same as the one given in Section 1.7.1. In this setup we do not precompute any terms and consider one graph topology with its nominal power injections. We use each method to solve for the synchronization manifold $[\theta^*]$, and average the computation time over 10 trials.

Test Case	*fsolve* / NR	Ord. 5 / NR	Ord. 7 / NR
IEEE 118	4.2072	0.4511	0.4539
IEEE 300	2.6501	0.7546	0.7539
Pegase 1354	1.2825	0.8582	0.8633
Polish 2383	1.1279	0.9559	0.9583

Table 1.3: Computational times of MATLAB's *fsolve*, 5th order series (Ord. 5), and 7th order series (Ord. 7) normalized by the computational time for Newton–Raphson (NR) for IEEE test cases. The computation time is how long it takes the various methods to compute the solution of the unconstrained edge balance equations, averaged over 10 trials. Certain values are precomputed for each graph, but the precomputation times are not included.

Summary evaluation The results in Table 1.3 show that, for IEEE test cases, the series approximations are computationally comparable to Newton–Raphson and they are computationally more efficient than MATLAB's *fsolve*.

1.8 Mathematica Code

We present an implementation of a Mathematica algorithm 1 to compute the coefficient of the power series expansion given in Theorem 72.

It is worth mentioning that the required computations increase exponentially with the order of the terms. Specifically, computing the $(2k+1)$th order coefficient of the

Algorithm 1 Mathematica algorithm to compute terms of series expansion

```
permCount[as_]:=Length[Permutations[Flatten[as]]]
getOddPartition[x1_,x2_]:=Select[IntegerPartitions[x1,{x2}],allOddQ]
getSymbol[val_]:=Symbol["A"<>ToString[val]]
A[1]=getSymbol[1]
A[i_/;OddQ[i]]:=
-Pcyc**(Sum[(2k-1)!!/((2k+1)(2k)!!)*
Sum[permCount[as]*Product[getSymbol[a],{a,as}],
{as,getOddPartition[i,2k+1]}],{k,1,(i-1)/2}])
```

power series requires finding all the odd-integer partitions of $2k + 1$.

1.9 Conclusion

This chapter proposes a novel equivalent characterization of the equilibrium equation for the Kuramoto coupled oscillator; we refer to this characterization as to the unconstrained edge balance equation. Using this characterization, we propose a Taylor series expansion for the synchronization manifold of the Kuramoto network and a recursive formula to symbolically compute all the terms in the Taylor series. We then use the truncated Taylor series as a tool to (i) find sharp approximation for the synchronization manifold and (ii) estimate the onset of frequency synchronization. Our numerical simulations illustrate the accuracy and computational efficiency of this method on various classes of random graphs and IEEE test cases. As future directions, it may be instructive to employ this series expansion method to study frequency synchronization in networks consisting of other important oscillators, such as FitzHugh–Nagumo systems. Additionally, it may be viable to adopt the series expansion approach to tackle more general nonlinear network flow problems, such as the coupled power flow equations and optimal power flow problems.

Chapter 2

Assign and Appraise: Achieving Optimal Performance in Collaborative Teams

2.1 Introduction

Research, technology, and innovation is increasingly reliant on teams of individuals with various specializations and interdisciplinary skill sets. In its simplest form, a group of individuals completing routine tasks is a resource allocation problem. However, tackling complex problems such as scientific research [50], software development [51], or problem solving [52] requires consideration of the team structure, cognitive affects, and interdependencies between team members [53]. In these complex scenarios, it is fundamental to discover what skills each member is endowed with, so as to devise a task assignment that maximizes the resulting collective team performance.

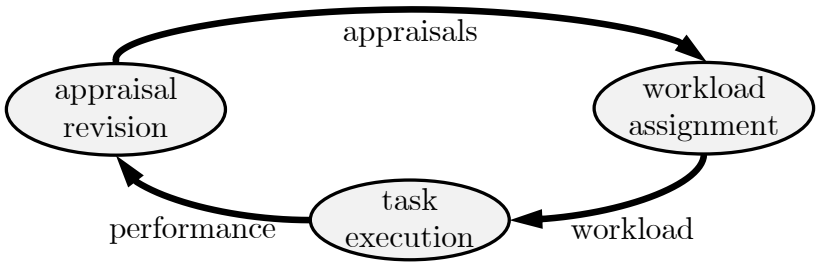

Figure 2.1: Architectural overview on the assign and appraise model studied in this manuscript. Given a complex task to complete, team members get assigned and execute an initial workload (right and bottom blocks). Each team member revises their appraisal of neighboring members based on each neighbor's individual performance (left), which in turn is used to reassign the workload. The objective is for the team to learn who has what skill, so as to assign tasks in a way that maximizes the collective team performance.

2.1.1 Problem description

In this chapter, we focus on a quantitative model describing the process by which individuals in a team evaluate one another while concurrently assigning work to each of the team members, in order to maximize the collective team performance (see Figure 2.1). More specifically, we assume each team member is endowed with a skill level (a-priori unknown), and that the team needs to divide a complex task among its members. We let each team member build their own local appraisal of neighboring team members' based on the performance exhibited on previous tasks. Upcoming tasks are then distributed according to the current appraisal estimates. Finally, the performance of each member is newly observed by neighboring members, who, in turn, update their appraisal. Any model satisfying these assumptions is composed of two building blocks: i) an appraisal component modeling how team members update their appraisals (left block in Figure 2.1), and ii) a work assignment component describing how the task is divided within the team (right block in Figure 2.1).

We model the appraisal process i) through the lens of transactive memory systems, a conceptual model introduced by Wegner [54], which assumes that a team is capable

of developing collective knowledge regarding who has what information and capabilities. Our choice of dynamics describing the evolution of the interpersonal appraisals is inspired from replicator dynamics, whereby each team member i updates their appraisal of a neighboring member j proportionally to the difference between member j performance and the (appraisal-weighted) average performance of the team.

We model the work assignment process ii) as a compartmental system [55], and utilize two natural dynamics to describe how the task is divided based on the current appraisals. These dynamics correspond to utilizing different centrality measures to subdivide a complex task. It is crucial to observe that the coupling between the appraisal revision and the work assignment process results in a *coevolutionary* network problem.

This chapter follows a trend initiated recently, whereby many traditionally qualitative fields such as social psychology and organizational sciences are developing *quantitative* models. In this regard, our aim is to quantify the development of transactive memory within a team and study what conditions cause a team to fail or succeed at allocating a task optimally among members. To do so, we leverage control theoretical tools as well as ideas from evolutionary game theory, and notions from graph theory.

2.1.2 Contributions

Our main contributions are as follows. 1. We formulate a quantitative model to capture the coevolution of the workload division and appraisal network, where the optimal workload assignment maximizing the collective team performance is an equilibrium of the model. While we let the appraisal network evolve according to a replicator-like dynamics, we consider two different mechanisms for workload division and show well-posedness of the model. 2. Regardless of the mechanism used for workload division, we derive conserved quantities associated to the cycles of the appraisal network. Leveraging this

result, for a team of n individuals, we significantly reduce the dimension of the system from n^2+n to a $2n$ dimensional submanifold. 3. We provide rigorous positive and negative results that characterize the asymptotic behavior for either of the workload division mechanisms. When adopting the first workload division mechanism, we show that under a mild assumption, strongly connected teams are always able to learn each member's correct skill level, and thus determine the optimal workload division. In the second model variation, strong connectivity is insufficient to guarantee that the team learns the optimal workload, but more specific assumptions allow the team to converge to the optimal workload. 4. Finally, we enrich our analysis by means of numerical experiments that provide further insight into the limiting behavior.

2.1.3 Related works

Quantitative models of transactive memory systems

Wegner's transactive memory systems (TMS) model [54] describes how cognitive states affect the collective performance of a team performing complex tasks. This widely established model captures both learning on the individual and collective level, as well as the evolution of the interaction between individuals within a team.

There are very few quantitative models attempting to describe TMS and most of these models rely on numerical analysis to study the evolution of team knowledge [56], or what events are disruptive to learning and productivity in groups [57]. However, numerical analysis alone has natural limitations, whereas a mathematical perspective to TMS can establish the emergence of learning behaviors for entire classes of models. Moreover, while our proposed model is agent-based with collective knowledge represented as a weighted digraph, [56, 57] are not agent-based models and use a scalar value to encode the team's collective knowledge.

The collective learning model introduced by Mei *et al.* [58] was the first to quantify TMS with appraisal networks and provide convergence analysis. In particular, for the *assign/appraise* model in [58], the appraisal update protocol is akin to one originally introduced in [59] and assumes each team member only updates their own appraisal based on performance comparisons. Additionally, the workload assignment is a centralized process determined by the eigenvector centrality of the network [60]. Our model significantly differs from [58] in that team members update their own and neighboring team members' appraisals. Additionally, the workload assignment is a distributed and dynamic process.

Distributed optimization

Our model has direct ties with the field of distributed optimization. Under suitable conditions discussed later, in fact, the team will be able to learn each other's skill levels, and thus agree on a work assignment maximizing the collective performance in a distributed fashion. Additionally, any change in the problem dimension, due to the addition or subtraction of agents, only requires local adaptions. In light of this observation, one could reinterpret the assign and appraisal model studied here as a distributed optimization algorithm, where the objective is that of maximizing the team performance through local communication. In comparison to our work, existing distributed optimization algorithms often require more complex dynamics. For example, [61] requires that the optimal solution estimates are projected back into the constrained set, while Newton-like methods [62] require higher order information.

Perhaps closest to this perspective on our problem is the work of Barreiro-Gomez *et al.* [63], where evolutionary game theory is used to design distributed optimization algorithms. Nevertheless, we observe that the objective we pursue here is that of quantifying if and to what extent team members learn how to share a task optimally. In this respect, the dynamics we consider do not arise as the result of a design choice (as it is in [63]),

but they are rather defining the problem itself.

Adaptive coevolutionary networks

Our model is an example of appraisal network coevolving with a resource allocation process. Research regarding adaptive networks has gained traction in recent decades, appearing in biological systems and game theoretical applications [64]. Wang *et al.* [65], for example, review coupled disease-behavior dynamics, while Ogura *et al.* [66] propose an epidemic model where awareness causes individuals to distance themselves from infected neighbors. Finally, we note that coevolutionary game theory considers dynamics on the population strategies and dynamics of the environment, where the payoff matrix evolves with the environment state [67, 68].

Chapter organization

Section 2.2 contains the problem framework, model definition, the model's well-posedness, and equilibrium corresponding to the optimal workload. Section 2.3 contains the properties of the appraisal dynamics and reduced order dynamics. Section 2.4 and 2.5 present the convergence results for the model with both workload division mechanisms. Section 2.6 contains numerical studies illustrating the various cases of asymptotic behavior.

Notation

Let $\mathbb{1}_n$ ($\mathbb{0}_n$ resp.) denote the n-dimensional column vector with all ones (zero resp.). Let I_n represent the $n \times n$ identity matrix. For a matrix or vector $B \in \mathbb{R}^{n\times m}$, let $B \geq 0$ and $B > 0$ denote component-wise inequalities. Given $x = [x_1, \ldots, x_n]^\top \in \mathbb{R}^n$, let $\mathrm{diag}(x)$ denote the $n \times n$ diagonal matrix such that the ith entry on the diagonal equals x_i. Let

$\odot$ ($\oslash$ resp.) denote Hadamard entrywise multiplication (division resp.) between two matrices of the same dimensions. For $x, y \in \mathbb{R}^n$ and $B \in \mathbb{R}^{n\times n}$, we shall use the property

$$xy^\top \odot B = \operatorname{diag}(x) B \operatorname{diag}(y). \tag{2.1}$$

Define the n-dimensional simplex as $\Delta_n = \{x \in \mathbb{R}^n \mid \mathbb{1}_n^\top x = 1, x \geq 0\}$ and the relative interior of the simplex as $\operatorname{int}(\Delta_n) = \{x \in \mathbb{R}^n \mid \mathbb{1}_n^\top x = 1, x > 0\}$.

A nonnegative matrix $B \geq 0$ is row-stochastic if $B\mathbb{1}_n = \mathbb{1}_n$. For a nonnegative matrix B, $G(B)$ is the weighted digraph associated to B, with node set $\{1, \ldots, n\}$ and directed edge (i, j) from node i to j if and only if $b_{ij} > 0$. A nonnegative matrix B is irreducible if its associated digraph is strongly connected. The Laplacian matrix of a nonnegative matrix B is defined as $L(B) = \operatorname{diag}(B\mathbb{1}_n) - B$. For B irreducible and row-stochastic, $v_{\text{left}}(B)$ denotes the left dominant eigenvector of B, i.e., the entry-wise positive left eigenvector normalized to have unit sum and associated with the dominant eigenvalue of B [69, Perron Frobenius theorem].

2.2 Problem Framework and ASAP Model

In this section, we first propose the Assignment and Appraisal (ASAP) model and establish that it is well-posed for finite time. The proposed ASAP model can be considered a socio-inspired, distributed, and online algorithm for optimal resource allocation problems. Our model captures two fundamental processes within teams: workload distribution and transactive memory. We consider two distributed, dynamic models for the workload division: a compartmental system model and a linear model that uses average-appraisal as the input for adjusting workload. The transactive memory is quantified by the appraisal network and reflects individualized peer evaluation in the team. The

development of the transactive memory system allows the team to estimate the work assignment that maximizes the collective team performance.

2.2.1 Workload assignment, performance observation, and appraisal network

Workload assignment

We consider a team of n individuals performing a sequence of tasks. Let $\boldsymbol{w} = [w_1, \ldots, w_n]^\top \in \text{int}(\Delta_n)$ denote the vector of *workload assignments* for a given task, where w_i is the work assignment of individual i.

Individual performance

Let $p(\boldsymbol{w}) : \text{int}(\Delta_n) \to \mathbb{R}^n_{>0}$ represent the vector of *individual performances* that change as a function of the work assignment, where $p(\boldsymbol{w}) = [p_1(w_1), \ldots, p_n(w_n)]^\top \in$ and $p_i(w_i)$ is the performance of individual i. In general, individuals will perform better if they have less workload; we formalize this notion with the following two assumptions.

Assumption 10. *(Smooth and strictly decreasing performance functions) Assume function $p_i : (0, 1] \to [0, \infty)$ is C^1, strictly decreasing, convex, integrable, and $\lim_{x \to 0^+} p_i(x) = +\infty$.*

Assumption 11. *(Power law performance functions) Assume function $p_i : (0, 1] \to [0, \infty)$ is of the form $p_i(x) = s_i x^{-\gamma}$ where $s_i > 0$ and $\gamma \in (0, 1)$.*

The first assumption is quite general and can be further weakened at the cost of additional notation. The second assumption is more restrictive than Assumption 10, but is well-motivated by the power law for individual learning [70]. Note that functions obeying Assumption 11 also satisfy Assumption 10.

Appraisal network

Let $A = \{a_{ij}\}_{i,j\in\{1,\dots,n\}}$ denote the $n \times n$ nonnegative, row-stochastic *appraisal matrix*, where a_{ij} is individual i's appraisal of individual j. The appraisal matrix represents the team's network structure and transactive memory system.

2.2.2 Model description and problem statement

In this work, we design a model where the workload assignment coevolves with the appraisals: the workload assignment changes as a function of the appraisals and the appraisals update based on perceived performance disparities for the assigned workload. Suppose at each time t, the team has a workload assignment $\boldsymbol{w}(t)$, individual performances $p(\boldsymbol{w}(t))$, and appraisal matrix $A(t)$. Since we are studying teams, it is reasonable to assume the appraisal network is strongly connected and each individual appraises themself. This translates to an irreducible initial appraisal matrix $A(0)$ with strictly positive self-appraisals $a_{ii}(0) > 0$ for all $i \in \{1, \dots, n\}$. All members also start with strictly positive workload $\boldsymbol{w}(0) \in \operatorname{int}(\Delta_n)$. For shorthand throughout the rest of the chapter, we use $A_0 = A(0)$ and $\boldsymbol{w}_0 = \boldsymbol{w}(0)$.

Before introducing the model, first we define the work flow function $F = [F_1(A, \boldsymbol{w}), \dots, F_n(A, \boldsymbol{w})]^\top$, where $F_i : [0,1]^{n\times n} \times \Delta_n \to \Delta_n$ describes how individual i adjusts their own work assignment. Then our coevolving assignment and appraisal process is quantified by the following dynamical system.

Definition 12 (ASAP (assignment and appraisal) model)**.** *Consider n performance functions p_i satisfying Assumption 10 or 11. The coevolution of the appraisal network*

$A(t)$ and workload assignment $\boldsymbol{w}(t)$ obey the following coupled dynamics,

$$\begin{aligned} \dot{a}_{ij} &= a_{ij}\Big(p_j(w_j) - \sum_{k=1}^{n} a_{ik}p_k(w_k)\Big), \\ \dot{w}_i &= F_i(A, \boldsymbol{w}), \end{aligned} \tag{2.2}$$

which reads in matrix form

$$\begin{aligned} \dot{A} &= A \odot \Big(\mathbb{1}_n p(\boldsymbol{w})^\top - Ap(\boldsymbol{w})\mathbb{1}_n^\top\Big), \\ \dot{\boldsymbol{w}} &= F(A, \boldsymbol{w}). \end{aligned} \tag{2.3}$$

The work flow function F obeys one of the following work flow models:

$$\textit{Donor-controlled:} \quad F_i(A, \boldsymbol{w}) = -w_i + \sum_{k=1}^{n} a_{ki}w_k, \tag{2.4}$$

$$\textit{Average-appraisal:} \quad F_i(A, \boldsymbol{w}) = -w_i + \frac{1}{n}\sum_{k=1}^{n} a_{ki}. \tag{2.5}$$

The matrix forms of the donor-controlled (2.4) *and average-appraisal* (2.5) *work flows are $F(A, \boldsymbol{w}) = -\boldsymbol{w} + A^\top \boldsymbol{w}$ and $F(A, \boldsymbol{w}) = -\boldsymbol{w} + \frac{1}{n}A^\top \mathbb{1}_n$, respectively.*

The appraisal weights of the ASAP model (2.2) update based on performance feedback between neighboring individuals. For neighboring team members i and j, i will increase their appraisal of j if j's performance is larger than the weighted average performance observed by i, i.e. $p_j(w_j) > \sum_{k=1}^{n} a_{ik}p_k(w_k)$. Individual i also updates their self-appraisal with the same mechanism. The irreducibility and strictly positive self-appraisal assumptions on the appraisal network means that every individual's performance is evaluated by themself and at least one other individual within the team.

The donor-controlled work flow (2.4) models a team where individuals exchange portions of their workload assignment with their neighbors, and the amount of work

exchanged depends on their current work assignments and the appraisal values. The work individual j gives to individual i has flow rate a_{ji} and is proportional to w_j. The average-appraisal work flow (2.5) assumes that each individual collects feedback from neighboring team members through appraisal evaluations. Each individual uses this feedback to calculate their average-appraisal $\frac{1}{n}\sum_{k=1}^{n} a_{ki}$, which is then used to adjust their own workload assignment. The average-appraisal is equivalent to the degree centrality of the appraisal network. Note that while the donor-controlled work flow is decentralized and distributed, the average-appraisal work flow is only distributed since it requires individuals to know the total number of team members.

In the following lemma, we show that the ASAP model is well-posed and the appraisal network maintains the same network topology for finite time.

Lemma 13 (Finite-time properties for the ASAP model)**.** *Consider the ASAP model 2.2 with donor controlled* (2.4) *or average appraisal* (2.5) *work flow. Assume A_0 is row-stochastic, irreducible, with strictly positive diagonal and $\boldsymbol{w}_0 \in \operatorname{int}(\Delta_n)$. Then for any finite $\Delta t > 0$, the following statements hold:*

1. *$\boldsymbol{w}(t) \in \operatorname{int}(\Delta_n)$ for $t \in [0, \Delta t]$;*

2. *$A(t)$ remains row-stochastic with the same zero/positive pattern for $t \in [0, \Delta t]$.*

Proof. Before proving statement 1, we give some properties of the appraisal dynamics. If $a_{ij}(t) = 0$, then $\dot{a}_{ij}(t) = 0$, which implies $a_{ij}(t) \geq 0$. By using the Hadamard product property (2.1), the matrix form of the appraisal dynamics can also be written as $\dot{A} = A\operatorname{diag}(p(\boldsymbol{w})) - \operatorname{diag}(Ap(\boldsymbol{w}))A$. Then for $A_0\mathbb{1}_n = \mathbb{1}_n$, $\dot{A}\mathbb{1}_n = \mathbb{0}_n$, so $A(t)$ remains row-stochastic for $t \geq 0$.

Next, we use $A(t)$ row-stochastic to prove $w(t) \in \operatorname{int}(\Delta_n)$ for donor-controlled work flow and $t \in [0, \Delta t]$. Left multiplying the $\boldsymbol{w}(t)$ dynamics by $\mathbb{1}_n^\top$, we have $\mathbb{1}_n^\top \dot{\boldsymbol{w}} = \mathbb{1}_n^\top(-\boldsymbol{w}+$

$A^\top \boldsymbol{w}) = \mathbb{0}_n$. Next, let $w_i(t) = \min_k\{w_k(t)\}$. For $\boldsymbol{w}_0 \in \text{int}(\Delta_n)$, $w_i(t) = \min_k\{w_k(t)\} = 0$, and $A(t) \geq 0$, then $\dot{w}_i(t) = \sum_{k=1}^n a_{ki}(t)w_k(t) \geq 0$. Therefore $\boldsymbol{w}(t) \in \Delta_n$. Lastly, we apply the Grönwall-Bellman Comparison Lemma to also show that $\boldsymbol{w}(t)$ lives in the relative interior of the simplex. For $w_i(0) > 0$ and $\dot{w}_i(t) = -w_i(t) + \sum_{k=1}^n a_{ki}(t)w_k(t) \geq -w_i(t)$, then $w_i(t) \geq w_i(0)e^{-t} > 0$ for $t \in [0, \Delta t]$. Therefore, if $\boldsymbol{w}_0 \in \text{int}(\Delta_n)$, then $\boldsymbol{w}(t) \in \text{int}(\Delta_n)$ for $t \in [0, \Delta t]$.

The proof for statement 1 can be extended to the average-appraisal work flow (2.5) following the same process, since $\dot{w}_i(t) = -w_i(t) + \frac{1}{n}\sum_{k=1}^n a_{ki}(t) \geq -w_i(t)$.

For statement 2, to prove that $A(t)$ maintains the same zero/positive pattern for $t \in [0, \Delta t]$, consider any i, j such that $a_{ij}(0) > 0$. Since $\boldsymbol{w}(t) \in \text{int}(\Delta_n)$, then $p(\boldsymbol{w}(t)) > 0$ by the performance function assumptions and $p_j(w_j) - \sum_{k=1}^n a_{ik}p_k(w_k)$ is finite for any i, j and $t \in [0, \Delta t]$. Let $p_{\max}(\boldsymbol{w}(t)) = \max_{k\in\{1,\dots,n\}}\{p_k(w_k)\}$. Then the convex combination of individual performances is upper bounded by $\sum_{k=1}^n a_{ik}p_k(w_k) \leq p_{\max}(\boldsymbol{w}(t))$. Now we can write the following lower bound for the time derivative of $a_{ij}(t)$,

$$\begin{aligned}\dot{a}_{ij}(t) &\geq a_{ij}(t)\big(p_j(w_j(t)) - \sum\nolimits_{k=1}^n a_{ik}(t)p_k(w_k(t))\big)\\ &\geq -a_{ij}(t)p_{\max}(\boldsymbol{w}(t)).\end{aligned}$$

Using the Grönwall-Bellman Comparison Lemma again, for $t \in [0, \Delta t]$, then

$$a_{ij}(t) \geq a_{ij}(0)\exp\left(-\int_0^t p_{\max}(\boldsymbol{w}(\tau))d\tau\right) > 0.$$

Therefore, $A(t)$ remains row-stochastic and maintains the same zero/positive pattern as A_0 for finite time. □

2.2.3 Team performance and optimal workload as model equilibria

We are interested in the collective team performance and while no single collective team performance function is widely accepted in the social sciences, we consider three such functions. Under minor technical assumptions, the optimal workload for all three is characterized by equal performance levels by the individuals and is an equilibrium point of the ASAP model. If $p_i(w_i)$ represents the marginal utility of individual i, then the collective team performance can be measured by the *total utility*,

$$\mathcal{H}_{\text{tot}}(\boldsymbol{w}) = \sum_{i=1}^{n} \int_0^{w_i} p_i(x)dx.$$

The team performance can alternatively be measured by the "weakest link" or *minimum performer*,

$$\mathcal{H}_{\min}(\boldsymbol{w}) = \min_{i\in\{1,\dots,n\}} \{p_i(w_i)\}.$$

Another metric often used is the *weighted average individual performance*:

$$\mathcal{H}_{\text{avg}}(\boldsymbol{w}) = \sum_{i=1}^{n} w_i p_i(w_i).$$

The next theorem clarifies when the workload maximizing either $\mathcal{H}_{\text{tot}}$, $\mathcal{H}_{\min}$, or $\mathcal{H}_{\text{avg}}$ is an equilibrium of the ASAP model.

Theorem 14 (Optimal performance as equilibria of dynamics)**.** *Consider performance functions p_i satisfying Assumption 10 for all $i \in \{1, \dots, n\}$. Then*

1. *there exists a unique pair $(p^*, \boldsymbol{w}^{\text{opt}})$ such that $p^* > 0$, $\boldsymbol{w}^{\text{opt}} \in \text{int}(\Delta_n)$, and $p(\boldsymbol{w}^{\text{opt}}) = p^* \mathbb{1}_n$.*

Additionally, let $\mathcal{H}$ denote $\mathcal{H}_{\text{tot}}$, $\mathcal{H}_{\min}$, or $\mathcal{H}_{\text{avg}}$. Let Assumption 11 hold when $\mathcal{H} =$

$\mathcal{H}_{\text{avg}}$. *Then*

2. $\boldsymbol{w}^{\text{opt}}$ *is the unique solution to*

$$\boldsymbol{w}^{\text{opt}} = \arg\max_{\boldsymbol{w}\in\Delta_n}\{\mathcal{H}(\boldsymbol{w})\}.$$

Finally, consider the ASAP model (2.2) *with donor-controlled work flow* (2.4) *and let* A_0 *be row-stochastic, irreducible, with strictly positive diagonal and* $\boldsymbol{w}_0 \in \text{int}(\Delta_n)$. *Then*

3. *there exists at least one matrix* A^* *with the same zero/positive pattern as* A_0 *that satisfies* $\boldsymbol{w}^{\text{opt}} = v_{\text{left}}(A^*)$*; and*

4. *every pair* $(A^*, \boldsymbol{w}^{\text{opt}})$*, such that* A^* *has the same zero/positive pattern as* A_0 *and* $\boldsymbol{w}^{\text{opt}} = v_{\text{left}}(A^*)$*, is an equilibrium.*

For average-appraisal work flow (2.5), statements 3-4 may not hold for $\boldsymbol{w}^{\text{opt}} = \frac{1}{n}(A^*)^\top \mathbb{1}_n$, since there may not exist an A^* with the same zero/positive pattern as A_0. Section 2.5 elaborates on these results.

Proof. Regarding statement 1, recall that p_i is C^1 and strictly decreasing by Assumption 10 or 11. Now we show that given our assumptions, there exists $\boldsymbol{w}^{\text{opt}} \in \text{int}(\Delta_n)$ such that $p(\boldsymbol{w}^{\text{opt}}) = p^*\mathbb{1}_n$ holds. Let p_i^{-1} denote the inverse of p_i and let $\circ$ denote the composition of functions where $f(g(x)) = (f \circ g)(x)$. Given $p_1(w_1) = p_i(w_i)$, then $w_i = (p_i^{-1} \circ p_1)(w_1)$ for all $i \neq 1$. Then taking into account $\boldsymbol{w}^{\text{opt}} \in \text{int}(\Delta_n)$,

$$w_1 + \sum\nolimits_{i=1}^{n} (p_i^{-1} \circ p_1)(w_1) = 1.$$

p_i strictly decreasing implies p_i^{-1} ($p_i^{-1} \circ p_1$ resp.) is strictly decreasing (strictly increasing resp.). Therefore the left hand side of the above equation is strictly increasing, so there

is a unique $w_1^{\text{opt}} \in (0,1)$ solving the equation. Therefore there is a unique $(p^*, \boldsymbol{w}^{\text{opt}})$ that satisfies $p(\boldsymbol{w}^{\text{opt}}) = p^* \mathbb{1}_n$, where $p^* = p_1(w_1^{\text{opt}}) > 0$.

Regarding statement 2, p_i is strictly decreasing, C^1, and convex by Assumption 10-11. Then $\mathcal{H}_{\text{tot}}$, $\mathcal{H}_{\min}$, and $\mathcal{H}_{\text{avg}}$ are all strictly concave. Since we are maximizing over a compact set, and $\mathcal{H}(\boldsymbol{w})$ is finite for $\boldsymbol{w} \in \Delta_n$, there exists a unique optimal solution $\boldsymbol{w}^{\text{opt}} \in \Delta_n$. Next we show that $\boldsymbol{w}^{\text{opt}}$ must satisfy $p(\boldsymbol{w}^{\text{opt}}) = p^* \mathbb{1}_n$ where $p^* > 0$ for each collective team performance measure and $\boldsymbol{w}^{\text{opt}} \in \text{int}(\Delta_n)$.

First, consider $\mathcal{H} = \mathcal{H}_{\text{tot}}$. Let $\boldsymbol{\mu} \in \mathbb{R}^n$ and $\lambda \in \mathbb{R}$. Then the KKT conditions are given by: $p(\boldsymbol{w}^{\text{opt}}) + \boldsymbol{\mu} - \lambda \mathbb{1}_n = \mathbb{0}_n$, $\boldsymbol{\mu} \odot \boldsymbol{w}^{\text{opt}} = \mathbb{0}_n$, and $\boldsymbol{\mu} \succeq \mathbb{0}_n$. If $\lambda \to \infty$, then $\boldsymbol{w}^{\text{opt}} = \mathbb{0}_n$ for the first KKT condition to hold, but we require $\boldsymbol{w}^{\text{opt}} \in \Delta_n$. Similarly, $w_i^{\text{opt}} = 0$ for any i would satisfy the second KKT condition, but violate the first KKT condition. As a result, $\lambda < \infty$ and $\boldsymbol{\mu} = \mathbb{0}_n$. This implies that $p_i(w_i^{\text{opt}}) = \lambda$ for all i. Therefore $\boldsymbol{w}^{\text{opt}} \in \text{int}(\Delta_n)$ and there exists $p^* = \lambda \in (0, \infty)$ such that $p(\boldsymbol{w}^{\text{opt}}) = p^* \mathbb{1}_n$.

Second, consider $\mathcal{H} = \mathcal{H}_{\min}$. Define the set $\arg\min(p(\boldsymbol{w})) = \{i \in \{1, \ldots, n\} \mid p_i(w_i) = \min_k\{p_k(w_k)\}\}$ and let $|\arg\min(p(\boldsymbol{w}))|$ denote the number of elements in $\arg\min(p(\boldsymbol{w}))$. We prove the claim by contradiction. Assume $\boldsymbol{w}^{\text{opt}}$ is the optimal solution such that there exists at least one $j \neq i$ such that $p_i(w_i^{\text{opt}}) < p_j(w_j^{\text{opt}})$ for $i \in \arg\min(p(\boldsymbol{w}))$. Then there exists a sufficiently small $\epsilon > 0$ and $\boldsymbol{w}^* \in \text{int}(\Delta_n)$ such that $\mathcal{H}_{\min}(\boldsymbol{w}^{\text{opt}}) < \mathcal{H}_{\min}(\boldsymbol{w}^*)$, where $w_i^* = w_i^{\text{opt}} - \epsilon$ and $w_j^* = w_j^{\text{opt}} + \epsilon |\arg\min(p(\boldsymbol{w}))|$. This contradicts the fact that $\boldsymbol{w}^{\text{opt}}$ is the optimal solution. Additionally, we can prove that $\boldsymbol{w}^{\text{opt}} \in \text{int}(\Delta_n)$ by assuming there exists at least one i such that $w_i = 0$ and following the same proof by contradiction process. Therefore $\boldsymbol{w}^{\text{opt}} \in \text{int}(\Delta_n)$ and $p(\boldsymbol{w}^{\text{opt}}) = p^* \mathbb{1}_n$.

Third, consider $\mathcal{H} = \mathcal{H}_{\text{avg}}$. Let $\boldsymbol{\mu} \in \mathbb{R}^n$ and $\lambda \in \mathbb{R}$. Then the KKT conditions are given by: $(1-\gamma)p(\boldsymbol{w}^*) + \boldsymbol{\mu} - \lambda \mathbb{1}_n = \mathbb{0}_n$, $\boldsymbol{\mu} \odot \boldsymbol{w}^* = \mathbb{0}_n$, and $\boldsymbol{\mu} \succeq \mathbb{0}_n$. The rest of the proof follows from the same argument as used for $\mathcal{H} = \mathcal{H}_{\text{tot}}$.

Regarding statements 3 and 4, let $a_d = [a_{11}, \ldots, a_{nn}]^\top \in [0,1]^n$ and $A(a_d, A_0) =$

$\mathrm{diag}(a_d) + (I_n - \mathrm{diag}(a_d))A_0$. We prove that there exists some $a_d^* > 0$ such that $\boldsymbol{w}^{\mathrm{opt}} = v_{\mathrm{left}}\big(A^*(a_d^*, A_0)\big)$. From the assumptions on A_0, then there exists $\bar{\boldsymbol{w}} = v_{\mathrm{left}}(A_0)$ such that $\sigma\bar{\boldsymbol{w}} = (I_n - \mathrm{diag}(a_d^*))\boldsymbol{w}^{\mathrm{opt}}$ for $\sigma \in \mathbb{R}$. Then solving for a_d^*, we have $a_d^* = \mathbb{1}_n - \sigma(\bar{\boldsymbol{w}} \oslash \boldsymbol{w}^{\mathrm{opt}})$. Next, we choose $\sigma = \epsilon / \max_i\{\bar{w}_i/w_i\}$ for $\epsilon \in (0,1)$, which gives the following bounds on a_{ii} for all i,

$$a_{ii} \in [1-\epsilon, 1-\epsilon \min_i\{\bar{w}_i/w_i\}(\max_i\{\bar{w}_i/w_i\})^{-1}] \subseteq (0,1).$$

With $a_d^* > \mathbb{0}_n$, then $A^*(a_d^*, A_0)$ has the same zero/positive pattern as $A(0)$. This shows that, given $\boldsymbol{w}^{\mathrm{opt}}$, there always exists a matrix A^* with left dominant eigenvector $\boldsymbol{w}^{\mathrm{opt}}$ and with the same pattern as $A(0)$.

Next, we prove that any such pair $(A^*, \boldsymbol{w}^{\mathrm{opt}})$ is an equilibrium. Our assumptions on A^* and the Perron-Frobenius theorem together imply that the $\mathrm{rank}(I_n - (A^*)^\top) = n-1$. For the ASAP model (2.2) with donor-controlled work flow (2.4), the equilibrium conditions on the self-appraisal states and work assignment read:

$$\mathbb{0}_n = \mathrm{diag}\left(a_d(A^*)\right)(I_n - A^*)p(\boldsymbol{w}^*), \tag{2.6}$$

$$\mathbb{0}_n = (A^* - I_n)^\top \boldsymbol{w}^*. \tag{2.7}$$

Equation (2.6) is satisfied because we know from statement 2 that $p(\boldsymbol{w}^{\mathrm{opt}}) = p^*\mathbb{1}_n$. Equation (2.7) is satisfied because we know $v_{\mathrm{left}}(A^*) = \boldsymbol{w}^{\mathrm{opt}}$. This concludes the proof of statements 3 and 4. □

The equilibria described in the above lemma also resemble an evolutionarily stable set [71], which is defined as the set of strategies with the same payoff. Our proof illustrates that at least one A^* always exists, but in general, there are multiple A^* matrices that satisfy a particular zero/positive irreducible matrix pattern with $\boldsymbol{w}^{\mathrm{opt}} = v_{\mathrm{left}}(A^*)$ with the same collective team performance. We will later show that, under mild conditions, this

optimal solution is an equilibrium of our dynamics with various attractivity properties (see Section 2.4 and 2.5).

2.3 Properties of Appraisal Dynamics: Conserved Quantities and Reduced Order Dynamics

In this section, we show that every cycle in the appraisal network is associated to a conserved quantity. Leveraging these conserved quantities, we reduce the appraisal dynamics to an $n-1$ dimensional submanifold. Before doing so, we introduce the notion of cycles, cycle path vectors, the cycle set, and the cycle space. For a given initial appraisal matrix A_0 with strictly positive diagonal, let m denote the total number of strictly positive interpersonal appraisals in the edge set $\mathcal{E}(A_0)$. Recall that if $a_{ij}(0) = 0$ for any i, j, then $\dot{a}_{ij} = 0$, which implies $a_{ij}(t) = 0$ for all $t \geq 0$. Therefore we can consider the total number of appraisal states to be the number of edges in A_0, which gives a total of $n + m$ appraisal states.

Definition 15 (Cycles, cycle path vectors, and cycle set)**.** *Consider the digraph $G(A)$ associated to matrix $A \in \mathbb{R}^{n\times n}_{\geq 0}$.*

A cycle *is an ordered sequence of nodes $r = \{r_1, \ldots, r_k, r_1\}$ with no node appearing more than once, that starts and ends at the same node, has at least two distinct nodes, and each sequential pair of nodes in the cycle denotes an edge $(r_i, r_{i+1}) \in \mathcal{E}(A)$. We do not consider self-loops, i.e. self-appraisal edges, to be part of any cycles.*

Let $C_r \in \{0, 1\}^m$ denote the cycle path vector *associated to cycle r. Let each off-diagonal edge of the appraisal matrix $(i, j) \in \mathcal{E}(A)$ be assigned to a number in the ordered*

set $\{1, \dots, m\}$. *For every edge* $e \in \{1, \dots, m\}$, *the* e*th component of* C_r *is defined as*

$$(C_r)_e = \begin{cases} +1, & \text{if edge } e \text{ is positively traversed by } C_r, \\ 0, & \text{otherwise.} \end{cases}$$

Let $\Phi(A)$ *denote the* cycle set, *i.e. the set of all cycles, in digraph* $G(A)$.

To refer to a particular cycle, we will use the cycle's associated cycle path vector, which then allows us to define the cycle space.

Definition 16 (Cycle space)**.** *A* cycle space *is a subspace of* $\mathbb{R}^m$ *spanned by cycle path vectors. By [72, pg. 29, Theorem 9], the cycle space of a strongly connected digraph* $G(A)$ *is spanned by a basis of* $\mu = m - n + 1$ *cycle path vectors.*

Let $C_B \in \{0,1\}^{m \times \mu}$ *denote a matrix where the columns are a basis of the cycle space.*

The following theorem 1. rigorously defines the conserved quantities associated to cycles in the appraisal network; 2. shows that the appraisal states can be reduced from dimension $n + m$ to $n - 1$ using the conserved quantities; and 3. uses both the previous properties to introduce reduced order dynamics that have a one-to-one correspondence with the appraisal trajectories.

Theorem 17 (Conserved cycle constants give reduced order dynamics)**.** *Consider the ASAP model* (12) *with donor-controlled* (2.4) *or average-appraisal* (2.5) *work flow. Given initial conditions* A_0 *row-stochastic, irreducible, with strictly positive diagonal and* $\boldsymbol{w}_0 \in \operatorname{int}(\Delta_n)$, *let* $(A(t), \boldsymbol{w}(t))$ *be the resulting trajectory. Then*

1. *for any cycle* r, *the quantity*

$$c_r = \prod_{(i,j) \in r} \frac{a_{ii}(t)}{a_{ij}(t)}, \tag{2.8}$$

is constant; we refer to $c_r \in (0,\infty)$ *as the cycle constant associated to cycle* $r \in \Phi(A_0)$*;*

2. *the appraisal matrix* $A(t)$ *takes value in a submanifold of dimension* $n-1$*;*

3. *given a solution* $(\boldsymbol{v}(t), \bar{\boldsymbol{w}}(t)) \in \mathbb{R}^n_{>0} \times \operatorname{int}(\Delta_n)$ *with initial condition* $(\boldsymbol{v}_0, \bar{\boldsymbol{w}}_0) = (\mathbb{1}_n, \boldsymbol{w}_0)$ *of the dynamics*

$$\begin{aligned} \dot{\boldsymbol{v}} &= \operatorname{diag}\big(p(\bar{\boldsymbol{w}}) - \bar{\boldsymbol{w}}^\top \mathcal{A}(\boldsymbol{v}) p(\bar{\boldsymbol{w}}) \mathbb{1}_n\big)\boldsymbol{v}, \\ \dot{\bar{\boldsymbol{w}}} &= F(\mathcal{A}(\boldsymbol{v}), \bar{\boldsymbol{w}}), \end{aligned} \tag{2.9}$$

where $\mathcal{A} : \mathbb{R}^n \to \mathbb{R}^{n\times n}$ *is defined by*

$$\mathcal{A}(\boldsymbol{v}) = \operatorname{diag}(A_0\boldsymbol{v})^{-1} A_0 \operatorname{diag}(\boldsymbol{v}), \tag{2.10}$$

then $A(t) = \mathcal{A}(\boldsymbol{v}(t))$ *and* $\boldsymbol{w}(t) = \bar{\boldsymbol{w}}(t)$*;*

4. *for every equilibrium* $(\boldsymbol{v}^*, \boldsymbol{w}^{\mathrm{opt}})$ *of* (2.9)*,* $(A^*, \boldsymbol{w}^{\mathrm{opt}})$ *is an equilibrium of* (12) *with* $A^* = \mathcal{A}(\boldsymbol{v}^*)$*;*

5. *if additionally* $A_0 > 0$*, then the positive matrix* $A(t) \oslash A_0$ *is rank 1 for all time* t*.*

Proof. Regarding statement 1, we show that c_r is constant for any $r \in \Phi(A_0)$ by taking the natural logarithm of both sides of (2.8) and showing that the derivative vanishes. By Lemma 13, $\ln(c_r)$ is well-defined since $a_{ii}(t), a_{ij}(t) > 0$ for any $a_{ij} \in r$ and finite time $t < \infty$.

$$\mathrm{d}t \ln(c_r) = \sum_{(i,j)\in r} \Big(\frac{\dot{a}_{ii}}{a_{ii}} - \frac{\dot{a}_{ij}}{a_{ij}}\Big) = \sum_{(i,j)\in r} \Big(\big(p_i(w_i) - \bar{p}_i(\boldsymbol{w})\big) - \big(p_j(w_j) - \bar{p}_i(\boldsymbol{w})\big)\Big) = 0.$$

Therefore, c_r is constant for all $r \in \Phi(A_0)$.

Regarding statement 2, first, we will introduce a change of variables from $A(t)$ to $B(t) = \{b_{ij}(t)\}_{i,j\in\{1,\dots,n\}} \in \mathbb{R}^{n\times n}_{\geq 0}$, that comes from the appraisal dynamics property that allows for row-stochasticity to be preserved. This allows the $n+m$ states of $A(t)$ to be reduced to m states of $B(t)$. Second, we show that there exists $\mu = m-n+1$ independent cycle constants, define constraint equations associated to the cycle constants, and apply the implicit function theorem to show that the m states of $B(t)$ further reduce to $n-1$ states.

Let $b_{ij}(t) = \frac{a_{ij}(t)}{a_{ii}(t)}$ for all i, j. This is well-defined in finite-time by Theorem 13 and the assumption that A_0 has strictly positive diagonal. Since the diagonal entries of $B(t)$ remain constant and zero-valued edges remain zero, then we can consider the total states of $B(t)$ to be the m off-diagonal edges of $B(t)$. Next, we introduce the cycle constant constraint functions and use the implicit function theorem to show that the m states can be further reduced to $n-1$ using the cycle constants. For edge $e = (i, j)$, let $b_{ij}(t) = b_e(t)$. Let $z = [x^\top, y^\top]^\top \in \mathbb{R}^m_{>0}$ where $x = [b_1, \dots, b_{m-\mu}]^\top \in \mathbb{R}^{m-\mu}_{>0}$ and $y = [b_{m-\mu+1}, \dots, b_m]^\top \in \mathbb{R}^\mu_{>0}$. Consider the cycle constant constraint function $g(x, y) = [g_1(x, y), \dots, g_\mu(x, y)]^\top : \mathbb{R}^{m-\mu}_{>0} \times \mathbb{R}^\mu_{>0} \to \mathbb{R}^\mu$, where $g_r(x, y) = \ln(c_r) - \sum_{(i,j)\in r} \ln(\frac{a_{ii}}{a_{ij}}) = 0$ is associated to cycle path vector C_r for all $r \in \{1, \dots, \mu\}$ and the selected cycles form a basis for the cycle subspace such that $C_{\mathrm{B}} = [C_1, \dots, C_\mu]$. In matrix form, $g(x, y)$ reads as

$$g(x, y) = \begin{bmatrix} \ln(c_1) \\ \vdots \\ \ln(c_\mu) \end{bmatrix} + C_B^\top \begin{bmatrix} \ln(b_1) \\ \vdots \\ \ln(b_m) \end{bmatrix} = \mathbb{0}_\mu.$$

We partition C_B into block matrices, $C_B = [\bar{C}_B^\top, \hat{C}_B^\top]^\top$ where $\bar{C}_B \in \{0, 1\}^{m-\mu\times\mu}$ and

$\hat{C}_B \in \{0,1\}^{\mu\times\mu}$. Then taking the partial derivative of $g(x,y)$ with respect to y,

$$\frac{\partial g(x,y)}{\partial y} = C_B^\top \begin{bmatrix} \mathbb{0}_{m-\mu\times\mu} \\ (\mathrm{diag}(y))^{-1} \end{bmatrix} = \hat{C}_B^\top (\mathrm{diag}(y))^{-1}.$$

The ordering of the rows of C_B is determined by the ordering of the edges $e \in \{1,\dots,m\}$. Since C_B is full column rank by definition, then there exists an edge ordering such that $\mathrm{rank}(\hat{C}_B) = \mu$. For this ordering with $\mathrm{rank}(\hat{C}_B) = \mu$, then $\mathrm{rank}(\frac{\partial g(x,y)}{\partial y}) = \mu$. By the implicit function theorem, $y \in \mathbb{R}^\mu_{>0}$ is a continuous function of $x \in \mathbb{R}^{m-\mu}_{>0} = \mathbb{R}^{n-1}$. Equivalently, B can then be reduced from m states to $m-\mu = m-(m-n+1) = n-1$. Therefore if $A(t)$ is irreducible with strictly positive diagonal, then $A(t)$ can be reduced to an $n-1$ dimensional submanifold.

Regarding statement 3, we show that, if $\boldsymbol{v}(t)$ satisfies the dynamics of (2.9), then $\mathcal{A}(\boldsymbol{v}(t))$ defined by equation (2.10) satisfies the original ASAP dynamics (12). For shorthand, let $\tilde{p}(\boldsymbol{v},\boldsymbol{w}) = \boldsymbol{w}^\top \mathcal{A}(\boldsymbol{v}) p(\boldsymbol{w})$. We compute:

$$\begin{aligned}
\dot{a}_{ij} &= \frac{a_{ij}(0)\dot{v}_j}{\sum_{k=1}^n a_{ik}(0)v_k} - \frac{a_{ij}(0)v_j \sum_{k=1}^n a_{ik}(0)\dot{v}_k}{\big(\sum_{k=1}^n a_{ik}(0)v_k\big)^2} \\
&= \frac{a_{ij}(0)v_j}{\sum_{k=1}^n a_{ik}(0)v_k}\left(p_j(w_j) - \tilde{p}(\boldsymbol{v},\boldsymbol{w}) - \sum_{k=1}^n \frac{a_{ik}(0)v_k\big(p_k(w_k) - \tilde{p}(\boldsymbol{v},\boldsymbol{w})\big)}{\sum_{h=1}^n a_{ih}(0)v_h}\right) \\
&= a_{ij}\left(p_j(w_j) - \sum\nolimits_{k=1}^n a_{ik}p_k(w_k)\right).
\end{aligned}$$

We also note that

$$A_0 = \mathcal{A}(\boldsymbol{v}(0)).$$

Our claim follows from the uniqueness of solutions to ordinary differential equations.

Statement 4 follows trivially from verifying that $(\boldsymbol{v}^*, \boldsymbol{w}^{\mathrm{opt}})$ and $(A^*, \boldsymbol{w}^{\mathrm{opt}})$ are equilibrium points of the corresponding dynamics with $A^* = \mathcal{A}(\boldsymbol{v}^*) > 0$.

Regarding statement 5, we first show that the positive matrix $A(t) \oslash A_0$ is rank 1 for all time t. First we multiply $A(t) \oslash A_0$ by the diagonal matrix $D = \mathrm{diag}([a_{11}(0)/a_{11}, \ldots, a_{n1}(0)/a_{n1}])$. Then we show that $D(A(t) \oslash A_0)$ is rank 1, which implies that $A(t) \oslash A_0$ is also rank 1.

$$D(A \oslash A_0) = \begin{bmatrix} 1 & \frac{a_{11}(0)}{a_{11}} \frac{a_{12}}{a_{12}(0)} & \cdots & \frac{a_{11}(0)a_{1n}}{a_{11}a_{1n}(0)} \\ \vdots & \vdots & \ddots & \vdots \\ 1 & \frac{a_{n1}(0)a_{n2}}{a_{n1}a_{n2}(0)} & \cdots & \frac{a_{n1}(0)a_{nn}}{a_{n1}a_{nn}(0)} \end{bmatrix}$$

By assumption $A_0 > 0$, $G(A)$ is a complete graph for finite t. Then the cycle constants (2.8), and any nodes $i \neq j \neq k$, we have $\frac{a_{kk}a_{jj}a_{ii}}{a_{kj}a_{ik}a_{ji}} = \frac{a_{kk}(0)a_{jj}(0)a_{ii}(0)}{a_{kj}(0)a_{ij}(0)a_{jk}(0)}$ and $\frac{a_{kk}a_{jj}}{a_{kj}a_{jk}} = \frac{a_{kk}(0)a_{jj}(0)}{a_{kj}(0)a_{jk}(0)}$. Rearranging these two equations gives $\frac{a_{ii}}{a_{ii}(0)} \frac{a_{ij}(0)}{a_{ij}} = \frac{a_{ki}}{a_{ki}(0)} \frac{a_{kj}(0)}{a_{kj}}$. This shows that every row of $D(A \oslash A_0)$ is equivalent and $\mathrm{rank}(D(A \oslash A_0)) = \mathrm{rank}(A \oslash A_0) = 1$. □

Case study for team of two

In order to illustrate the role of the cycle constants (2.8), we consider an example of a two-person team with performance functions $p_1(w_1) = (\frac{0.45}{w_1})^{0.9}$ and $p_2(w_2) = (\frac{0.55}{w_2})^{0.8}$. Figure 2.2 shows the evolution of the trajectories for various initial conditions of the ASAP model with donor-controlled work flow. The trajectories illustrate the conserved quantities associated to the cycles in the appraisal network, which is

$$c = \frac{a_{11}(0)a_{22}(0)}{(1 - a_{11}(0))(1 - a_{22}(0))} \tag{2.11}$$

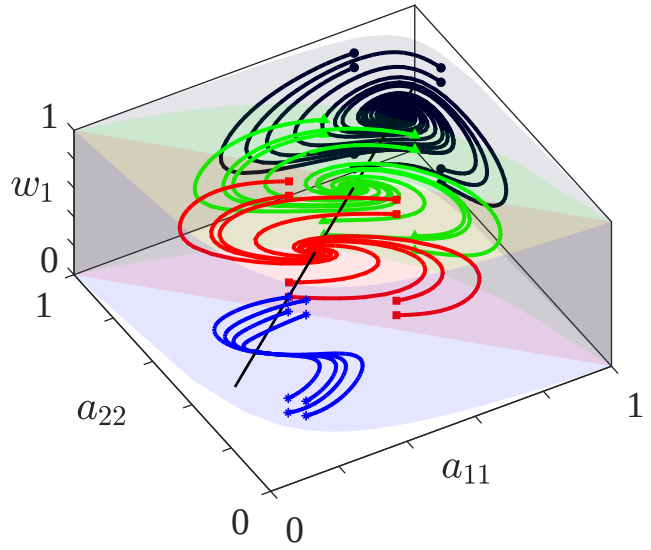

Figure 2.2: Trajectories of the ASAP (2.2) with donor-controlled work flow (2.4) for various initial conditions. The markers designate the initial values. All trajectories starting on a particular colored surface, remain on that colored surface, where the surfaces are associated to the conserved cycle constants. For $n = 2$, the dynamics reduce to the system (2.12) with cycle constant c given by (2.11). The color blue corresponds to $c < 1$, red to $c = 1$, and green and black to $c > 1$.

for the two-node case. Then the cycle constant c with Theorem 172 allows us to write the dynamics for $n = 2$ as

$$\begin{aligned} \dot{a}_{11} &= a_{11}(1 - a_{11})\big(p_1(w_1) - p_2(1 - w_1)\big), \\ \dot{w}_1 &= -w_1 + \left(\frac{a_{11}(1 - a_{11})(1 - c)w_1 + a_{11}}{c + a_{11}(1 - c)}\right). \end{aligned} \tag{2.12}$$

The cycle constants can be thought of as a parameter that measures the level of deviation between individual's initial perception of each other's skills. When $c_r = 1$ for some $r \in \Phi(A)$, then all individuals along cycle r are in agreement over the appraisals for every other individual.

2.4 Stability Analysis for the ASAP Model with Donor-Controlled Work Flow

In this section, we study the asymptotic behavior of the ASAP model with donor-controlled work flow. Our analysis is based on a Lyapunov argument. Utilizing this approach, we identify initial appraisal network conditions for teams with complete graphs where the optimal workload is learned without any other additional assumptions. Under a technical assumption, we also rigorously prove that for any strongly connected team, the dynamics will converge to the optimal workload.

The next lemma defines the performance-entropy function, which we show to be a Lyapunov function for the ASAP model under certain structural assumptions on the appraisal network.

Lemma 18 (Performance-entropy function)**.** *Consider the ASAP model* (12) *with donor-controlled work flow* (2.4)*. Assume A_0 row-stochastic, $\boldsymbol{w}_0 \in \operatorname{int}(\Delta_n)$, and there exists some A^* with the same zero/positive pattern as A_0 such that $\boldsymbol{w}^{\mathrm{opt}} = v_{\mathrm{left}}(A^*)$. Define the* performance-entropy function $V : \{a_{ij}\}_{(i,j)\in\mathcal{E}(A_0)} \times \operatorname{int}(\Delta_n) \to \mathbb{R}$ *by*

$$V(A, \boldsymbol{w}) = -\sum_{i=1}^{n} \left(\int_{w_i^{\mathrm{opt}}}^{w_i} p_i(x)dx + w_i^{\mathrm{opt}} \sum\nolimits_{\substack{k \text{ s.t.} \\ (i,k)\in\mathcal{E}(A_0)}} a_{ik}^* \ln\left(\frac{a_{ik}}{a_{ik}^*}\right) \right). \tag{2.13}$$

Then

1. *$V(A, \boldsymbol{w}) > 0$ for $A \neq A^*$ or $\boldsymbol{w} \neq \boldsymbol{w}^{\mathrm{opt}}$, and*

2. *the Lie derivative of V is*

$$\dot{V}(A, \boldsymbol{w}) = p(\boldsymbol{w})^\top (I_n - A^\top)(\boldsymbol{w} - \boldsymbol{w}^{\mathrm{opt}}). \tag{2.14}$$

The first term of the function is the rescaled total utility, $\mathcal{H}_{\text{tot}}(\boldsymbol{w}^{\text{opt}}) - \mathcal{H}_{\text{tot}}(\boldsymbol{w}) = -\sum_{i=1}^{n} \int_{w_i^{\text{opt}}}^{w_i} p_i(x)dx$. The second term, $w_i^{\text{opt}} \sum_{\substack{k \text{ s.t.} \\ (i,k)\in\mathcal{E}(A_0)}} a_{ik}^* \ln \frac{a_{ik}}{a_{ik}^*}$, is the Kullback-Liebler relative entropy measure [73].

Proof. By Assumption 10, $-\sum_{i=1}^{n} \int_{w_i^{\text{opt}}}^{w_i} p_i(x)dx$ is convex with minimum value if and only if $w_i = w_i^{\text{opt}}$. Therefore this term is positive definite for $\boldsymbol{w} \neq \boldsymbol{w}^{\text{opt}}$. Since the function $-\ln(\cdot)$ is strictly convex and $\sum_{k=1}^{n} a_{ik}^* = 1$, Jensen's inequality can be used to give the following lower bound,

$$-\sum_{\substack{k \text{ s.t.} \\ (i,k)\in\mathcal{E}(A_0)}} a_{ik}^* \ln\left(\frac{a_{ik}}{a_{ik}^*}\right) \geq 0,$$

where the inequality holds strictly if and only if $A \neq A^*$.

For the last statement of the lemma and with the assumption $\boldsymbol{w}^{\text{opt}} = v_{\text{left}}(A^*)$, the Lie derivative of V is

$$\begin{aligned}
\dot{V}(A, \boldsymbol{w}) &= -p(\boldsymbol{w})^\top \dot{\boldsymbol{w}} - (\boldsymbol{w}^{\text{opt}})^\top \big(A^* \odot (\dot{A} \oslash A)\big)\mathbb{1}_n \\
&= -p(\boldsymbol{w})^\top \dot{\boldsymbol{w}} - (\boldsymbol{w}^{\text{opt}})^\top \big(A^* \odot (\mathbb{1}_n p(\boldsymbol{w})^\top - Ap(\boldsymbol{w})\mathbb{1}_n^\top)\big)\mathbb{1}_n.
\end{aligned}$$

Then using Hadamard product property (2.1) and $\boldsymbol{w}^{\text{opt}} = v_{\text{left}}(A^*)$, $\dot{V}(A, \boldsymbol{w})$ further simplifies to

$$\begin{aligned}
\dot{V}(A, \boldsymbol{w}) &= -p(\boldsymbol{w})^\top \dot{\boldsymbol{w}} - (\boldsymbol{w}^{\text{opt}})^\top \big(A^* \operatorname{diag}(p(\boldsymbol{w})) - \operatorname{diag}(Ap(\boldsymbol{w}))A^*\big)\mathbb{1}_n \\
&= -p(\boldsymbol{w})^\top \dot{\boldsymbol{w}} - (\boldsymbol{w}^{\text{opt}})^\top \big(A^* p(\boldsymbol{w}) - Ap(\boldsymbol{w})\big) \\
&= p(\boldsymbol{w})^\top (I_n - A^\top)(\boldsymbol{w} - \boldsymbol{w}^{\text{opt}}).
\end{aligned}$$

□

The next theorem states the convergence results to the optimal workload for various cases on the connectivity of the initial appraisal matrix. For donor-controlled work flow, the optimal workload is equal to the eigenvector centrality of the network [74], which is

a measure of the individual's importance as a function of the network structure and appraisal values. Therefore the equilibrium workload value quantifies each team member's contribution to the team and learning the optimal workload reflects the development of TMS within the team. Note that statement 3 relies on the assumption that conjecture given in the statement holds. This conjecture is discussed further at the end of the section, where we provide extensive simulations to illustrate its high likelihood.

Theorem 19 (Convergence to optimal workload for strongly connected teams)**.** *Consider the ASAP model* (2.2) *with donor-controlled work flow* (2.4)*. Given initial conditions* A_0 *row-stochastic, irreducible, with strictly positive diagonal and* $\boldsymbol{w}_0 \in \operatorname{int}(\Delta_n)$*. The following statements hold:*

1. *if* $n = 2$ *and* $A_0 > 0$*, then* $\lim_{t\to\infty}(A(t), \boldsymbol{w}(t)) = (A^*, \boldsymbol{w}^{\text{opt}})$ *such that* $A^* > 0$ *is row-stochastic and* $\boldsymbol{w}^{\text{opt}} = v_{\text{left}}(A^*)$*;*

2. *if there exists* $a_d(0) = [a_{11}(0), \dots a_{nn}(0)]^\top \in \operatorname{int}(\Delta_n)$ *such that* $A_0 = \mathbb{1}_n a_d(0)^\top$ *is also rank* 1*, then* $\lim_{t\to\infty}(A(t), \boldsymbol{w}(t)) = (\mathbb{1}_n(\boldsymbol{w}^{\text{opt}})^\top, \boldsymbol{w}^{\text{opt}})$*.*

Moreover, define $\boldsymbol{v}(t) \in \mathbb{R}^n_{>0}$ *as in Theorem 173.*

3. *If* $\boldsymbol{v}(t)$ *is uniformly bounded for all* $(A_0, \boldsymbol{w}_0)$ *and* $t \geq 0$*, then* $\lim_{t\to\infty}(A(t), \boldsymbol{w}(t)) = (A^*, \boldsymbol{w}^{\text{opt}})$ *such that* A^* *is row-stochastic, has the same zero/positive pattern as* A_0*, and* $\boldsymbol{w}^{\text{opt}} = v_{\text{left}}(A^*)$*.*

Proof. Statement 1 follows directly from the fact that the function defined by (2.13) is a Lyapunov function for the system. For brevity, we omit the proof of Statement 1, since it follows a similar proof to statement 2.

Regarding statement 2, if A_0 is the rank 1 form given by the theorem assumptions, then $c_r = 1$ for all cycles $r \in \Phi(A_0)$ by Theorem 171. This implies that $a_{ij} = a_{kj}$ for any

j, all $i \neq k$, and $t \geq 0$. For the storage function $V(A, \boldsymbol{w})$ as defined by (2.13), the Lie derivative (2.14) simplifies to,

$$\begin{aligned}\dot{V} &= p(\boldsymbol{w})^\top (I_n - a_d \mathbb{1}_n^\top)\boldsymbol{w} - p(\boldsymbol{w})^\top (I_n - a_d \mathbb{1}_n^\top)\boldsymbol{w}^{\text{opt}} \\ &= p(\boldsymbol{w})^\top (\boldsymbol{w} - a_d - \boldsymbol{w}^{\text{opt}} + a_d) = p(\boldsymbol{w})^\top (\boldsymbol{w} - \boldsymbol{w}^{\text{opt}}).\end{aligned}$$

From $\boldsymbol{w}, \boldsymbol{w}^{\text{opt}} \in \Delta_n$, then $p(\boldsymbol{w})^\top (\boldsymbol{w} - \boldsymbol{w}^{\text{opt}}) = (p(\boldsymbol{w}) - p(\boldsymbol{w}^{\text{opt}}))^\top (\boldsymbol{w} - \boldsymbol{w}^{\text{opt}}) = (p(\boldsymbol{w}) - p^* \mathbb{1}_n)^\top (\boldsymbol{w} - \boldsymbol{w}^{\text{opt}})$. Since $p_i(w_i)$ strictly decreasing by Assumption 10 or 11, then $\dot{V} < 0$ for $\boldsymbol{w} \neq \boldsymbol{w}^{\text{opt}}$. Then V is a Lyapunov function for the rank 1 initial appraisal case and $\lim_{t\to\infty}(A(t), \boldsymbol{w}(t)) = (\mathbb{1}_n(\boldsymbol{w}^{\text{opt}})^\top, \boldsymbol{w}^{\text{opt}})$.

Regarding statement 3, we start by considering the equivalent reduced order appraisal dynamics (2.9) and by proving asymptotic convergence using LaSalle's Invariance Principle. Define the function $\bar{V} : \mathbb{R}^n_{>0} \times \text{int}(\Delta_n) \to \mathbb{R}$, which is a modification of the storage function (2.13) by replacing the term $\frac{a_{ij}}{a^*_{ij}}$ with v_i for all i, j,

$$\bar{V}(\boldsymbol{v}, \boldsymbol{w}) = -\sum_{i=1}^{n} \left(\int_{w_i^{\text{opt}}}^{w_i} p_i(x)dx + w_i^{\text{opt}} \ln(v_i) \right). \tag{2.15}$$

The Lie derivative of $\bar{V}$ is

$$\begin{aligned}\dot{\bar{V}} &= -p(\boldsymbol{w})^\top \dot{\boldsymbol{w}} - (\dot{\boldsymbol{v}} \oslash \boldsymbol{v})^\top \boldsymbol{w}^{\text{opt}} \\ &= p(\boldsymbol{w})^\top (I_n - A^\top)\boldsymbol{w} - \left(p(\boldsymbol{w}) - p(\boldsymbol{w})^\top A^\top \boldsymbol{w} \mathbb{1}_n\right)^\top \boldsymbol{w}^{\text{opt}} \\ &= p(\boldsymbol{w})^\top (\boldsymbol{w} - \boldsymbol{w}^{\text{opt}}) \leq 0.\end{aligned}$$

We can now define the sublevel set $\Omega = \{\boldsymbol{v} \in \mathbb{R}^n_{>0}, \boldsymbol{w} \in \text{int}(\Delta_n) \mid \bar{V}(\boldsymbol{v}, \boldsymbol{w}) \leq \bar{V}(\boldsymbol{v}_0, \boldsymbol{w}_0), t \geq 0\}$, which is closed and positively invariant. Note that if there exists any i such that $\lim_{t\to\infty} v_i = 0$, then $\lim_{t\to\infty} \bar{V}(\cdot) = \infty$. However, $\dot{\bar{V}} \leq 0$ and $\bar{V}(\boldsymbol{v}_0, \boldsymbol{w}_0)$

is finite, so $\boldsymbol{v}(t)$ must be bounded away from zero by a positive value for $t \geq 0$. By our assumption, $\boldsymbol{v}(t)$ is also upper bounded. Then there exists constants $v_{\min}, v_{\max} > 0$ such that $\boldsymbol{v} \in [v_{\min}, v_{\max}]^n$. Then by LaSalle's Invariance Principle, the trajectories must converge to the largest invariant set contained in the intersection of

$$\{\boldsymbol{v} \in [v_{\min}, v_{\max}]^n, \boldsymbol{w} \in \operatorname{int}(\Delta_n) \mid \dot{\tilde{V}} = 0\} \cap \Omega.$$

By Theorem 14, if $\dot{\tilde{V}} = 0$, then $w = \boldsymbol{w}^{\text{opt}}$ and $p(\boldsymbol{w}^{\text{opt}}) = p^* \mathbb{1}_n$. This implies $\dot{\boldsymbol{v}} = \operatorname{diag}(\boldsymbol{v})(p(\boldsymbol{w}^{\text{opt}}) - p^* \mathbb{1}_n) = 0$, so $\boldsymbol{v} = \boldsymbol{v}^* > 0$. By Theorem 174, $(\boldsymbol{v}^*, \boldsymbol{w}^{\text{opt}})$ corresponds to equilibrium $(A^*, \boldsymbol{w}^{\text{opt}})$. Therefore $\lim_{t\to\infty}(\boldsymbol{v}(t), \boldsymbol{w}(t)) = (\boldsymbol{v}^*, \boldsymbol{w}^{\text{opt}})$ is equivalent to $\lim_{t\to\infty}(A(t), \boldsymbol{w}(t)) = (A^*, \boldsymbol{w}^{\text{opt}})$ such that $\boldsymbol{w}^{\text{opt}} = v_{\text{left}}(A^*)$ and $A^* = \mathcal{A}(\boldsymbol{v}^*)$, where A^* and A_0 have the same zero/positive pattern. □

Theorem 193 establishes asymptotic convergence from all initial conditions of interest under the assumption that the trajectory $\boldsymbol{v}(t)$ is uniformly bounded. Throughout our numerical simulation studies, we have empirically observed that this assumption has always been satisfied. We now present a Monte Carlo analysis [75] to estimate the probability that this uniform boundedness assumption holds.

For any randomly generated pair $(A_0, \boldsymbol{w}_0)$, which corresponds to $\boldsymbol{v}_0 = \mathbb{1}_n$, define the indicator function $\mathbb{I} : \mathbb{R}^n_{\geq 0} \times \operatorname{int}(\Delta_n) \to \{0, 1\}$ as

1. $\mathbb{I}(A_0, \boldsymbol{w}_0) = 1$ if there exists $v_{\max}$ such that $\boldsymbol{v}(t) \leq v_{\max} \mathbb{1}_n$ for all $t \in [0, 1000]$;
2. $\mathbb{I}(A_0, \boldsymbol{w}_0) = 0$, otherwise.

Let $p = \mathbb{P}[\mathbb{I}(A_0, \boldsymbol{w}_0) = 0]$. We estimate p as follows. We generate $N \in \mathbb{N}$ independent identically distributed random sample pairs, $(A_0^{(i)}, \boldsymbol{w}_0^{(i)})$ for $i \in \{1, \ldots, N\}$, where $A_0^{(i)} \in [0, 1]^{n \times n}$ is row-stochastic, irreducible, with strictly positive diagonal and $\boldsymbol{w}_0^{(i)} \in \operatorname{int}(\Delta_n)$.

Finally, we define the empirical probability as

$$\hat{p}_N = \frac{1}{N}\sum_{i=1}^{N} \mathbb{I}(A_0^{(i)}, \boldsymbol{w}_0^{(i)}).$$

For any accuracy $1-\epsilon \in (0,1)$ and confidence level $1-\xi \in (0,1)$, then by the Chernoff Bound [75, Equation 9.14], $|\hat{p}-p| < \epsilon$ with probability greater than confidence level $1-\xi$ if

$$N \geq \frac{1}{2\epsilon^2} \log \frac{2}{\xi}. \tag{2.16}$$

For $\epsilon = \xi = 0.01$, the Chernoff bound (2.16) is satisfied by $N = 27\,000$.

Our simulation setup is as follows. We run 27 000 independent MATLAB simulations for the ASAP model (2.2) with donor-controlled work flow (2.5). We consider $n = 6$, irreducible with strictly positive diagonal A_0 generated using the Erdös-Renyi random graph model with edge connectivity probability 0.3, and performance functions of the form $p_i(w_i) = (\frac{s_i}{w_i})^{\gamma_i}$ for $\gamma_i \in (0,1)$ and $[s_1, \ldots, s_n] \in \text{int}(\Delta_n)$. We find that $\hat{p}_N = 1$. Therefore, we can make the following statement.

Consider 1. $n = 6$*; 2.* A_0 *irreducible with strictly positive diagonal generated by the Erdös-Renyi random graph model with edge connectivity probability* 0.3*, and randomly generated edge weights normalized to be row-stochastic; and 3.* $\boldsymbol{w}_0 \in \text{int}(\Delta_n)$*. Then with* 99% *confidence level, there is at least* 0.99% *probability that* $\|\boldsymbol{v}(t)\|$ *is uniformly upper bounded for* $t \in [0, 1000]$*.*

2.5 Stability Analysis for the ASAP Model with Average-Appraisal Work Flow

This section investigates the asymptotic behavior of the ASAP model (2.2) with average-appraisal work flow (2.5). In contrast with the eigenvector centrality model, we observe that strongly connected teams obeying this work flow model are not always able to learn their optimal work assignment. First we give a necessary condition on the initial appraisal matrix and optimal work assignment for convergence to the optimal team performance. Second, we prove that learning the optimal work assignment can be guaranteed if the team has a complete network topology or if the collective team performance is optimized by an equally distributed workload. Note that the results in Sections 2.2-2.3 also hold for average-appraisal work flow, only if the equilibrium satisfies $\boldsymbol{w}^{\text{opt}} = \frac{1}{n}(A^*)^\top \mathbb{1}_n$.

Let $\lceil x \rceil$ denote the ceiling function which rounds up all elements of x to the nearest integer. The following lemma gives a condition that guarantees when the team is unable to learn the optimal workload assignment.

Lemma 20 (Condition for failure to learn optimal work assignment for the degree centrality model)**.** *Consider the ASAP model* (2.2) *with average-appraisal work flow* (2.5)*. Assume A_0 row-stochastic and $\boldsymbol{w}_0 \in \text{int}(\Delta_n)$. If there exists at least one $i \in \{1, \dots, n\}$ such that $w_i^{\text{opt}} > \max\{\frac{1}{n}\sum_{k=1}^n \lceil a_{ki}(0) \rceil, w_i(0)\}$. Then $\boldsymbol{w}(t) \neq \boldsymbol{w}^{\text{opt}}$ for any $t \geq 0$.*

Proof. By the Grönwall-Bellman Comparison Lemma, $\dot{w}_i \leq -w_i + \frac{1}{n}\sum_{k=1}^n \lceil a_{ki}(0) \rceil$ implies that

$$\begin{aligned} w_i(t) &\leq -w_i(0)e^{-t} + \frac{1}{n}\sum\nolimits_{k=1}^n \lceil a_{ki}(0) \rceil (e^{-t} - 1) \\ &\leq \max\Big\{\frac{1}{n}\sum\nolimits_{k=1}^n \lceil a_{ki}(0) \rceil, w_i(0)\Big\}. \end{aligned}$$

Therefore if there exists at least one i such that $w_i^{\text{opt}} > \max\{\frac{1}{n}\sum_{k=1}^{n}\lceil a_{ki}(0)\rceil, w_i(0)\}$, then $w_i(t) \neq w_i^{\text{opt}}$. □

This sufficient condition for failure to learn the optimal workload can also be stated as a necessary condition for learning the optimal workload. In other words, if $\lim_{t\to\infty} \boldsymbol{w}(t) = \boldsymbol{w}^{\text{opt}}$, then $\boldsymbol{w}_i^{\text{opt}} \leq \max\{\frac{1}{n}\sum_{k=1}^{n}\lceil a_{ki}(0)\rceil, w_i(0)\}$ for all i.

While the average-appraisal work flow does not converge to the optimal equilibrium for strongly connected teams and general initial conditions, the following lemma describes two cases that do guarantee learning of the optimal workload.

Lemma 21 (Convergence to optimal workload for average-appraisal work flow)**.** *Consider the ASAP model* (2.2) *with average-appraisal work flow* (2.5)*. The following statements hold.*

1. *If A_0 is row-stochastic, irreducible, with strictly positive diagonal, $\boldsymbol{w}(0) \in \text{int}(\Delta_n)$, and $\boldsymbol{w}^{\text{opt}} = \frac{1}{n}\mathbb{1}_n$, then $\lim_{t\to\infty}(A(t), \boldsymbol{w}(t)) = (A^*, \frac{1}{n}\mathbb{1}_n)$ where A^* has the same zero/positive pattern as A_0 and is doubly-stochastic with $\frac{1}{n}(A^*)^\top\mathbb{1}_n = \frac{1}{n}\mathbb{1}_n$;*

2. *if $A_0 > 0$ is row-stochastic and $\boldsymbol{w}(0) \in \text{int}(\Delta_n)$, then $\lim_{t\to\infty}(A(t), \boldsymbol{w}(t)) = (A^*, \boldsymbol{w}^{\text{opt}})$ where $A^* > 0$ and $\boldsymbol{w}^{\text{opt}} = \frac{1}{n}(A^*)^\top\mathbb{1}_n$.*

Proof. Regarding statement 1, the storage function from (2.13) is a Lyapunov function for the given dynamics with assumption $\boldsymbol{w}^{\text{opt}} = \frac{1}{n}\mathbb{1}_n = \frac{1}{n}(A^*)^\top\mathbb{1}_n$. The Lie derivative $\dot{V}$ is

$$\begin{aligned}\dot{V}(A, \boldsymbol{w}) &= -p(\boldsymbol{w})^\top\dot{\boldsymbol{w}} - (\boldsymbol{w}^{\text{opt}})^\top(A^* - A)p(\boldsymbol{w}).\\ &= p(\boldsymbol{w})^\top\Big(\boldsymbol{w} - \frac{1}{n}A^\top\mathbb{1}_n - \frac{1}{n}(A^*)^\top\mathbb{1}_n + \frac{1}{n}A^\top\mathbb{1}_n\Big)\\ &= p(\boldsymbol{w})^\top(\boldsymbol{w} - \boldsymbol{w}^{\text{opt}}) \leq 0.\end{aligned}$$

By Lemma 18, $V = 0$ if and only if $\boldsymbol{w} = \boldsymbol{w}^{\text{opt}} = \frac{1}{n}\mathbb{1}_n$ and $A = A^*$ such that $\frac{1}{n}(A^*)^\top \mathbb{1}_n = \frac{1}{n}\mathbb{1}_n$. Therefore $\lim_{t\to\infty}(A(t), \boldsymbol{w}(t)) = (A^*, \frac{1}{n}\mathbb{1}_n)$ where A_0 and A^* have the same zero/positive pattern.

Regarding statement 2, consider the reduced order dynamics (2.9), with the following shorthand notation $\tilde{p}(\boldsymbol{v}, \boldsymbol{w}) = \boldsymbol{w}^\top \mathcal{A}(\boldsymbol{v}) p(\boldsymbol{w})$. Define the function $\bar{V} : \mathbb{R}^n_{>0} \times \text{int}(\Delta_n) \to \mathbb{R}$ as

$$\bar{V}(\boldsymbol{v}, \boldsymbol{w}) = \sum_{i=1}^{n} \Big(- \int_{w_i^{\text{opt}}}^{w_i} p_i(x)dx - w_i^{\text{opt}} \ln(v_i) + \frac{1}{n} \ln\Big(\sum\nolimits_{k=1}^{n} a_{ik}(0) v_k \Big) \Big).$$

First, we show that $\bar{V}$ is lower bounded. Second, we illustrate that $\bar{V}$ is monotonically decreasing for $\boldsymbol{w} \neq \boldsymbol{w}^{\text{opt}}$. Then this allows us to show convergence to an optimal equilibrium.

Let $a_{\min} = \min_{i,j}\{a_{ij}(0)\}$. From the proof of Lemma 18, $-\int_{w_i^{\text{opt}}}^{w_i} p_i(x)dx \geq 0$ for all i. Then $\bar{V}$ is lower bounded by

$$\begin{aligned} \bar{V} &\geq -\sum_{i=1}^{n} \left(w_i^{\text{opt}} \ln(v_i) + \frac{1}{n} \ln\Big(\frac{1}{a_{\min} \|\boldsymbol{v}\|_1} \Big) \right) \\ &\geq \ln(a_{\min}) - \sum_{i=1}^{n} w_i^{\text{opt}} \ln\Big(\frac{v_i}{\|\boldsymbol{v}\|_1} \Big) \geq \ln(a_{\min}). \end{aligned}$$

Now we show that $\dot{\bar{V}} \leq 0$. Define the function $\boldsymbol{u} : \mathbb{R}^n_{>0} \to \mathbb{R}^n_{>0}$, where $\boldsymbol{u}(\boldsymbol{v}) = \text{diag}(A_0 \boldsymbol{v})^{-1}$, which reads element-wise as $u_i(\boldsymbol{v}) = \sum_{k=1}^{n} a_{ik}(0) v_k$. Using $A(t) = \mathcal{A}(\boldsymbol{v}(t))$ as in (2.10), then the rate of change of $\boldsymbol{u}$ is given by

$$\dot{\boldsymbol{u}} = -\,\text{diag}(\boldsymbol{u})^2 A_0 \dot{\boldsymbol{v}} = -\,\text{diag}(\boldsymbol{u})\big(Ap(\boldsymbol{w}) - \tilde{p}(\boldsymbol{v}, \boldsymbol{w}) \mathbb{1}_n \big).$$

Plugging $\boldsymbol{u}$ into $\bar{V}$, the Lie derivative of $\bar{V}$ is

$$\begin{aligned}
\dot{\bar{V}}(\boldsymbol{v},\boldsymbol{w}) &= -p(\boldsymbol{w})^\top \dot{\boldsymbol{w}} - (\dot{\boldsymbol{v}} \oslash \boldsymbol{v})^\top \boldsymbol{w}^{\mathbf{opt}} - \frac{1}{n}(\dot{\boldsymbol{u}} \oslash \boldsymbol{u})^\top \mathbb{1}_n \\
&= -p(\boldsymbol{w})^\top \left(-\boldsymbol{w} + \frac{1}{n} A^\top \mathbb{1}_n \right) - \left(p(\boldsymbol{w}) - \tilde{p}(\boldsymbol{v},\boldsymbol{w})\mathbb{1}_n\right)^\top \boldsymbol{w}^{\mathrm{opt}} \\
&- \qquad \frac{1}{n}\left(-Ap(\boldsymbol{w}) + \tilde{p}(\boldsymbol{v},\boldsymbol{w})\mathbb{1}_n\right)^\top \mathbb{1}_n \\
&= p(\boldsymbol{w})^\top \left(\boldsymbol{w} - \boldsymbol{w}^{\mathrm{opt}}\right) + \tilde{p}(\boldsymbol{v},\boldsymbol{w})\left(\mathbb{1}_n^\top \boldsymbol{w}^{\mathrm{opt}} - \frac{1}{n}\mathbb{1}_n^\top \mathbb{1}_n\right) \\
&= p(\boldsymbol{w})^\top (\boldsymbol{w} - \boldsymbol{w}^{\mathrm{opt}}) \leq 0.
\end{aligned}$$

Since $\dot{\bar{V}} \leq 0$, implies that $\bar{V}(\boldsymbol{v},\boldsymbol{w}) \leq \bar{V}(\boldsymbol{v}_0,\boldsymbol{w}_0) < \infty$, we can conclude that there exists some strictly positive constant $v_{\min} > 0$ such that $\boldsymbol{v} \geq v_{\min}\mathbb{1}_n$.

Note that $\dot{\bar{V}} = 0$ if and only if $\boldsymbol{w} = \boldsymbol{w}^{\mathrm{opt}}$ by Lemma 18. Because $\bar{V}$ has a finite lower bound and is monotonically decreasing for $\boldsymbol{w} \neq \boldsymbol{w}^{\mathrm{opt}}$, then as $t \to \infty$, $\bar{V}$ will decrease to the level set where $\boldsymbol{w} = \boldsymbol{w}^{\mathrm{opt}}$. Then $\boldsymbol{w} = \boldsymbol{w}^{\mathrm{opt}}$ implies $\dot{\boldsymbol{w}} = 0$ and $\dot{\boldsymbol{v}} = 0$. Therefore $\lim_{t\to\infty}(\boldsymbol{v},\boldsymbol{w}) = (\boldsymbol{v}^*, \boldsymbol{w}^{\mathrm{opt}})$ such that $\boldsymbol{w}^{\mathrm{opt}} = \frac{1}{n}\mathcal{A}(\boldsymbol{v}^*)^\top \mathbb{1}_n = \frac{1}{n}(A^*)^\top \mathbb{1}_n$. □

2.6 Numerical Simulations

In this section, we utilize numerical simulations to investigate various cases of the ASAP model to illustrate when teams succeed and fail at optimizing their collective performance.

For all the simulations in this section, we consider performance functions of the form $p_i(w_i) = (\frac{s_i}{w_i})^\gamma$ for $\gamma \in (0,1)$ and all i, which satisfy Assumptions 10-11. Then the same optimal workload maximizes any choice of collective team performance we have introduced.

First, we provide an example of a team with a strongly connected appraisal net-

work and strictly positive self-appraisal weights, i.e. satisfying the assumptions of Theorem 193, to illustrate a case where the team learns the optimal work assignment. Figure 2.3 illustrates the evolution of the appraisal network and work assignment of the ASAP model (2.2) with donor-controlled work flow (2.4).

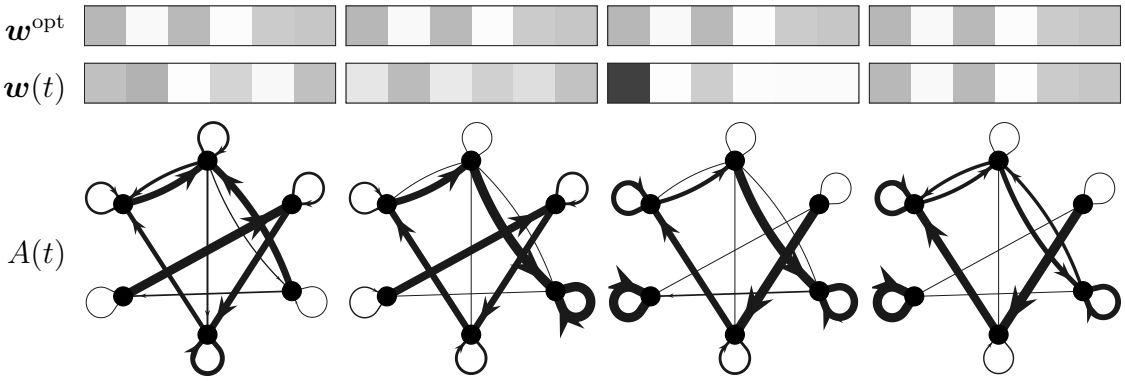

Figure 2.3: Visualization of the evolution of $\boldsymbol{w}(t)$ and $A(t)$ obeying the ASAP Model (2.2) with donor-controlled work flow (2.4). For the work assignment vector, the darker the entry, the higher value it has. For the appraisal matrix, the thicker the edge is, the higher the appraisal edge weight is. The team's initial appraisal network is strongly connected with strictly positive self-appraisals, and is an example of a team that successfully learns the work assignment that maximizes the collective team performance. The plots pictured are at times $t = \{0, 1, 10, 1000\}$, from left to right.

2.6.1 Distributed optimization illustrated with switching team members

Next we consider another example of the ASAP model (2.2) with donor-controlled work flow (2.4), where individuals are switching in and out of the team. Under the behavior governed by the ASAP model, only affected neighboring individuals need to be aware of an addition or subtraction of a team member, since the model is both distributed and decentralized. In this example, when individual j is added to the team as a neighbor of individual i, i allocates a portion of their work assignment to the new individual j.

Similarly, if individual j is removed, then j's neighbors will absorb j's workload. Let $k = 1$, $k = 2$, and $k = 3$ denote the subteams from time intervals $t \in [0, 5)$, $t \in [5, 15)$, and $t \in [15, \infty)$, respectively. Then let $\mathcal{H}_{\text{tot}}^{(k)}$ denote the collective performance for the kth subteam. Figure 2.4 illustrates the appraisal network topologies of each subteam and the evolution of the workload $\boldsymbol{w}(t)$ and normalized collective team performance $\mathcal{H}_{\text{tot}}^{(k)}$.

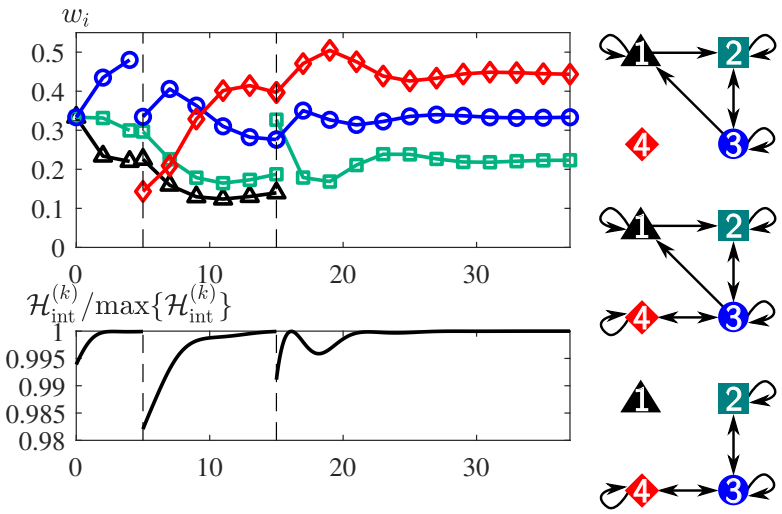

Figure 2.4: Evolution of the ASAP model (2.2) with donor-controlled work flow (2.4) where individuals are being added and removed from the team. From top to bottom, the digraphs depict the topology of the team for $t \in [0, 5)$, $t \in [5, 15)$ and $t \in [15, \infty)$. At $t = 10$, individual 4 (in red diamond) is added to the team and individual 3 gives a portion of their work to individual 4. At $t = 20$, individual 1 (in black triangle) is removed from the team, and 1's work assignment is given to individual 2.

2.6.2 Failure to learn

Partial observation of performance feedback does not guarantee learning optimal work assignment

Partial observation occurs when the appraisal network does not have the desired strongly connected property, resulting in team members having insufficient feedback

to determine their optimal work assignment. We consider an example of the ASAP model (2.2) with donor-controlled work flow (2.4) and reducible initial appraisal network A_0. Figure 2.5 illustrates how some appraisal weights between neighboring individuals approach zero asymptotically, resulting in the team not being capable of learning the work distribution that maximizes the collective team performance.

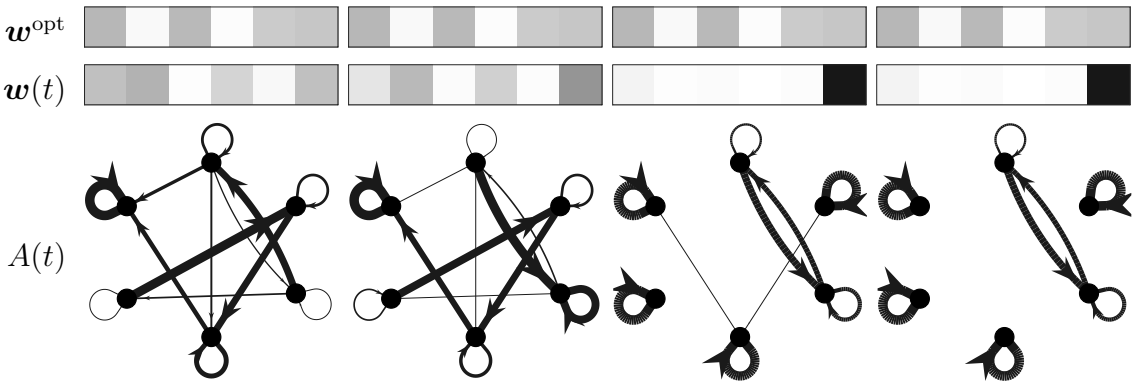

Figure 2.5: Example of failure to learn the optimal work assignment. Visualization of the evolution of $\boldsymbol{w}(t)$ and $A(t)$ obeying the ASAP model (2.2) with donor-controlled work flow (2.4) and A_0 weakly connected. For the work assignment vector, the darker the entry, the higher value it has. For the appraisal matrix, the thicker the edge is, the higher the appraisal edge weight is. The plots pictured are at times $t = \{0, 1, 10, 1000\}$, from left to right.

Average-appraisal feedback limits direct cooperation

Figure 2.6 is an example of a team obeying the ASAP model (2.2) with average-appraisal work flow (2.5). Even if the team does not satisfy the sufficient conditions for failure from Lemma 20, when individuals adjust their work assignment with only their average-appraisal as the input, the team may still not succeed in learning the correct workload to maximize the team performance.

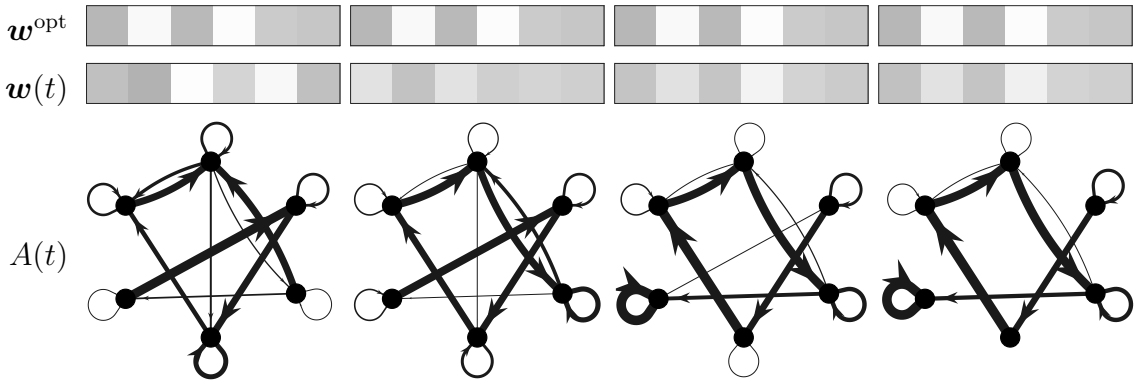

Figure 2.6: Example of failure to learn the optimal work assignment. Visualization of the evolution of $\boldsymbol{w}(t)$ and $A(t)$ obeying the ASAP model (2.2) with average-appraisal work flow (2.5). A_0 is strongly connected and $\boldsymbol{w}^{\text{opt}}$, $\boldsymbol{w}_0$, and A_0 satisfy the sufficient condition for failure to learn the optimal workload given by Lemma 20. For the work assignment vector, the darker the entry, the higher value it has. For the appraisal matrix, the thicker the edge is, the higher the appraisal edge weight is. The plots pictured are at times $t = \{0, 1, 10, 1000\}$, from left to right.

2.7 Conclusion

This chapter proposes novel models for the evolution of interpersonal appraisals and the assignment of workload in a team of individuals engaged in a sequence of tasks. We propose appraisal networks as a mathematical multi-agent model for the applied psychological concept of TMS. For two natural models of workload assignment, we establish conditions under which a correct TMS develops and allows the team to achieve optimal workload assignment and optimal performance. Our two proposed workload assignment mechanisms feature different degrees of coordination among team members. The donor-controlled work flow model requires a higher level of coordination compared to the average-appraisal work flow and, as a result, achieves optimal behavior under weaker requirements on the initial appraisal matrix.

Possible future research directions include studying team's behavior when individuals in the team update their appraisals and work assignments asynchronously. The updates could be modeled using an additional contact network with switching topology. More

investigation can also be done to determine if it is possible to predict which appraisal weights in a weakly connected network approach zero asymptotically, using only information on the initial work distribution and appraisal values.

Chapter 3

Estimating Influence Networks Using Cognitive Dynamic Models

3.1 Introduction

Inevitably, relationships among collaborating actors evolve over time, with people changing their opinions or appraisals of one another. Such relationships form a network structure called an influence/appraisal network [76–81] with signed edges that may portray trust/distrust, friendship/enmity, and like/dislike [82]. In our study, we use the terms *influence* and *appraisal* interchangeably. Investigations of the evolution of such networks draw on a rich body of literature on opinion dynamics. DeGroot *et al.* [76], and Friedkin *et al.* [77] propose widely-established models of opinion change and the conditions of consensus formation. Altafini *et al.* [83]'s model considers diverging opinions under antagonistic interactions. Such models are surveyed in Proskurnikov *et al.* [84]. Influence system specifications play a pivotal role in all of these studies. Note that these opinion dynamic models assume the influence network of a group is given a prior. Our goal is to quantitatively estimate the influence network among individuals in a group,

where the influence network within the group is represented by a row-stochastic matrix. The estimation of this matrix paves the way for solving problems such as influence maximization [85, 86]; viral marketing [87, 88]; personalized recommendation [89]; feed rankings [90]; target advertisement [91]; selecting influential tweeters [92, 93]; and selecting informative blogs [94].

Literature review

Classic studies of the antecedents of interpersonal influence include French and Raven's work [95] on the bases of social power, and cognitive biases research [96] showed that individuals are accorded influence based on their job titles, past performance, friends' opinions, etc. There has also been mathematical modeling of the endogenous evolution of appraisal networks. Friedkin *et al.* [59] showed how reflected appraisal mechanisms elevate or dampen the self-weights of group members along a sequence of issues. Jia *et al.* [80] proposed the DeGroot-Friedkin model, where the appraisal network evolves as a function of the social power within the group. Jia *et al.* [97] also studied how over time, the coevolution of appraisal and influence networks leads to a generalized model of structural balance theory [98–104]. Mei *et al.* [58] modeled collective learning in teams of individuals using appraisal networks, where the appraisal dynamics change as a function of the performance of individuals within the team.

Research on transactive memory systems (TMS) [105–108] provide an approach to formation of influence systems. A TMS is characterized by individuals' skills and knowledge, combined with members' collective understanding of which members possess what knowledge [107, 109, 110]. As members observe the task performances of each other, their understanding of "who knows what" tends to converge to an accurate assessment, leading to greater coordination and integration of members' skills. Empirical research [105–108]

across a range of team types and settings demonstrate a strong positive relationship between the development of a team TMS and team performance. The research indicates for the purpose of improving self performance, individuals tend to find experts via demonstrability in their group during intellective tasks [103]. Unlike judgemental issues, for intellective tasks there exists a demonstrable mathematical or verbal correct answer that can be distinguished by high-performing teammates [103].

Research in social comparison theory has shown that individuals tend to evaluate their own abilities by biased comparisons with their peers. In particular, Woods [111] describes several motivations behind biased social comparison such as self-esteem protection [112], lack of appropriate incentives [113], or the existence of dominant individuals who skew member contributions [114, 115]. Davison *et al.* [115]'s experimental results show that low-performing individuals tend to overestimate (resp. underestimate) low-performers (resp. high-performers), i.e. high-performing individuals are better able to recognize other experts than low-performing individuals. To study such psychological cognitive biases, several scientists have conducted group experimental studies by self and peer evaluations [114, 116, 117].

Research on confidence heuristics [118, 119] has shown that the more self-confident individuals are, the more influence they are accorded by others. Confidence heuristics is defined based on a social and psychological norm, whereby more confidently expressed arguments signal better information, allowing an efficient revelation of information and decision-making based on expressed confidence [118].

We build on the above three lines of research. Although the problem of estimating social power [80, 120], and influence networks have been studied before [121–123], existing research lacks empirical studies as they are mostly based on theory and grounded on simulation-based analyses [58]. Moreover, previous studies on influence estimation has focused on proxies of influence such as propagation of hashtags, quotes, and retweets [123–

128]. An impactful study by Almaatouq *et al.* [129] finds that social influence is significantly correlated with confidence and correctness. However, no estimation method is proposed that mathematically formulates how these factors contribute to the underlying dynamics of influence. Furthermore, we find these two factors alone do not lead to the most accurate predictions of self-reported influence for small teams with static networks in this empirical setting. Studies on the empirical estimation of the weighted network of who-influences-whom are rare [130, 131]. In the present work, we probe more deeply into the foundations of the links between individual performance, self-confidence and social comparison on interpersonal influence. Our work bridges the gap between empirical and simulation-based results by utilizing sociology-inspired mechanisms and machine-learning based models to estimate the social influence in groups. Overall, to the best of our knowledge, this study is the first to estimate the influence matrices in a text-based shared media among individuals, collected from a human subject experiment, where teammates communicate via a broadcast system to solve intellective tasks.

3.1.1 Contributions

We have the following two main contributions in this chapter. First, we find empirical support for widely established theories in psychology, sociology and management regarding the effect of TMS [105, 106, 108], confidence heuristics [118, 119] and social comparison theory [111, 115] on individuals' influence over their teammates. Second, we introduce a novel cognitive dynamic model based on the aforementioned theory regarding how influence is accorded from others. This cognitive dynamic model is validated against the empirical data and can be used to estimate influence matrices using past reported influence matrices and individual performance. We provide analytical and simulation results on the asymptotic behavior of the model for the case with identically performing

individuals.

Chapter organization

Section 3.2 describes the experiment setup, hypotheses for how interpersonal influence is accorded, and regression analysis supporting our hypotheses in the data. Section 3.3 introduces the dynamical models. Section 3.4 contains the analysis of the models and numerical simulation examples. Section 3.5 validates our main cognitive dynamic model on the experimental data, including a comparison to machine learning based models.

Notation

Let $\mathbb{1}_n$ ($\mathbb{0}_n$ resp.) denote the n-dimensional column vector with all ones (zero resp.). Let I_n represent the $n \times n$ identity matrix. For a matrix or vector $B \in \mathbb{R}^{n \times m}$, let $B \geq 0$ and $B > 0$ denote component-wise inequalities. Given $x = [x_1, \ldots, x_n]^\top \in \mathbb{R}^n$, let $\mathrm{diag}(x)$ denote the $n \times n$ diagonal matrix such that the ith entry on the diagonal equals x_i. Define the n-dimensional simplex as $\Delta_n = \{x \in \mathbb{R}^n \mid \mathbb{1}_n^\top x = 1, x \geq 0\}$ and the relative interior of the simplex as $\mathrm{int}(\Delta_n) = \{x \in \mathbb{R}^n \mid \mathbb{1}_n^\top x = 1, x > 0\}$.

A nonnegative matrix $B \geq 0$ is row-stochastic if $B\mathbb{1}_n = \mathbb{1}_n$. For B irreducible and row-stochastic, $v_{\mathrm{left}}(B)$ denotes the left dominant eigenvector of B, i.e., the entry-wise positive left eigenvector normalized to have unit sum and associated with the dominant eigenvalue of B [69, Perron Frobenius theorem].

3.2 Experimental Design and Data Analysis

3.2.1 Experimental design

We collected data for 31 teams comprising of $n = 4$ human members each. Each team is presented with the same sequence of 45 trivia questions that fall into three categories: Science and Technology, History and Mythology, and Literature and Media. Every team has two minutes to answer each question. First, team members answer individually before the answers are revealed to the team. Second, they are asked to collaborate on a single unanimous response. Lastly, the platform reveals the correct answer immediately after a team submits their answer. Thus, they are provided with immediate feedback on their performance after every response. The design also incorporates a multi-part incentive for subjects to seek the correct answer on each question: an evolving team performance score; an option to consult with one of four available AI-agents after the team discussion (the AI-agents may or may not provide a correct answer) which, if exercised, must lower the team's performance score regardless of whether provides a correct or incorrect answer; and feedback to each team on correct and incorrect answers. This multi-part incentive structure operated to concentrate the attention of the team on the evaluation of the relative expertise of their members.

This experimental setting was run on the Platform for Online Group Studies (POGS) and tests the participants' intellective memory. Each experiment consists of nine rounds of five intellective questions each, with teams surveyed after each round. At the end of each round, subjects are asked to record the influence of their teammates in their decision-making process as a percent value, such that the sum of all values adds up to 100. Every subject assumes they are given a total of 100 chips and instructed to distribute these chips to indicate the relative importance of each member in determining their own final answer on all past problems. Thus, the number of chips that a subject allocates to a particular

member should indicate the extent to which they were personally influenced by that member. The number of chips that subjects allocate to themselves should indicate the extent to which their final answer was not affected by the conversation. If an individual felt that all conversations so far provided no influence to their choice of answer, then they would put 100 besides their own name. If the conversation caused them to abandon their approach to the problem, then they are instructed to put zero beside their own name and allocate all the chips to one or more of the other members.

After normalization, the self-reported interpersonal influences form a row-stochastic influence matrix for every round, containing only non-negative entries (in a row-stochastic matrix every row sums up to one). The platform ensures that in each inquiry, the reported influence matrix has non-negative entries and is row-stochastic. Additionally, the platform collects a log of all the instant messages including time of message and content during every question, the individual and group answers, and the self-reported influence matrices.

Since the platform displays the correct answer to every question immediately after the group submits its response, attentive subjects can use the individual responses and text discussion to keep track of which individual teammates may have expertise in one or more areas over the course of the experiment. Thus, along the problem sequence, the team may solve problems more efficiently and also more accurately.

The experimental logs show that most teams reached a consensus when answering the questions. Every team reached a consensus on average 42 times on the sequence of 45 questions posed to them. All self-reported influence networks are found to be unilaterally connected and the majority are strongly connected. More precisely, out of 279 influence matrices reports, only six ($\sim$2%) are not strongly connected which happen only when one person assigns all their influence to only themselves. Almost all of the not strongly connected cases were reported early in the experiment. With respect to the convergence

of influence, in the last round, in 90% of the teams, at least half of the subjects reported the same ranking order of influences for all members including themselves. Additionally, we observe that in ∼74% of the teams the influence assignments converge to a single person as being the most influential unanimously reported by the team, and that ∼23% of the teams converge to two individuals as being equally the most influential members.

In this experiment, subjects read and answer every question individually. Ergo, the individual performance (expertise) can be measured by the ratio of correct answers one gives individually, prior to seeing others' answers and the discussion phase. Assuming individuals can potentially keep track of others' expertise by recalling their answers or their chat messages, we study if individual expertise plays a prominent role in the amount of social influence one receives. Note that M shows the ground truth influence matrix.

3.2.2 Origins of Interpersonal Influence

The following hypotheses, motivated from past research, are empirically supported by our experimental results and are captured by the cognitive dynamic models we introduce.

Hypothesis 1. *Individuals with higher expertise are accorded higher interpersonal influence from the group.*

Hypothesis 2. *Individuals with lower expertise have diminished ability to recognize experts in the group.*

Hypothesis 3. *Individuals with higher confidence are accorded higher interpersonal influence from the group.*

3.2.3 Regression study of origins of influence

In order to support our previously introduced hypotheses for the origins of influence, we use the Generalized Linear Model (GLM) method to show that the there is empirical

support of the hypotheses within our dataset.

To quantitatively test the three hypotheses, we use the following definitions for confidence, expertise, and influence. Within our dataset, we consider teams of $n = 4$ individuals, rounds indexed by $t \in \{1, \ldots, 9\}$, and teams $m \in \{1, \ldots, 31\}$. Let $M^m(t) \in [0,1]^{n \times n}$ be team m's row-stochastic influence networks reported in round t of the experimental data. The ith row and jth column of the influence network, $M^m_{ij}(t)$, represents i's appraisal of j, or equivalently the amount of influence individual j has on i. In this chapter, we use appraisal network and influence network interchangeably. Let *confidence* be defined as an individual's self influence, such that $a^m_{ii}(t)$ is individual i's confidence. Define the confidence vector for team m at round t as $M^m_d(t) = [m^m_{11}(t), ..., m^m_{nn}(t)]^\top \in [0,1]^n$. The performance vector of team m is denoted by $p^m(t) = [p^m_1(t), \ldots, p^m_n(t)]^\top \in \Delta_n$, where $p^m_i(t)$ represents the normalized individual performance of individual i at round t. For the experimental data, the performance is defined as the normalized cumulative correctness rate up to the given round. The cumulative correctness rate vector is defined as $r^m(t) = [r^m_1, \ldots, r^m_n]^\top \in [0,1]^n$, where $r^m_i(t) = \frac{\text{\# of correct answers up to round } t}{\text{\# of questions up to round } t}$. Then the performance from the data is defined as $p^m(t) = \frac{1}{\mathbb{1}_n^\top r^m(t)} r^m(t)$. The performance reflects the expertise of an individual, so we refer to $p(t)$ as the expertise or performance, interchangeably.

Regression study of individual expertise versus reversion to mean We use the Generalized Linear Model (GLM) method to solve the regression problem for individual expertise versus mean reversion, in order to empirically support Hypothesis 2. We define the following measure for mean reversion of individual i,

$$D^m_i(t) = \sum_{j=1}^{n} \left| M^m_{ij}(t) - \frac{1}{n} \right|^2. \tag{3.1}$$

The empirical evidence for Hypothesis 2 is obtained via regression on expertise and mean reversion. Table 3.1 shows the regression results for predicting mean reversion for every individual. Our results show the more expert one individual is, the more different than equal they appraise their teammates as the expertise is positively and statistically significant of predictive power of the reversion to the mean ($p - value < 0.05$) in all teams.

Table 3.1: Regression result for predicting mean reversion, with Generalized Linear Model (GLM) regression coefficients and their statistical significance in estimating mean reversion over all rounds and teams within the experiment (all 45 questions and 31 teams). The statistical significance using the p-value is portrayed with *** for $p < 0.01$ and ** for $p < 0.05$. This result shows that expertise is statistically and positively predictive of mean reversion.

Predicting mean reversion, $D_i^m(t)$	Feature-set 1
Intercept	0.10 ***
Expertise, $p_i^m(t)$	**0.07 ****
	Log-likelihood: 384.4 AIC: -764.8 BIC: -754.4

Regression study of performance and confidence versus total influence Here, GLM method is used to solve the regression problem for performance and confidence versus total influence. The results of these regression analyses provide empirical support for Hypothesis 1 and 3. Let the *total influence* of individual i at time t represent the total influence of i, defined as $\sum_{k=1}^{n} m_{ik}^m(t)$. Table 3.2 shows the coefficients and their statistical significance in three least-squares problems performance versus total influence, confidence versus total influence, and performance and confidence versus total influence.

Table 3.2 shows that introducing more variables in columns has increased log-likelihood, Bayesian Information Criterion (BIC), and Akaike Information Criterion (AIC). It shows that expertise has a consistently positive and statistical predictive-power

Table 3.2: Regression result for predicting total influence, with Generalized Linear Model (GLM) regression coefficients and their statistical significance in estimating local total influence over all rounds and teams within the experiment (all 45 questions and 31 teams). The statistical significance using the p-value is portrayed with *** for $p < 0.01$ and ** for $p < 0.05$. The amount of Variance Inflation Factor (VIF) is provided in parenthesis; this factor estimates how much the variance of a regression coefficient is inflated due to multicollinearity in the model. It is known [132] that statistical results remain significant in models with multicorrelated independent variables when VIF < 5. Let LL stand for log-likelihood. Taking into account the interactions of all variables, we find that expertise and confidence are consistently statistically predictive of total influence.

Predicting total influence, $\sum_{k=1}^{n} m_{ki}^{m}(t)$	Feature-set 1	Feature-set 2	Feature-set 3
Intercept	0.13 ***	0.19 ***	0.12 ***
Expertise, $p_i^m(t)$	**0.20 *** **		**0.17 *** (VIF: 1.05)**
Confidence, $m_{ii}^m(t)$		**0.14 *** **	**0.11 *** (VIF: 1.05)**
	LL: 162.86 AIC: -321.7 BIC: -316.3	LL: 162.90 AIC: -321.8 BIC: -316.4	LL: 168.12 AIC: -330.2 BIC: -322.1

on persuasiveness (the empirical evidence for Hypothesis 1). The statistical significance is robust even when considering expertise and confidence, together. Also, confidence has a positive statistical predictive-power to predict total influence (the empirical evidence for Hypothesis 3). However, its coefficient (importance) is less than the expertise (aligned with research in confidence heuristics [118]). This result is found when the platform provides immediate feedback for every question. If no feedback is provided or there is no right or wrong answer (i.e. judgmental questions), people might use confidence as a more substantial metric in their appraisal distribution.

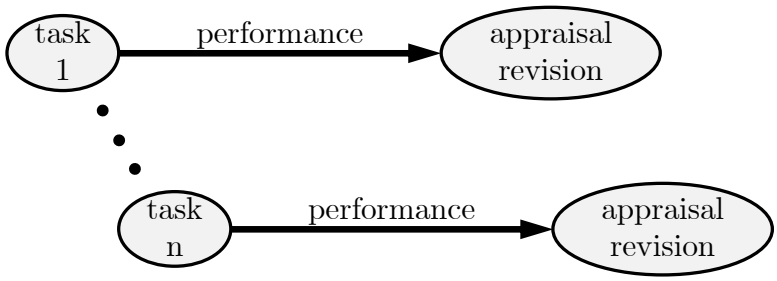

Figure 3.1: Architectural overview on the appraisal model with constant workload studied in this chapter. Given an intellective task to complete, team members divide the work evenly and revises their appraisals of neighboring members based on each neighbor's individual performance. The objective is for the team to learn who has the highest expertise within the team, and accurately evaluate one another relative to skill level.

3.3 Problem Framework for Modeling Evolution of Influence Networks

In this section, we introduce several dynamical models that capture how interpersonal influence evolves over time. The models are formulated such that established sociological concepts are baked into their equations. Our main model, called the Differentiation, Reversion, Perceived Expertise (DRP) model, encodes all three of our proposed hypotheses. Later in this chapter, we validate our model with the dataset, and show that it is capable of forecasting the team's influence networks.

Our models assume that each team obeys the architecture shown in Figure 3.1, where each team is given a sequence of tasks and the work assignment is distributed equally per task. After each task, we assume that individuals can observe their team members' performance and confidence levels, which drive changes in the influence network.

Recall that $M^m(t)$ represents the ground truth influence matrix from the dataset for team m at round t. Let $A^m(t) \in [0,1]^{n\times n}$ be the row-stochastic influence network given by a particular dynamical model for $t \geq 0$. Note that $A^m(t)$ can be considered an estimate of $M^m(t)$. Let $A_d(t) = [a_{11}(t), ..., a_{nn}(t)]^\top \in [0,1]^n$ be the associated *confidence* vector,

where $a_{ii}^m(t)$ represents individual i's *confidence* level. Let $p^m = [p_1^m, \ldots, p_n^m] \in \Delta_n$ denote the normalized performance, where p_i^m is the individual performance of person i. For our dynamical models, we assume that since performance is a reflection of the expertise of an individual, then performance is constant. When only discussing the dynamical models, we drop the m superscript denoting the team from $A^m(t)$ and $p^m(t)$.

Consider the perceived expertise, defined as follows.

Definition 22. *The* perceived expertise*, denoted by* $\hat{p}(p, A_d(t)) \in \Delta_n$*, is defined as*

$$\hat{p}\big(p, A_d(t)\big) = \frac{1}{p^\top A_d(t)\big)} \operatorname{diag}\big(A_d(t)\big)p. \tag{3.2}$$

For shorthand, we will refer to $\hat{p}(p, A_d(t))$ *as* $\hat{p}(t)$*.*

We propose several discrete-time dynamical models, of the form

$$A(t+1) = T(p, A(t)), \quad \text{for } t \geq 0.$$

Our proposed models also use a scaling parameter $\tau \in (0, 1)$ that can be adjusted to change the time-scale of the dynamics. If we have information on past reported influence matrices and expertise levels of team members, these models can be used to predict future influence matrices.

Model 23 (Differentiation model (D model))**.** *Motivated by Hypothesis 1, this model assumes individuals assign influence based on the individual expertise, where individuals with higher expertise are accorded higher influence. The model is defined for all* $i, j \in \{1, \ldots, n\}$ *as*

$$a_{ij}(t+1) = (1-\tau)a_{ij}(t) + \tau p_j, \tag{3.3}$$

which reads in matrix form as $A(t+1) = (1-\tau)A(t) + \tau \mathbb{1}_n p^\top$*.*

Model 24 (Differentiation, Reversion model (DR model))**.** *Motivated by Hypotheses 1 and 2, this model is based on the D model and assumes high-performing individuals are accorded more influence and low-performing individuals tend to assign influence weights uniformly amongst team members. The model is defined for all* $i, j \in \{1, \ldots, n\}$ *as*

$$a_{ij}(t+1) = (1-\tau)a_{ij}(t) + \tau\Big(p_i p_j + \big(1-p_i\big)\frac{1}{n}\Big), \tag{3.4}$$

which reads in matrix form as

$$A(t+1) = (1-\tau)A(t) + \tau\Big(pp^\top + \frac{1}{n}\big(\mathbb{1}_n - p\big)\mathbb{1}_n^\top\Big).$$

Model 25 (Cognitive dynamic model based on Differentiation, Reversion, Perceived expertise model (DRP model))**.** *Motivated by Hypotheses 1, 2 and 3, this model is an extension of* (3.5)*, where everyone's expertise is misevaluated based on their own self-confidence. The model then uses the perceived expertise* (3.2) *to learn how much influence is accorded to one another. Figure 3.4 depicts for both single-round and multi-round prediction, using all three hypotheses baked in this model provides the most accurate and consistent estimation. This model is defined for all* $i, j \in \{1, \ldots, n\}$ *as*

$$a_{ij}(t+1) = (1-\tau)a_{ij}(t) + \tau\Big(\hat{p}_i(t)\hat{p}_j(t) + \big(1-\hat{p}_i(t)\big)\frac{1}{n}\Big). \tag{3.5}$$

3.4 Stability Analysis

In this section, provide remarks and analysis on convergence behavior for the DRP model under uniform expertise. We omit examples of the D and DR models, since these affine models have straightforward asymptotic behavior.

Remark 26. *For the DRP model, the dynamics of the self-influence matrix weights is closed from the dynamics of the interpersonal influence weights, and can be written as only a function of* $a_d(t)$*,*

$$A_d(t+1) = (1-\tau)A_d(t) + \tau\Big(\operatorname{diag}(\hat{p}(t))\hat{p}(t) + \operatorname{diag}(\mathbb{1}_n - \hat{p}(t))\frac{1}{n}\mathbb{1}_n\Big). \tag{3.6}$$

Then the dynamics of the interpersonal influence evolve as a function of the self-influence weights and the initial condition $A(0)$*. This cascading effect illustrates how confidence drives influence.*

The following Lemma states that the D, DR, and DRP model are well-posed and the dynamics preserves row-stochasticity of the influence matrices.

Lemma 27 (Dynamic models preserve row-stochasticity)**.** *Consider the D model* (3.3)*, DR model* (3.4)*, and DRP model* (3.5) *with* $\tau \in (0,1)$ *and* $p(t) = p = [0,1]^n$*. If* $A(0)$ *is row-stochastic, then* $A(t)$ *remains row-stochastic for all* $t \geq 0$ *under the D and DR model.*

If additionally, there exists at least one i *such that* $a_{ii}(0) > 0$ *and* $p_i > 0$*, then the DRP models are well-posed for finite* t *and* $A(t)$ *remains row-stochastic for all* $t \geq 0$*.*

Proof. It is straightforward to see that the first statement holds by verifying $A(t+1)\mathbb{1}_n = T\big(p, A(t)\big)\mathbb{1}_n = \mathbb{1}_n$ for the D and DR models.

For the DRP models, per our assumption that there exists at least one i such that $a_{ii}(0) > 0$ and $p_i > 0$, then $p^\top A_d(0) > 0$. Additionally, both models guarantee that $a_{ij}(t) \geq (1-\tau)^{(t-1)}a_{ij}(0) \geq 0$ for all i, j and $t \geq 0$. Then by our assumptions, $p^\top A_d(t) > 0$ for finite time $t \geq 0$. Therefore the DP and DRP model dynamics are well-posed.

Next we show that the DRP dynamics preserves row-stochasticity. By definition, the

sum of the perceived expertise is $\mathbb{1}_n^\top \hat{p} = \big(A_d(t)^\top \hat{p}(t)\big)^{-1} A_d(t)^\top \hat{p}(t) = 1$. Then

$$\begin{aligned} A(t+1)\mathbb{1}_n &= (1-\tau)A(t)\mathbb{1}_n + \tau\Big(\operatorname{diag}\big(\hat{p}(t)\big)\mathbb{1}_n \hat{p}(t)^\top \mathbb{1}_n + \frac{1}{n}\operatorname{diag}\big(\mathbb{1}_n - \hat{p}(t)\big)\mathbb{1}_n \mathbb{1}_n^\top \mathbb{1}_n\Big) \\ &= (1-\tau)\mathbb{1}_n + \tau\Big(\hat{p}(t) + \big(\mathbb{1}_n - \hat{p}(t)\big)\Big) = \mathbb{1}_n. \end{aligned}$$

Therefore, $A(t)$ remains row-stochastic and well-posed for finite time $t \geq 0$ under the DRP models. □

It is clear that the affine D and DR models, converge. In simulations (see Section 3.4), we also observe that the DRP model exhibits convergence behaviors to a unique equilibrium. The next Lemma illustrates convergence of the DRP model for the simpler uniform expertise case, $p = c\mathbb{1}_n$ with $c \in (0, 1]$.

Theorem 28 (Equilibrium and convergence of DRP model with uniform expertise)**.** *Consider the DRP model* (3.5)*. Assume for $\tau \in (0,1)$, constant uniform expertise values $p(t) = p = c\mathbb{1}_n$ with $c \in (0,1]$, $A(0)$ row-stochastic, and that there exists at least one i such that $a_{ii}(0) > 0$. Then $\lim_{t\to\infty} A(t) = \frac{1}{n}\mathbb{1}_n\mathbb{1}_n^\top$.*

Proof. Since the dynamics of $A(t+1)$ can be described as a function of $A_d(t)$, then it is sufficient to prove convergence of the self-influence weights given by the dynamics (3.6). Note that $\hat{p}(t) = (p^\top A_d(t))^{-1}\operatorname{diag}(p)A_d(t) = (cp^\top A_d(t))^{-1}\operatorname{diag}(cp)A_d(t)$ for any $c > 0$. Then per our assumption that $y = c\mathbb{1}_n$, we can assume $y = \mathbb{1}_n$ without loss of generality and $\hat{p}(t) = \big(\mathbb{1}_n^\top A_d(t)\big)^{-1} A_d(t)$. For our proof, first, we show that all trajectories satisfying our initial condition assumptions reach the forward-invariant set $\Omega = \{A_d(t) \in [0,1]^n \mid \mathbb{1}_n^\top A_d(t) \geq 1\}$. Second, we define a function $V : [0,1]^n \to \mathbb{R}$ that we prove is a Lyapunov function for $A_d(t) \in \Omega$.

From the dynamics, all influence weight values become strictly positive for $t \geq 0$, regardless of the initial condition. If $a_{ij}(0) = 0$, then $a_{ij}(1) = \frac{\tau}{n}$ and if $a_{ij}(0) > 0$, then

$a_{ij}(1) > (1-\tau)a_{ij}(0)$. Consider $A_d(t) \notin \Omega$ where $\mathbb{1}_n^\top A_d(t) < 1$, then

$$\begin{aligned}\mathbb{1}_n^\top A_d(t+1) &= (1-\tau)\mathbb{1}_n A_d(t) + \tau \hat{p}(t)^\top \hat{p}(t) + \tau - \frac{\tau}{n} \\ &> \mathbb{1}_n^\top A_d(t) - \tau + \frac{\tau}{n} + \tau - \frac{\tau}{n} = \mathbb{1}_n^\top A_d(t).\end{aligned}$$

The inequality from the last line follows from the fact that $\hat{p}(t)^\top \hat{p}(t) \geq \frac{1}{n}$, which can be found by formulating the minimization problem of $\hat{p}(t)^\top \hat{p}(t)$ as a constrained convex optimization problem and applying the KKT conditions. Therefore if $A_d(t) \notin \Omega$ and $\mathbb{1}_n^\top A_d(t+1) > \mathbb{1}_n^\top A_d(t)$, there exists some finite time $T > t$ such that $A_d(t) \in \Omega$. Next, consider $A_d(t) \in \Omega$ implies

$$\mathbb{1}_n^\top A_d(t+1) \geq (1-\tau)\mathbb{1}_n^\top A_d(t) - \tau + \frac{\tau}{n} + \tau - \frac{\tau}{n} \geq 1.$$

Since the dynamics also preserves row-stochasticity of the influence network by Lemma 1, then $\mathbb{1}_n^\top A_d(t) \leq n$ and we have shown that Ω is a compact forward-invariant set, where trajectories that enter Ω remain in Ω.

Now we prove that all trajectories in Ω converge to the equilibrium A_d^*. It is straightforward to verify that the equilibrium of (3.6) is $A_d^* = \frac{1}{n}\mathbb{1}_n$, which corresponds to the influence network equilibrium $A^* = \frac{1}{n}\mathbb{1}_n\mathbb{1}_n^\top$. We define $V(A_d(t))$ as

$$V\big(A_d(t)\big) = \max_{i\in\{1,\dots,n\}} \Big\{ a_{ii}(t) - \frac{1}{n} \Big\},$$

where $V(\frac{1}{n}\mathbb{1}_n) = 0$ and $V(A_d(t)) > 0$ for $A_d(t) \in \Omega \setminus \frac{1}{n}\mathbb{1}_n$. Next we show that $V(A_d(t+1)) < V(A_d(t))$ for $A_d(t) \in \Omega \setminus \frac{1}{n}\mathbb{1}_n$. Note that for $\hat{p}(t) \in \Delta_n$ and $A_d(t) \in \Omega$, then

$\hat{p}_i(t) \leq a_{ii}(t)$ and $\max_i\{a_{ii}(t)\} \geq \frac{1}{n}$, which are used for the following bounds.

$$
\begin{aligned}
V(A_d(t+1)) - V(A_d(t)) &= \max_{i\in\{1,\dots,n\}} \Big\{a_{ii}(t+1) - \frac{1}{n}\Big\} - \max_{i\in\{1,\dots,n\}} \Big\{a_{ii}(t) - \frac{1}{n}\Big\} \\
&\leq (1-\tau) \max_{i\in\{1,\dots,n\}} \Big\{a_{ii}(t) - \frac{1}{n}\Big\} + \tau \max_{i\in\{1,\dots,n\}} \Big\{\hat{p}_i(t)\big(\hat{p}_i(t) - \frac{1}{n}\big)\Big\} - \max_{i\in\{1,\dots,n\}} \Big\{a_{ii}(t) - \frac{1}{n}\Big\} \\
&\leq -\tau \max_{i\in\{1,\dots,n\}} \Big\{a_{ii}(t) - \frac{1}{n}\Big\} + \tau \max_{i\in\{1,\dots,n\}} \big\{a_{ii}(t)\big\} \max_{i\in\{1,\dots,n\}} \Big\{a_{ii}(t) - \frac{1}{n}\Big\} < 0.
\end{aligned}
$$

As a result, all trajectories reach Ω in finite time and trajectories in Ω approach $\lim_{t\to\infty} \max_i\{a_{ii}(t)\} = \frac{1}{n}$, which can only occur for $A_d^* = \frac{1}{n}\mathbb{1}_n$. For $A_d(t) = A_d^*$, the dynamics of the interpersonal influence weights simplify to a stable affine system,

$$
a_{ij}(t+1) = (1-\tau)a_{ij}(t) + \tau\Big(\hat{p}_i(t)\hat{p}_j(t) + \big(1-\hat{p}_i(t)\big)\frac{1}{n}\Big).
$$

Therefore, for any $A(0) \in [0,1]^{n\times n}$ with at least one strictly positive diagonal entry, then $\lim_{t\to\infty} A(t) = \frac{1}{n}\mathbb{1}_n^\top \mathbb{1}_n$. □

Numerical Simulations In general for the DRP model, we observe that for any given p, then any initial condition $A(0)$ will converge to a unique $A^* = A^*(p)$. Figure 3.2 illustrates how the influence weights of the DRP model with $p = [0.05, 0.2, 0.3, 0.45]^\top$ and time scale $\tau = 0.4$ evolves over time. The example shows that each person is capable of determining the correct order of who has the least to most expertise. However, we observe that lower performing team members do not have large differentiations in their appraisals relative to expertise compared to higher performing team members. Figure 3.3 illustrates how the influence weights of the DRP model with constant expertise p and time scale $\tau = 0.4$ evolves over time. As shown in Theorem 28, all influence weights converge to $\frac{1}{n}$.

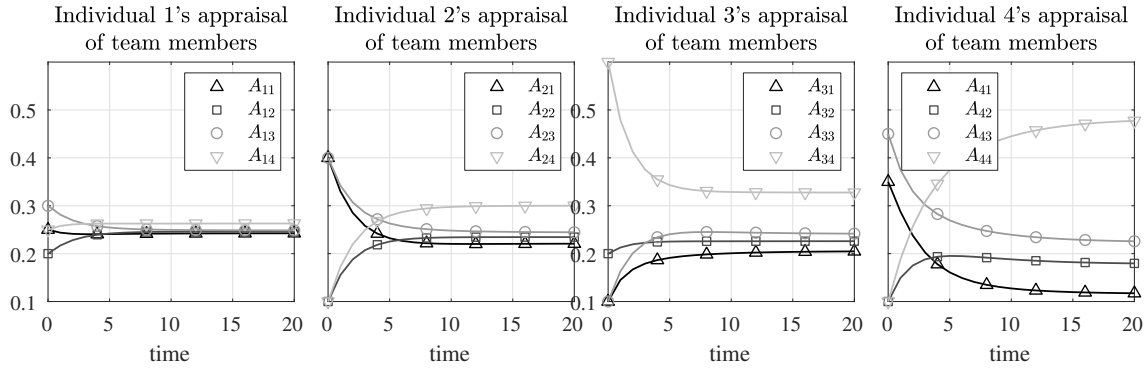

Figure 3.2: Evolution of the influence matrix for a given team using the Differentiation, Reversion, Perceived expertise (DRP) model (3.5) with expertise levels $p = [0.05, 0.2, 0.3, 0.45]^\top$ and time scale $\tau = 0.4$. Every panel depicts how much influence each team member has on a particular individual. Higher performing individuals are more capable of determining which team members have higher expertise. Note that higher performance does not imply an individual will have higher confidence as $t \to \infty$.

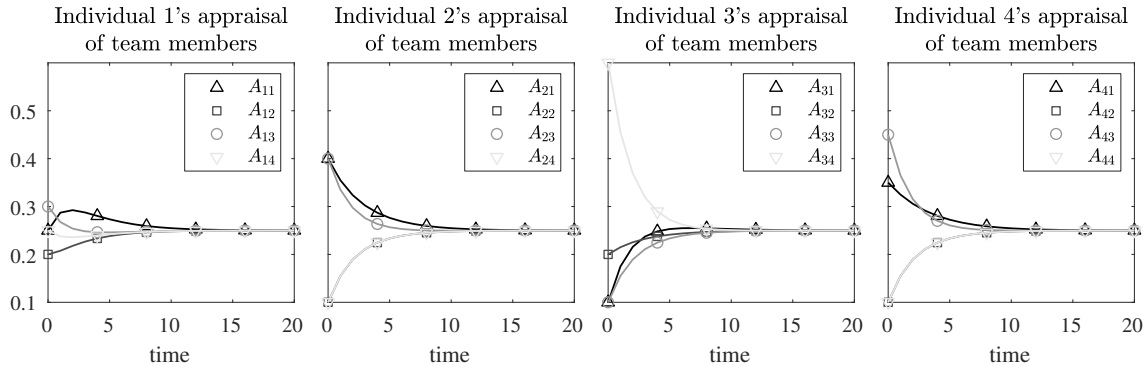

Figure 3.3: Evolution of the influence matrix for a given team using the Differentiation, Reversion, Perceived expertise (DRP) model 3.5 with uniform expertise $p = \frac{1}{n}\mathbb{1}_n$ and time scale $\tau = 0.4$. Every panel depicts how much influence each team member has on a particular individual and $A(t)$ converges to $\frac{1}{n}\mathbb{1}_n\mathbb{1}_n^\top$.

3.5 Cognitive Dynamic Model Validation

Studying the problem of estimating the influence matrix is a novel and applicable problem for any team-based organization. Our data presents an unprecedented opportunity to understand team behavior and estimate the interpersonal influence system within a team. Since our dynamic models only take the history of past influence weight informa-

tion and individuals' performance values, these models can be used to provide a single or multi-round forecast of the influence matrices for successive rounds of the experiment. We also compare our dynamic models to other machine-learning based estimation methods, which use a history of influence matrices, text embeddings, and individual performance.

Before studying how to use the models to estimate influence matrices, we need a set of measures (metrics) to gauge the accuracy of the estimated influence matrices with the ground truth ones. We use two classical metrics: Mean Square Error (MSE) and the Kullback-Liebler (KL) divergence. Together they portray two different measures of accuracy. MSE pays more attention to the exact estimation of each number in the matrix while KL divergence on each row of the influence matrix focuses on the similarity of the distributions.

The MSE and KL divergence of two $n \times n$ row-stochastic matrices A^{real} and A^{pred} are defined as follows,

$$\text{MSE}(A^{\text{real}}, A^{\text{pred}}) = \tfrac{1}{n} \left\| A^{\text{real}} - A^{\text{pred}} \right\|_{\text{F}}^2 = \tfrac{1}{n} \sum_{i=1}^{n} \sum_{j=1}^{n} |A_{ij}^{\text{real}} - A_{ij}^{\text{pred}}|^2, \tag{3.7}$$

$$\text{KL}(A^{\text{real}}, A^{\text{pred}}) = \tfrac{1}{n} \sum_{i=1}^{n} \left(\sum_{j=1}^{n} A_{ij}^{\text{real}} \log \left(\frac{A_{ij}^{\text{pred}}}{A_{ij}^{\text{real}}} \right) \right). \tag{3.8}$$

Depending on the application, one may choose any of these metrics, with $A^{\text{real}} = M^m(t)$ and $A^{\text{pred}} = A^m(t)$. To showcase the generality of our proposed models, we present our results for both metrics.

3.5.1 Accuracy Comparison of the Dynamic Models

Our results compare the accuracy of our various dynamical models: the D model (3.3), DR model (3.4), DRP model (3.5), and the baseline constant model (3.17). The models

assume that individuals can observe each other's normalized, cumulative expertise $p(t) \in \Delta_n$, which they take into account when readjusting the influence weights for their team members.

We consider single-round and multi-round forecast, to compare how the models perform when using the previous round's influence matrix versus only the initial round's influence matrix, respectively.

Single-round forecast The single-round forecast estimates the influence matrix $\hat{A}^m(t+1)$ for any round $t \in \{t_0, \ldots, T\}$, using the reported influence matrix from the previous round $M^m(t)$ and the expertise $p^m(t)$. Recall that for our dataset, $t_0 = 1$ and $T = 9$. For the single-round forecast, the estimation of the influence network for team m comes from the method using any given model,

$$A^m(t+1) = T(p^m(t), M^m(t)), \qquad \text{for } t \geq t_0. \tag{3.9}$$

Figure 3.4 (left) illustrates the error of a given model.

Multi-round forecast The multi-round forecast predicts $\hat{A}^m(t+1)$ for any round $\in \{t_0, \ldots, T\}$, using the initial reported influence matrix $M^m(0)$ and the previous round's expertise values $p^m(t)$ as inputs. The following details how the dynamical models are modified to give multi-round forecasts. The influence network is estimated for team m using the following for any given model,

$$\begin{aligned} A^m(t_0+1) &= T(p(t_0), M^m(t_0)) \\ A^m(t+1) &= T(p^m(t), M^m(t)), \qquad \text{for } t > t_0. \end{aligned} \tag{3.10}$$

In summary, the ground truth influence matrix data is propagated over a sequence of rounds to predict the influence matrix at future rounds. Figure 3.4 (right) illustrates the error of a given model.

Summary of results Figure 3.4 illustrates the error for a given model for single-round forecast (left) and multi-round forecast (right). Overall for the single and multi-round forecast, we observe increased estimation accuracy for the models that capture more hypotheses. For the single-round forecast, we observe that the accuracy increases for later rounds since individuals adjust influence weights less as the experiment goes on. However, the accuracy for later rounds does not give significant improvements compared to the constant baseline model, since the influence weights remain relatively constant for rounds $t \geq 3$. For the multi-round forecast, as expected, we see that the accuracy decreases for predictions of later rounds; yet consistently provides the most accurate predictions of the influence matrices regardless of whether the model is given the most up-to-date ground truth values. In the following, we also show that the cognitive dynamic model gives competitive predictions compared to the machine learning models.

3.5.2 Accuracy comparison of the DRP model to machine learning based models

We also introduce two machine learning models to predict the influence matrix at every round: a linear maximum likelihood estimation model using convex optimization and a deep neural network model. These models are able to use features extracted from the logs of the experiment and learn a mapping to estimate the corresponding influence matrix. Learning the mappings require training data, so a portion of the logs is reserved for training, and the remaining portion is used to test the trained model.

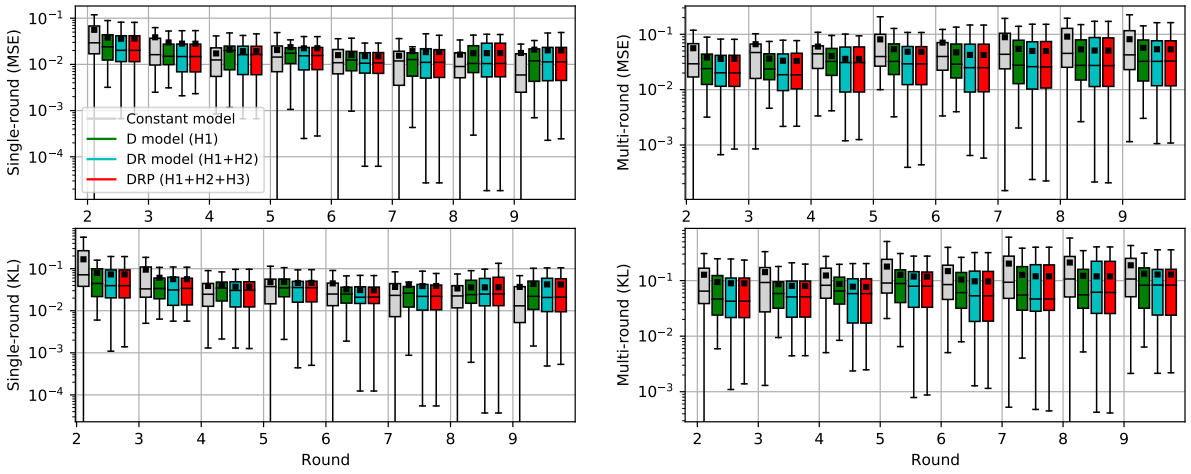

Figure 3.4: Cognitive dynamic model evaluation: The mean squared error (MSE) and the Kullback-Leibler (KL) divergence for different dynamical models over nine rounds of influence matrix estimation. Differentiation (D model) takes into account hypothesis 1. Differentiation, Reversion (DR model) is inspired by hypotheses 1 and 2. Differentiation, Reversion, Perceived (DRP model) uses hypotheses 1, 2, and 3. All models use the hyperparameter $\tau = 0.4$. In this figure boxes show the interquartile range of the errors, the whiskers show minimum and maximum of the range of the distribution. In each box, the dot shows the average and the line shows the median of the portrayed distribution. Outliers are not shown for better readability. **Left:** Single-round forecast error of various dynamical models for predicting the influence matrix one round ahead. The models estimate $M^m(t+1)$ using the algorithm with inputs of expertise $p^m(t)$ and the reported influence matrix from the previous round $M^m(t)$. **Right:** Multi-round forecast error of various dynamical models for predicting the influence matrix multiple rounds ahead. The models estimate $M^m(t+1)$ using the algorithm (3.10) with inputs of expertise $p^m(t)$ and the initial ground truth $A^m(0)$ influence matrix reported by individuals.

Since the machine learning based models require training, we only test their accuracy using single-round forecasting. The time scale for the DRP model is also selected through training data, but otherwise the dynmaic model requires no other training. In the following, we introduce the results of estimation using these models.

Proposed linear model Using machine learning models we can take advantage of all available data to estimate influence matrices. Combining text, connectivity network, expertise, and historical appraisals produce a multi-dimensional prediction model. We

have N teams of n individuals that go through T game rounds. To have a general format, we represent influence matrix for team m at round t by $\hat{A}^m(t)$. We represent all aforementioned features in matrix format (shown by $X_k^m(t)$ for matrix feature k of team m at round t). We need to estimate the weight variables that maps the features to the influence matrix. In total, we assume there are K matrix variables, shown as $W_k; \quad k = 1$ to K. Ergo, a convex objective function for estimating the influence matrix is defined as

$$\begin{aligned}
&\min_{\substack{W_k\ \forall k\in\{1,\dots,K\},\\ B}} \sum_{m=1}^{N}\sum_{t=1}^{T}\Big\|\sum_{k=1}^{K} X_k^m(t)W_k^T + B - M^m(t)\Big\|_F^2 + \lambda\Big(\sum_{k=1}^{K}\|W_k\|_{1,1} + \|B\|_{1,1}\Big),\\
&\text{Subject to } \sum_{k=1}^{K} X_k^m(t)W_k^T + B \geq 0,\ \ \forall m \in [1,N],\ \forall t \in [1,T],\\
&\qquad\qquad \mathbb{1}_n^T\Big(\sum_{k=1}^{K} X_k^m(t)W_k^T + B\Big) = \mathbb{1}_n^T.\ \ \forall m \in [1,N],\ \forall t \in [1,T].
\end{aligned} \tag{3.11}$$

Variables to be calculated via optimization are the $n \times n$ weight matrices W_k. B is the $n \times n$ bias matrix also to be estimated. We also use an $l1$-norm regularization to introduce sparsity to the estimated parameters that is commonly used in many real applications and also decrease the potential search space and therefore provides efficiency for the optimization solver.

Based on the application, when only the probability distribution and the order of influence toward others is more important than exact values, we use cross-entropy as the loss function and KL divergence as the metric. In such a case, we can formulate the matrix estimation problem as the estimation of each row, which is a discrete distribution comprised of four numbers. Cross-entropy for two probability distribution of p and q is

defined as $H(p,q) = -\sum_{i=1}^{n} p_i \log q_i$. In this study, the two probabilities are

$$p = [M_{i1}^m, \ldots, M_{in}^m]^\top \qquad \forall i \in \{1, \ldots, n\},$$
$$q = [A_{i1}^m, \ldots, A_{in}^m]^\top = \sigma(O_{i,.}) = \sigma(W^T X_{i,.} + b) \qquad \forall i \in \{1, \ldots, n\},$$

where σ represents Softmax function, and W and b show the weight and bias variables to be estimated.

Table 3.3 sheds light on the importance of every feature set in the linear model optimized using convex optimization which was trained with 80% of the data. This table shows entry-wise l1-norm of estimated parameters in (3.11). The values in table 3.3 are sorted from most to least important top to bottom. This result shows the previous influence matrix is the most important feature used to predict the next influence matrix. Interestingly, it also shows expertise is the second most of predictive power and text embedding is third. It shows sentiment, emotion, and quick responsiveness (response network) network are far less substantial in the estimation. It is worth mentioning that due to the origin of memory questions, there is only a brief chat happening for many of the members since they simply do not know the answer. That is probably the reason that text embedding is not as important as the correct answer rate.

Proposed deep neural network-based model We can also learn the mapping defined by the three weight matrices as deep encoders in a two-tower model [134]. In this regard, we apply end-to-end models to estimate the social influence matrices using multi-layered encoders from raw features to an influence matrix. This is described in Fig. 3.5. Each encoder is comprised of three fully connected Exponential Linear Unit (ELU) [135] layers, initialized by He *et al.* [136] Normal initialization, such that it draws samples from a truncated normal distribution centered on 0 with a standard deviation of $\sqrt{\frac{2}{f}}$ where f

Table 3.3: Importance features in predicting influence. Entry-wise $l1$-norm of estimated parameter matrix in linear model given in (3.11) which is trained with 80% of the data. This table shows the importance of each features in the proposed linear model. The embeddings [133], sentiments, and emotions all are computed from the message text content; however, responsiveness is computed from the timestamps of the messages.

	$l1$-norm of estimated parameters
Previous influence matrix	0.2137 ± 0.0027
Expertise	0.0239 ± 0.0027
Message content embedding	0.0111 ± 0.0003
Message sentiment	0.0078 ± 0.0010
Message emotion	0.0050 ± 0.0007
Message responsiveness	0.0041 ± 0.0004

is the number of input units in the weight tensor. We use Dropout [137] after each fully connected layer to decrease overfitting. Then, all three outputs are concatenated and fed to another three fully connected layers with the same activation function to decrease the dimensionality of embedding vectors to an $n \times n$ matrix $\tilde{M}^m(t)$. Finally, cosine similarity of the two matrices $M^m(t)$ and $\tilde{M}^m(t)$ is computed and the error is back-propagated using stochastic gradient descent.

The deep method description is shown in Fig. 3.5. In this figure, the weights matrices in (3.11) are framed as a layers of deep neural networks. This model creates a non-convex problem; however, arguably with the abundance of data, a more effective model. In order to predict the influence matrix at round t, we use time and content of text messages from the broadcast communication logs until round t, individual correct percent until round t, and reported influence matrices before round t in the following.

- Connectivity networks: In broadcast communication logs, the time between two messages can reveal a directed and weighted evolving network structure among teammates. This approach implies a basic assumption: if a message B appears on a chat log close enough in time to an earlier sent message A, then B is likely a response to A; and,

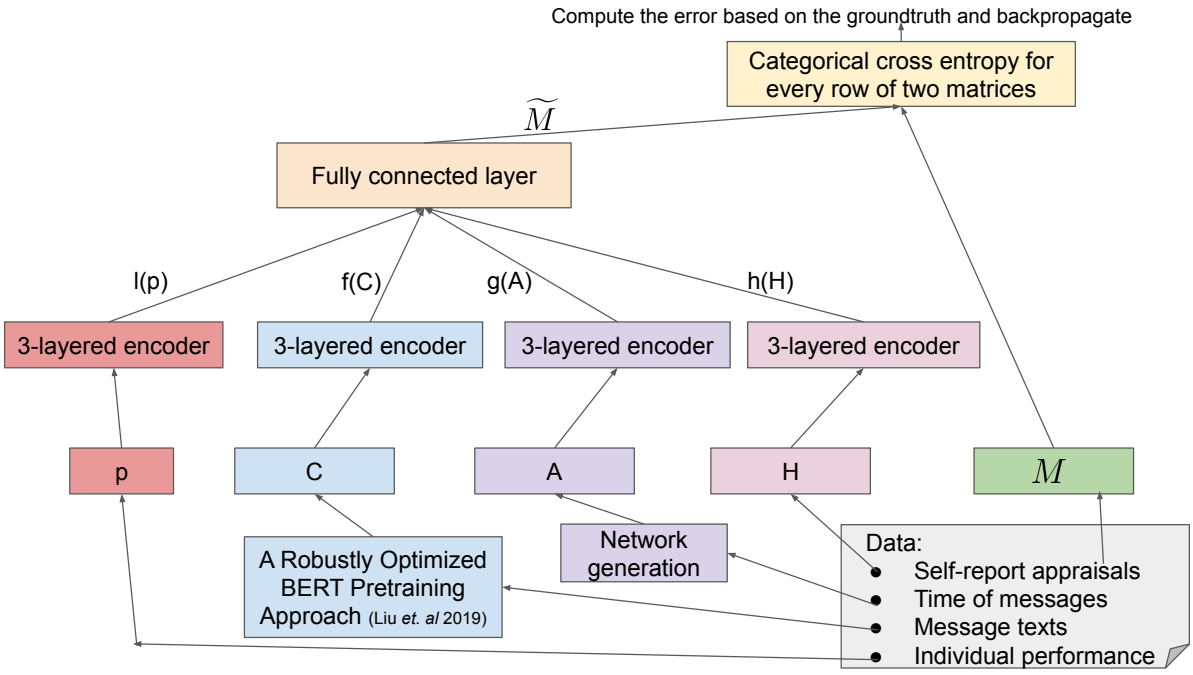

Figure 3.5: Deep learning model architecture. A deep encoder model in a two-tower framework [134] for learning the three mappings of connectivity network, content of messages, and history of appraisals. The final layer computes the cosine similarity with the ground truth influence matrix and back-propagates the error using Stochastic Gradient Descent (SGD).

the larger the time gap between two messages is, the less likely the later message is a response to the earlier message. For a message m occurring at time $m.time$ on the log, we define the set of its responses as

$$R(m) = \{r \mid m.time < r.time \wedge\ t_1 \leq r.time - m.time \leq t_2 \wedge\ r.sender \neq m.sender\},$$

and the connectivity networks as

$$C_{ij} = \sum_{\substack{p.sender=i \\ q.sender=j \\ q \in R(p)}} \text{weight}(p, q). \tag{3.12}$$

We define the weights in the connectivity networks (given in (3.12)) in three dif-

ferent ways. First is Response network in which the weights in the network, similar to Amelkin *et al.* [138], are calculated based on the duration a response as $\text{weight}(p, q) = e^{-\gamma|p.time - q.time|}$. This networks represents the responsiveness of every individuals toward every other member. The likelihood of a message being a response degrades with the increase of the time gap between the two messages. Second is Sentiment network in which we use Valence Aware Dictionary and sEntiment Reasoner (VADER) as the sentiment analysis toolbox [139] on words in the response message as $\text{weight}(p, q) = \text{sentiment}(q)$. Third is the Emotion network in which Affective norms for English words (ANEW) are used as the emotion analysis toolbox [140] that examines arousal, valence, and dominance of words in the response message. The weight for emotion network is computed as $\text{weight}(p, q) = \text{emotion}(q)$. In all networks, the summation is performed over all suitable pairs (p, q) of messages p and q in a team's chat log. Thus, these networks are represented as a $n \times n$ matrix with float values and no self-loop.

- Message content embeddings: We use natural language processing to analyze the content of messages. The text embeddings for sentences [141] are generated from a pretrained sentence embedding model by the last layer of the encoder in the state-of-the-art model, a Robustly Optimized BERT Pretraining Approach (RoBERTa) [133, 142], is generated.

- History of influence matrix: Previous influence matrices.

- Expertise: Individual cumulative correctness rate.

Fig. 3.5 shows the architecture of the neural network model. They both similarly intend to find a linear or nonlinear combination of the aforementioned input features to estimate a row-stochastic influence matrix. We compare the proposed models to the

baseline models with a variation of different input features. All models are trained with 80% of the data and tested on the withheld 20%. To compute the statistical significance, we draw 1000 bootstraps with replacement from the hold-out test set.

Baseline dynamical models We also include several baseline dynamical models, for comparison with the dynamic models. The following provides definitions of several baseline models for estimating the influence matrix using data history.

- *Random.* Randomly generated row-stochastic matrix.

$$A^m(t+1) = \text{diag}(B\mathbb{1}_n)^{-1}B, \qquad \text{for } B = \text{rand}(n,n) \tag{3.13}$$

- *First.* Assumes influence matrix remains constant over time, where t_0 is the initial round from the dataset.

$$A^m(t+1) = M^m(t_0) \tag{3.14}$$

- *SBT.* Structural balance theory (SBT) is a long-established theory describing the dynamics that govern the sentiment of interpersonal relationships. This baseline is inspired by earlier research of Kulakowski *et al.* [143].

$$A^m(t+1) = M^m(t)M^m(t) \tag{3.15}$$

- *Uniform.* Influence is accorded equally.

$$A^m(t+1) = \frac{1}{n}\mathbb{1}_n\mathbb{1}_n^\top \tag{3.16}$$

- *Constant.* Assumes the estimated influence matrix equals the previously reported

influence matrix.

$$A^m(t+1) = M^m(t) \tag{3.17}$$

- *Average.* Predicts the influence matrix as the average reported influence matrix.

$$A^m(t+1) = \frac{1}{T}\sum_{t=1}^{T} M^m(t) \tag{3.18}$$

- *Reflected appraisal.* Uses the reflected appraisal mechanism for prediction and is based on the model proposed in [58].

$$A^m(t+1) = A^m(t) + \text{diag}\left(p(t) - M^m(t)p(t)\right)\text{diag}\left(M_d^m(t)\right)\left(I_n - M^m(t)\right) \tag{3.19}$$

Summary of results Since the linear and neural network-based models require training, we only test them using the single-round forecast case, where we assume we have access to the previous influence matrix and expertise to predict the next influence matrix. For this setting, there are more baselines that we can compare our proposed models against. Fig. 3.6 (left) shows MSE divergence error for models using previous influence matrix and expertise. Similarly, the neural network-based model surpasses all baselines and provides statistically significant lower MSE. It is worth mentioning that proposed linear model (3.11) is competitive with the proposed neural network model (Fig. 3.5). Also, interestingly, the proposed cognitive dynamical model (3.5) which does not require any training and is described by a mechanism that postulates past research in social psychology works significantly better than other baselines and competitively close to the proposed machine learning models. Note that both machine learning models use optimization methods for training that requires several steps to converge.

Fig. 3.6 shows MSE and KL divergence of the estimated influence matrix from the

ground truth reported by individuals. This figure shows that for both error measurements, the DRP model is competitive against the two machine-learning based models, and even surpasses the linear model.

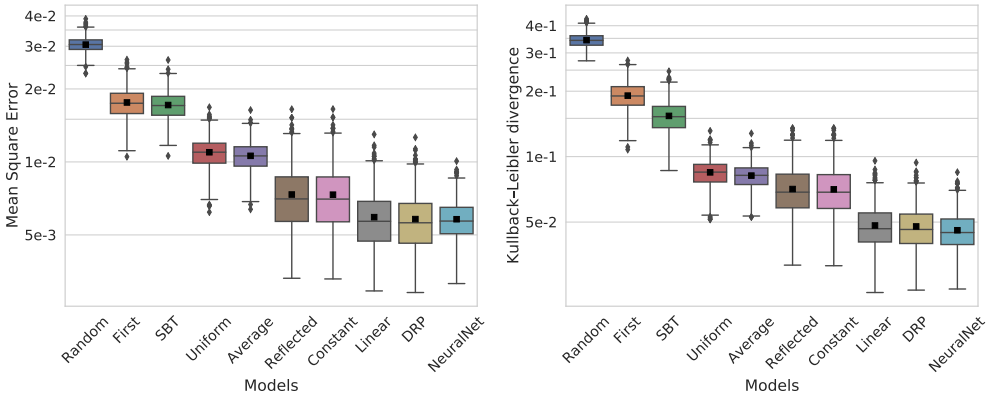

Figure 3.6: Comparison of all models. Mean squared error (MSE) and Kullback–Leibler (KL) divergence of single-round influence matrix prediction for baseline algorithms and the proposed models. Evaluations are applied on 1000 bootstraps of the holdout test dataset (20% of the entire data). All models have access to the expertise and previous influence matrix for every team. The box shows the interquartile range of the errors, the whisker shows minimum and maximum of the range of the distribution, and the dots show the outliers. Baseline models are: *Random* (3.13), *First* (3.14), *SBT* (3.15), *Uniform* (3.16), *Average* (3.18), *Reflected* (3.19), and *Constant* (3.17). The proposed models are: 1. the cognitive theory *DRP* (Differentiation, Reversion, Perceived expertise) model which encodes hypotheses (1, 2, 3) to predict influence matrices; 2. the *Linear* model using convex optimization; and 3. the Neural Networks model (*NeuralNet*) which learns important features from the logs to estimate influence matrices. The figure depicts that all our proposed models outperform baselines and the DRP model works competitively with the learning models, showing the power behind our empirically proven hypotheses.

3.6 Conclusion

Interpersonal appraisal networks can be modeled as an influence matrix, where weighted edges signify positive or negative appraisals among people. Being able to estimate these influence matrices has important applications such as marketing advertisements, creating successful political campaigns, and improving the efficiency of commu-

nication among team members. The problem of influence matrix estimation has been studied previously either with simulated data or with a focus on estimating the total amount of influence from websites rather than estimating interpersonal influence within groups.

We collected data from human subjects answering trivia questions in teams of four. After individually answering a question, they then collaborated to agree on a final answer through a chat system. The participants were periodically asked to assess their appraisals of each other. We built a machine learning-based model using text content, the time of messages, and individual task performance to estimate the collective influence matrix. We sought to find underlying factors that contribute to the accorded influence. We proposed a dynamical cognitive dynamic model, a linear model using convex optimization, and a neural network model alongside baselines from dynamical models and sociology literature to test our hypotheses. From these findings, we concluded that task performance and higher values of confidence were the two most salient factors in determining the amount of influence one receives in collaborative group settings. We believe this study on estimating underlying influence systems in a collaborative environment will spur the establishment of connections with a variety of fields and advance an interdisciplinary understanding of the design of social experiments.

Bibliography

[1] S. Jafarpour, E. Y. Huang, and F. Bullo, *Synchronization of Kuramoto oscillators: Inverse Taylor expansions*, *SIAM Journal on Control and Optimization* **57** (2019), no. 5 3388–3412.

[2] Y. Kuramoto, *Self-entrainment of a population of coupled non-linear oscillators*, in *Int. Symposium on Mathematical Problems in Theoretical Physics* (H. Araki, ed.), vol. 39 of *Lecture Notes in Physics*, pp. 420–422. Springer, 1975.

[3] J. A. Acebrón, L. L. Bonilla, C. J. P. Vicente, F. Ritort, and R. Spigler, *The Kuramoto model: A simple paradigm for synchronization phenomena*, *Reviews of Modern Physics* **77** (2005), no. 1 137–185.

[4] D. J. Hill and G. Chen, *Power systems as dynamic networks*, in *IEEE Int. Symposium on Circuits and Systems*, (Kos, Greece), pp. 722–725, May, 2006.

[5] F. Dörfler and F. Bullo, *Synchronization and transient stability in power networks and non-uniform Kuramoto oscillators*, *SIAM Journal on Control and Optimization* **50** (2012), no. 3 1616–1642.

[6] D. J. Klein, P. Lee, K. A. Morgansen, and T. Javidi, *Integration of communication and control using discrete time Kuramoto models for multivehicle coordination over broadcast networks*, *IEEE Journal on Selected Areas in Communications* **26** (2008), no. 4 695–705.

[7] R. Sepulchre, D. A. Paley, and N. E. Leonard, *Stabilization of planar collective motion: All-to-all communication*, *IEEE Transactions on Automatic Control* **52** (2007), no. 5 811–824.

[8] Y. Wang and F. J. Doyle III, *Exponential synchronization rate of Kuramoto oscillators in the presence of a pacemaker*, *IEEE Transactions on Automatic Control* **58** (2013), no. 4 989–994.

[9] O. Simeone, U. Spagnolini, Y. Bar-Ness, and S. H. Strogatz, *Distributed synchronization in wireless networks*, *IEEE Signal Processing Magazine* **25** (2008), no. 5 81–97.

[10] G. B. Ermentrout and N. Kopell, *Multiple pulse interactions and averaging in systems of coupled neural oscillators*, *Journal of Mathematical Biology* **29** (1991), no. 3 195–217.

[11] F. Bullo, *Lectures on Network Systems*. CreateSpace, 1 ed., July, 2018. With contributions by J. Cortés, F. Dörfler, and S. Martínez.

[12] D. Aeyels and J. A. Rogge, *Existence of partial entrainment and stability of phase locking behavior of coupled oscillators*, *Progress of Theoretical Physics* **112** (2004), no. 6 921–942.

[13] R. E. Mirollo and S. H. Strogatz, *The spectrum of the locked state for the Kuramoto model of coupled oscillators*, *Physica D: Nonlinear Phenomena* **205** (2005), no. 1-4 249–266.

[14] M. Verwoerd and O. Mason, *Global phase-locking in finite populations of phase-coupled oscillators*, *SIAM Journal on Applied Dynamical Systems* **7** (2008), no. 1 134–160.

[15] F. Dörfler, M. Chertkov, and F. Bullo, *Synchronization in complex oscillator networks and smart grids*, *Proceedings of the National Academy of Sciences* **110** (2013), no. 6 2005–2010.

[16] N. Chopra and M. W. Spong, *On exponential synchronization of Kuramoto oscillators*, *IEEE Transactions on Automatic Control* **54** (2009), no. 2 353–357.

[17] F. Dörfler and F. Bullo, *On the critical coupling for Kuramoto oscillators*, *SIAM Journal on Applied Dynamical Systems* **10** (2011), no. 3 1070–1099.

[18] C. J. Tavora and O. J. M. Smith, *Stability analysis of power systems*, *IEEE Transactions on Power Apparatus and Systems* **91** (1972), no. 3 1138–1144.

[19] N. Ainsworth and S. Grijalva, *A structure-preserving model and sufficient condition for frequency synchronization of lossless droop inverter-based AC networks*, *IEEE Transactions on Power Systems* **28** (2013), no. 4 4310–4319.

[20] A. Jadbabaie, N. Motee, and M. Barahona, *On the stability of the Kuramoto model of coupled nonlinear oscillators*, in *American Control Conference*, (Boston, USA), pp. 4296–4301, June, 2004.

[21] S. Jafarpour and F. Bullo, *Synchronization of Kuramoto oscillators via cutset projections*, *IEEE Transactions on Automatic Control* **64** (2019), no. 7 2830–2844.

[22] J. G. Restrepo, E. Ott, and B. R. Hunt, *Synchronization in large directed networks of coupled phase oscillators*, *Chaos: An Interdisciplinary Journal of Nonlinear Science* **16** (2006), no. 1 015107–015107.

[23] R. Delabays, P. Jacquod, and F. Dörfler, *The Kuramoto model on oriented and signed graphs*, *SIAM Journal on Applied Dynamical Systems* **18** (2019), no. 1 458–480.

[24] T. Menara, G. Baggio, D. Bassett, and F. Pasqualetti, *Stability conditions for cluster synchronization in networks of heterogeneous Kuramoto oscillators*, *IEEE Transactions on Control of Network Systems* (2019). to appear.

[25] E. Y. Huang, S. Jafarpour, and F. Bullo, *Synchronization of coupled oscillators: The Taylor expansion of the inverse Kuramoto map*, in *IEEE Conf. on Decision and Control*, (Miami, USA), pp. 5340–5345, Dec., 2018.

[26] R. Kyng and S. Sachdeva, *Approximate Gaussian elimination for Laplacians – Fast, sparse, and simple*, in *IEEE Annual Symposium on Foundations of Computer Science*, (New Brunswick, USA), pp. 573–582, 2016.

[27] D. A. Spielman and S.-H. Teng, *Nearly linear time algorithms for preconditioning and solving symmetric, diagonally dominant linear systems*, *SIAM Journal on Matrix Analysis and Applications* **35** (2014), no. 3 835–885.

[28] B. Stott, J. Jardim, and O. Alsac, *DC power flow revisited*, *IEEE Transactions on Power Systems* **24** (2009), no. 3 1290–1300.

[29] N. K. Vishnoi, *$Lx = b$, Laplacian solvers and their algorithmic applications*, *Theoretical Computer Science* **8** (2013), no. 1-2 1–141.

[30] B. Stott and O. Alsac, *Fast decoupled load flow*, *IEEE Transactions on Power Apparatus and Systems* **93** (1974), no. 3 859–869.

[31] W. F. Tinney and C. E. Hart, *Power flow solution by Newton's method*, *IEEE Transactions on Power Apparatus and Systems* **PAS-86** (1967), no. 11 1449–1460.

[32] A. F. Glimn and G. W. Stagg, *Automatic calculation of load flows*, *Transactions of the American Institute of Electrical Engineers. Part III: Power Apparatus and Systems* **76** (1957), no. 3 817–825.

[33] D. Mehta, N. S. Daleo, F. Dörfler, and J. D. Hauenstein, *Algebraic geometrization of the Kuramoto model: Equilibria and stability analysis*, *Chaos: An Interdisciplinary Journal of Nonlinear Science* **25** (2015), no. 5 053103.

[34] C. Wang, N. Rubido, C. Grebogi, and M. S. Baptista, *Approximate solution for frequency synchronization in a finite-size Kuramoto model*, *Physical Review E* **92** (2015), no. 6 062808.

[35] A. Trias, *The holomorphic embedding load flow method*, in *IEEE Power & Energy Society General Meeting*, pp. 1–8, 2012.

[36] S. Rao, Y. Feng, D. J. Tylavsky, and J. K. Subramanian, *The holomorphic embedding method applied to the power-flow problem*, *IEEE Transactions on Power Systems* **31** (2016), no. 5 3816–3828.

[37] J. A. Momoh, R. Adapa, and M. E. El-Hawary, *A review of selected optimal power flow literature to 1993. I. Nonlinear and quadratic programming approaches*, *IEEE Transactions on Power Systems* **14** (1999), no. 1 96–104.

[38] J. A. Momoh, M. E. El-Hawary, and R. Adapa, *A review of selected optimal power flow literature to 1993. II. Newton, linear programming and interior point methods*, *IEEE Transactions on Power Systems* **14** (1999), no. 1 105–111.

[39] D. K. Molzahn, F. Dörfler, H. Sandberg, S. H. Low, S. Chakrabarti, R. Baldick, and J. Lavaei, *A survey of distributed optimization and control algorithms for electric power systems*, *IEEE Transactions on Smart Grid* **8** (2017), no. 6 2941–2962.

[40] J. Munkres, *Topology*. Pearson, 2 ed., 2000.

[41] R. Abraham, J. E. Marsden, and T. S. Ratiu, *Manifolds, Tensor Analysis, and Applications*, vol. 75 of *Applied Mathematical Sciences*. Springer, 2 ed., 1988.

[42] L. Hörmander, *An Introduction to Complex Analysis in Several Variables*, vol. 7 of *North-Holland Mathematical Library*. North-Holland Publishing Co, third ed., 1990.

[43] L. Hörmander, *An Introduction to Complex Analysis in Several Variables*. North-Holland Publishing Co., revised ed., 1973.

[44] R. D. Zimmerman, C. E. Murillo-Sánchez, and R. J. Thomas, *MATPOWER: Steady-state operations, planning, and analysis tools for power systems research and education*, *IEEE Transactions on Power Systems* **26** (2011), no. 1 12–19.

[45] A. B. Birchfield, T. Xu, K. M. Gegner, K. S. Shetye, and T. J. Overbye, *Grid structural characteristics as validation criteria for synthetic networks*, *IEEE Transactions on Power Systems* **32** (2017), no. 4 3258–3265.

[46] C. Josz, S. Fliscounakis, J. Maeght, and P. Panciatici, *AC power flow data in MATPOWER and QCQP format: iTesla, RTE snapshots, and PEGASE*, Mar., 2016.

[47] F. Dörfler and F. Bullo, *Synchronization in complex networks of phase oscillators: A survey*, *Automatica* **50** (2014), no. 6 1539–1564.

[48] G. Chen, X. Wang, and X. Li, *Fundamentals of Complex Networks: Models, Structures and Dynamics*. John Wiley & Sons, 2015.

[49] D. J. Watts and S. H. Strogatz, *Collective dynamics of 'small-world' networks*, *Nature* **393** (1998) 440–442.

[50] S. W. J. Kozlowski, W. J. Steve, and B. S. Bell, *Evidence-based principles and strategies for optimizing team functioning and performance in science teams*, in *Strategies for Team Science Success*, pp. 269–293. Springer, 2019.

[51] S. Ryan and R. V. O'Connor, *Acquiring and sharing tacit knowledge in software development teams: An empirical study*, *Information and Software Technology* **55** (2013), no. 9 1614–1624.

[52] C. Hsiung, *The effectiveness of cooperative learning*, *Journal of Engineering Education* **101** (2012), no. 1 119–137.

[53] A. C. Graesser, S. M. Fiore, S. Greiff, J. Andrews-Todd, P. W. Foltz, and F. W. Hesse, *Advancing the science of collaborative problem solving*, *Psychological Science in the Public Interest* **19** (2018), no. 2 59–92.

[54] D. M. Wegner, *Transactive memory: A contemporary analysis of the group mind*, in *Theories of Group Behavior* (B. Mullen and G. R. Goethals, eds.), pp. 185–208. Springer, 1987.

[55] J. A. Jacquez and C. P. Simon, *Qualitative theory of compartmental systems*, *SIAM Review* **35** (1993), no. 1 43–79.

[56] J. A. Grand, M. T. Braun, G. Kuljanin, S. W. J. Kozlowski, and G. T. Chao, *The dynamics of team cognition: A process-oriented theory of knowledge emergence in teams*, *Journal of Applied Psychology* **101** (2016), no. 10 1353–1385.

[57] E. G. Anderson Jr and K. Lewis, *A dynamic model of individual and collective learning amid disruption*, *Organization Science* **25** (2014), no. 2 356–376.

[58] W. Mei, N. E. Friedkin, K. Lewis, and F. Bullo, *Dynamic models of appraisal networks explaining collective learning*, *IEEE Transactions on Automatic Control* **63** (2018), no. 9 2898–2912.

[59] N. E. Friedkin, *A formal theory of reflected appraisals in the evolution of power*, *Administrative Science Quarterly* **56** (2011), no. 4 501–529.

[60] P. Bauer, *A sequential elimination procedure for choosing the best population(s) based on multiple testing*, *Journal of Statistical Planning and Inference* **21** (1989), no. 2 245–252.

[61] A. Nedić, A. Ozdaglar, and P. A. Parrilo, *Constrained consensus and optimization in multi-agent networks*, *IEEE Transactions on Automatic Control* **55** (2010), no. 4 922–938.

[62] E. Wei, A. Ozdaglar, and A. Jadbabaie, *A distributed Newton method for network utility maximization, I: Algorithm*, *IEEE Transactions on Automatic Control* **58** (2013), no. 9 2162–2175.

[63] J. Barreiro-Gomez, G. Obando, and N. Quijano, *Distributed population dynamics: Optimization and control applications*, *IEEE Transactions on Systems, Man, and Cybernetics: Systems* **47** (2016), no. 2 304–314.

[64] T. Gross and B. Blasius, *Adaptive coevolutionary networks: A review*, *Journal of The Royal Society Interface* **5** (2008), no. 20 259–271.

[65] Z. Wang, M. A. Andrews, Z. X. Wu, L. Wang, and C. T. Bauch, *Coupled disease-behavior dynamics on complex networks: A review*, *Physics of Life Reviews* **15** (2015) 1–29.

[66] M. Ogura and V. M. Preciado, *Stability of spreading processes over time-varying large-scale networks*, *IEEE Transactions on Network Science and Engineering* **3** (2016) 44–57.

[67] J. S. Weitz, C. Eksin, S. P. B. K. Paarporn, and W. C. Ratcliff, *An oscillating tragedy of the commons in replicator dynamics with game-environment feedback*, *Proceedings of the National Academy of Sciences* **113** (2016), no. 47 E7518–E7525.

[68] L. Gong, J. Gao, and M. Cao, *Evolutionary game dynamics for two interacting populations in a co-evolving environment*, in *IEEE Conf. on Decision and Control*, pp. 3535–3540, 2018.

[69] F. Bullo, *Lectures on Network Systems*. Kindle Direct Publishing, 1.4 ed., July, 2020. With contributions by J. Cortés, F. Dörfler, and S. Martínez.

[70] A. Newell and P. S. Rosenbloom, *Mechanisms of skill acquisition and the law of practice*, in *Cognitive Skills and Their Acquisition* (J. R. Anderson, ed.), vol. 1, pp. 1–55. Taylor & Francis, 1981.

[71] J. Hofbauer and K. Sigmund, *Evolutionary Games and Population Dynamics*. Cambridge University Press, 1998.

[72] C. Berge, *Graphs and Hypergraphs*. North-Holland, 1973.

[73] J. W. Weibull, *Evolutionary Game Theory*. MIT Press, 1997.

[74] P. Bonacich, *Power and centrality: A family of measures*, *American Journal of Sociology* **92** (1987), no. 5 1170–1182.

[75] R. Tempo, G. Calafiore, and F. Dabbene, *Randomized Algorithms for Analysis and Control of Uncertain Systems*. Springer, 2005.

[76] M. H. DeGroot, *Reaching a consensus*, *Journal of the American Statistical Association* **69** (1974), no. 345 118–121.

[77] N. E. Friedkin and E. C. Johnsen, *Social influence and opinions*, *Journal of Mathematical Sociology* **15** (1990), no. 3-4 193–206.

[78] A. Das, S. Gollapudi, and K. Munagala, *Modeling opinion dynamics in social networks*, in *Proceedings of the 7th ACM International Conference on Web Search and Data Mining*, pp. 403–412, 2014.

[79] N. E. Friedkin and F. Bullo, *How truth wins in opinion dynamics along issue sequences*, *Proceedings of the National Academy of Sciences* **114** (2017), no. 43 11380–11385.

[80] P. Jia, A. MirTabatabaei, N. E. Friedkin, and F. Bullo, *Opinion dynamics and the evolution of social power in influence networks*, *SIAM Review* **57** (2015), no. 3 367–397.

[81] C. Ravazzi, R. Tempo, and F. Dabbene, *Learning influence structure in sparse social networks*, *IEEE Transactions on Control of Network Systems* **5** (2017), no. 4 1976–1986.

[82] X. Zheng, D. Zeng, and F.-Y. Wang, *Social balance in signed networks*, *Information Systems Frontiers* **17** (2015), no. 5 1077–1095.

[83] C. Altafini, *Consensus problems on networks with antagonistic interactions*, *IEEE Transactions on Automatic Control* **58** (2013), no. 4 935–946.

[84] A. V. Proskurnikov and R. Tempo, *A tutorial on modeling and analysis of dynamic social networks. Part I*, *Annual Reviews in Control* **43** (2017) 65–79.

[85] W. Chen, Y. Wang, and S. Yang, *Efficient influence maximization in social networks*, in *Proceedings of the 15th ACM SIGKDD International Conference on Knowledge Discovery and Data Mining*, pp. 199–208, 2009.

[86] O. Askarisichani and M. Jalili, *Influence maximization of informed agents in social networks*, *Applied Mathematics and Computation* **254** (2015) 229–239.

[87] J. Leskovec, L. A. Adamic, and B. A. Huberman, *The dynamics of viral marketing*, *ACM Transactions on the Web* **1** (2007), no. 1 5.

[88] W. Chen, C. Wang, and Y. Wang, *Scalable influence maximization for prevalent viral marketing in large-scale social networks*, in *Proceedings of the 16th ACM SIGKDD International Conference on Knowledge Discovery and Data Mining*, pp. 1029–1038, ACM, 2010.

[89] X. Song, B. L. Tseng, C. Lin, and M. Sun, *Personalized recommendation driven by information flow*, in *Proceedings of the 29th Annual International ACM SIGIR Conference on Research and development in information retrieval*, pp. 509–516, 2006.

[90] D. Ienco, F. Bonchi, and C. Castillo, *The meme ranking problem: Maximizing microblogging virality*, in *IEEE International Conference on Data Mining Workshops*, pp. 328–335, 2010.

[91] Y. Li, D. Zhang, and K. Tan, *Real-time targeted influence maximization for online advertisements*, *Proceedings of the VLDB Endowment* **8** (2015), no. 10 1070–1081.

[92] J. Weng, E. Lim, J. Jiang, and Q. He, *Twitterrank: finding topic-sensitive influential twitterers*, in *Proceedings of the third ACM International Conference on Web Search and Data Mining*, pp. 261–270, 2010.

[93] E. Bakshy, J. M. Hofman, W. A. Mason, and D. J. Watts, *Everyone's an influencer: quantifying influence on twitter*, in *Proceedings of the fourth ACM International Conference on Web Search and Data Mining*, pp. 65–74, 2011.

[94] J. Leskovec, A. Krause, C. Guestrin, C. Faloutsos, J. VanBriesen, and N. Glance, *Cost-effective outbreak detection in networks*, in *Proceedings of the 13th ACM SIGKDD International Conference on Knowledge Discovery and Data Mining*, pp. 420–429, ACM, 2007.

[95] J. R. P. French Jr. and B. Raven, *The bases of social power*, in *Studies in Social Power* (D. Cartwright, ed.), pp. 150–167. Institute for Social Research, University of Michigan, 1959.

[96] E. B. Goldsmith, *Social influence history and theories*, in *Social Influence and Sustainable Consumption*, pp. 23–39. Springer, 2015.

[97] P. Jia, N. E. Friedkin, and F. Bullo, *The coevolution of appraisal and influence networks leads to structural balance*, *IEEE Transactions on Network Science and Engineering* **3** (2016), no. 4 286–298.

[98] F. Heider, *Attitudes and cognitive organization*, *The Journal of Psychology* **21** (1946), no. 1 107–112.

[99] S. A. Marvel, J. Kleinberg, R. D. Kleinberg, and S. H. Strogatz, *Continuous-time model of structural balance*, *Proceedings of the National Academy of Sciences* **108** (2011), no. 5 1771–1776.

[100] A. Srinivasan, *Local balancing influences global structure in social networks*, *Proceedings of the National Academy of Sciences* **108** (2011), no. 5 1751–1752.

[101] G. Facchetti, G. Iacono, and C. Altafini, *Computing global structural balance in large-scale signed social networks*, *Proceedings of the National Academy of Sciences* **108** (2011), no. 52 20953–20958.

[102] M. Szell, R. Lambiotte, and S. Thurner, *Multirelational organization of large-scale social networks in an online world*, *Proceedings of the National Academy of Sciences* **107** (2010), no. 31 13636–13641.

[103] P. R. Laughlin and A. L. Ellis, *Demonstrability and social combination processes on mathematical intellective tasks*, *Journal of Experimental Social Psychology* **22** (1986), no. 3 177–189.

[104] O. Askarisichani, J. Ng Lane, F. Bullo, N. E. Friedkin, A. K. Singh, and B. Uzzi, *Structural balance emerges and explains performance in risky decision-making*, *Nature Communications* **10** (2019), no. 2648.

[105] J. R. Austin, *Transactive memory in organizational groups: the effects of content, consensus, specialization, and accuracy on group performance*, *Journal of Applied Psychology* **88** (2003), no. 5 866.

[106] K. Lewis, *Measuring transactive memory systems in the field: Scale development and validation*, *Journal of Applied Psychology* **88** (2003), no. 4 587–604.

[107] K. Lewis, *Knowledge and performance in knowledge-worker teams: A longitudinal study of transactive memory systems*, *Management Science* **50** (2004) 1519–1533.

[108] K. Lewis, D. Lange, and L. Gillis, *Transactive memory systems, learning, and learning transfer*, *Organization Science* **16** (2005), no. 6 581–598.

[109] Y. C. Yuan, I. Carboni, and K. Ehrlich, *The impact of awareness and accessibility on expertise retrieval: A multilevel network perspective*, *Journal of the American Society for Information Science and Technology* **61** (2010), no. 4 700–714.

[110] D. W. Liang, R. Moreland, and L. Argote, *Group versus individual training and group performance: The mediating role of transactive memory*, *Personality and Social Psychology Bulletin* **21** (1995), no. 4 384–393.

[111] J. V. Wood, *Theory and research concerning social comparisons of personal attributes*, *Psychological Bulletin* **106** (1989), no. 2 231–248.

[112] J. A. Shepperd, *Productivity loss in performance groups: A motivation analysis.*, *Psychological bulletin* **113** (1993), no. 1 67.

[113] J. A. Shepperd and R. A. Wright, *Individual contributions to a collective effort: An incentive analysis*, *Personality and social psychology bulletin* **15** (1989), no. 2 141–149.

[114] J. R. Beatty, R. W. Haas, and D. Sciglimpaglia, *Using peer evaluations to assess individual performances in group class projects*, *Journal of Marketing Education* **18** (1996), no. 2 17–27.

[115] H. K. Davison, V. Mishra, M. N. Bing, and D. D. Frink, *How individual performance affects variability of peer evaluations in classroom teams: A distributive justice perspective*, *Journal of Management Education* **38** (2014), no. 1 43–85.

[116] J. A. Drexler Jr, T. A. Beehr, and T. A. Stetz, *Peer appraisals: Differentiation of individual performance on group tasks*, *Human Resource Management* **40** (2001), no. 4 333–345.

[117] J. S. Miller and R. L. Cardy, *Self-monitoring and performance appraisal: rating outcomes in project teams*, *Journal of Organizational Behavior: The International Journal of Industrial, Occupational and Organizational Psychology and Behavior* **21** (2000), no. 6 609–626.

[118] J. P. Thomas and R. G. McFadyen, *The confidence heuristic: A game-theoretic analysis*, *Journal of Economic Psychology* **16** (1995), no. 1 97–113.

[119] P. C. Price and E. R. Stone, *Intuitive evaluation of likelihood judgment producers: Evidence for a confidence heuristic*, *Journal of Behavioral Decision Making* **17** (2004), no. 1 39–57.

[120] O. Askarisichani and J. Jalili, *Inference of hidden social power through opinion formation in complex networks*, *IEEE Transactions on Network Science and Engineering* **4** (2017), no. 3 154–164.

[121] L. E. Castro and N. I. Shaikh, *A particle-learning-based approach to estimate the influence matrix of online social networks*, *Computational Statistics & Data Analysis* **126** (2018) 1–18.

[122] L. E. Castro and N. I. Shaikh, *Influence estimation and opinion-tracking over online social networks*, *International Journal of Business Analytics* **5** (2018), no. 4 24–42.

[123] S. T. Smith, E. K. Kao, D. C. Shah, O. Simek, and D. B. Rubin, *Influence estimation on social media networks using causal inference*, in *IEEE Statistical Signal Processing Workshop (SSP)*, pp. 328–332, 2018.

[124] M. Gomez-Rodriguez, L. Song, N. Du, H. Zha, and B. Schölkopf, *Influence estimation and maximization in continuous-time diffusion networks*, *ACM Transactions on Information Systems* **34** (2016), no. 2 1–33.

[125] N. Du, L. Song, M. G. Rodriguez, and H. Zha, *Scalable influence estimation in continuous-time diffusion networks*, in *Advances in Neural Information Processing Systems*, pp. 3147–3155, 2013.

[126] Q. Deng and Y. Dai, *How your friends influence you: Quantifying pairwise influences on twitter*, in *International Conference on Cloud and Service Computing*, pp. 185–192, IEEE, 2012.

[127] S. Ye and S. F. Wu, *Measuring message propagation and social influence on twitter.com*, in *International Conference on Social Informatics*, pp. 216–231, Springer, 2010.

[128] F. Riquelme and P. González-Cantergiani, *Measuring user influence on twitter: A survey*, *Information Processing & Management* **52** (2016), no. 5 949–975.

[129] A. Almaatouq, A. Noriega-Campero, A. Alotaibi, P. M. Krafft, M. Moussaid, and A. Pentland, *Adaptive social networks promote the wisdom of crowds*, *Proceedings of the National Academy of Sciences* **117** (2020), no. 21 11379–11386.

[130] C. Manteli, B. V. D. Hooff, and H. V. Vliet, *The effect of governance on global software development: An empirical research in transactive memory systems*, *Information and Software Technology* **56** (2014), no. 10 1309–1321.

[131] C. Huang and P. Chen, *Exploring the antecedents and consequences of the transactive memory system: An empirical analysis*, *Journal of Knowledge Management* **22** (2018) 92–118.

[132] B. Everitt and A. Skrondal, *The Cambridge dictionary of statistics*, vol. 106. Cambridge University Press Cambridge, 2002.

[133] Y. Liu, M. Ott, N. Goyal, J. Du, M. Joshi, D. Chen, O. Levy, M. Lewis, L. Zettlemoyer, and V. Stoyanov, *Roberta: A robustly optimized bert pretraining approach*, *arXiv preprint arXiv:1907.11692* [**cs**] (2019).

[134] X. He, L. Liao, H. Zhang, L. Nie, X. Hu, and T. Chua, *Neural collaborative filtering*, in *Proceedings of the 26th International Conference on World Wide Web*, pp. 173–182, International World Wide Web Conferences Steering Committee, 2017.

[135] D. Clevert, T. Unterthiner, and S. Hochreiter, *Fast and accurate deep network learning by exponential linear units (elus)*, *arXiv preprint arXiv:1511.07289* [**cs**] (2015).

[136] K. He, X. Zhang, S. Ren, and J. Sun, *Delving deep into rectifiers: Surpassing human-level performance on imagenet classification*, in *Proceedings of the IEEE International Conference on Computer Vision*, pp. 1026–1034, 2015.

[137] N. Srivastava, G. Hinton, A. Krizhevsky, I. Sutskever, and R. Salakhutdinov, *Dropout: a simple way to prevent neural networks from overfitting*, *Journal of Machine Learning Research* **15** (2014), no. 1 1929–1958.

[138] V. Amelkin, O. Askarisichani, Y. J. Kim, T. W. Malone, and A. K. Singh, *Dynamics of collective performance in collaboration networks*, *PloS One* **13** (2018), no. 10 e0204547.

[139] C. J. Hutto and E. Gilbert, *Vader: A parsimonious rule-based model for sentiment analysis of social media text*, in *Eighth International AAAI Conference on weblogs and social media*, 2014.

[140] M. M. Bradley and P. J. Lang, *Affective norms for english words (anew): Instruction manual and affective ratings*, tech. rep., Technical report C-1, the center for research in psychophysiology ..., 1999.

[141] D. Cer, Y. Yang, S. Kong, N. Hua, N. Limtiaco, R. S. John, N. Constant, M. Guajardo-Cespedes, S. Yuan, C. Tar, *et. al.*, *Universal sentence encoder*, *ArXiv preprint arXiv:1803.11175* [**cs**] (2018).

[142] J. Devlin, M. Chang, K. Lee, and K. Toutanova, *Bert: Pre-training of deep bidirectional transformers for language understanding*, *arXiv preprint arXiv:1810.04805* [**cs**] (2018).

[143] K. Kułakowski, P. Gawroński, and P. Gronek, *The Heider balance: A continuous approach*, *International Journal of Modern Physics C* **16** (2005), no. 05 707–716.